Hydrodesulphurization of dibenzothiophene using carbon supported NiMoS catalysts

by

Majed Alamoudi

B.Sc., King Abdulaziz University, 2012

A THESIS SUBMITTED IN PARTIAL FULFILLMENT OF

THE REQUIREMENTS FOR THE DEGREE OF

MASTER OF APPLIED SCIENCE

in

THE FACULTY OF GRADUATE AND POSTDOCTORAL STUDIES

(CHEMICAL AND BIOLOGICAL ENGINEERING)

THE UNIVERSITY OF BRITISH COLUMBIA

(Vancouver)

April 2016

Abstract

Hydrodesulphurization (HDS) is the major process used to remove S from crude oil feedstocks in order to improve fuel quality and meet environmental regulations. The goal of this study was to determine if petroleum coke (petcoke), derived from Alberta oilsands, could be converted into a useful catalyst support. Hence the HDS activity and selectivity of nickel molybdenum sulfided catalysts supported on activated carbon (NiMoS/AC), petroleum coke (NiMoS/PC) and conventional alumina (NiMo/γ-Al_2O_3) have been compared using dibenzothiophene (DBT) as a model reactant. The reactions were carried out in a novel slurry-phase batch microreactor at different reaction times (30-120 min) and temperatures (588-638 K) and a fixed H_2 pressure (4.8 MPa).

The results showed that NiMoS/PC had higher activity towards the HDS of DBT when compared with NiMoS/AC, although the catalysts had very similar product selectivities. The highest activity for DBT HDS, corresponding to 90% DBT conversion, occurred at 638 K for the NiMoS/AC catalyst and at 623K for the NiMoS/PC catalyst. The reaction proceeded by two pathways: the direct desulphurization (DDS) reaction route and the hydrogenation (HYD) reaction route. The power law pseudo 1^{st}-order kinetic model was applied to the HDS of DBT. The estimated kinetic parameters showed similar magnitudes for the HYD versus the DDS routes over both catalysts, whereas the DDS pathway had higher apparent activation energy compared to the HYD route for both catalysts.

Preface

All the work reported in this thesis was performed in the Department of Chemical and Biological Engineering at the University of British Colombia, Vancouver campus.

I, Majed Alamoudi, was the investigator of this research and responsible for preparing the catalysts, running the microreactor, obtaining and discussing the results, and stating the major findings as well as constructing this thesis. Kevin J Smith supervised the research, providing guidance, instructions, approving the work, and editing this thesis. Ross Kukard commissioned the novel slurry-phase batch microreactor described in section 2.3 which was used to carry out the experiments and collect the data reported in section 3.3.

Table of Contents

List of Tables

List of Figures

Nomenclature

A_j	Pre-exponential factor of reaction, 1/s or $cm^3/(g_{cat}s)$
a_j	Catalyst deactivation factor of reaction *j*
C_i	Concentration of species *i*, mol/L
E_{aj}	Activation energy of reaction *j*, kJ/mol
ΔH	Enthalpy of reaction, kJ/mol
k	Rate constant, 1/s
k_j'	Catalytic rate constant, $cm^3/(g_{cat}s)$
R^2	Degree of explanation
v	Volumetric flow rate, m^3/min
V	Volume, m^3

Greek

Ω_j	Catalyst effectiveness factor of reaction *j*
ρ	Density, kg/m^3

List of Abbreviations

AAC	Alumina-activated carbon
AC	Activated carbon
BET	Brunauer-Emmett-Teller
BP	Biphenyl
BCH	Bicyclohexyl
CAC	Commercial active carbon
CHB	Cyclohexylbenzene
CMC	Mesoporous carbon
DAC	Delayed coke
DBT	Dibenzothiophene
DMDBT	Dimethyldibenzothiophene
DDS	Direct desulphurization
EXAFS	Extended X-ray absorption fine structure
HC	Hydrocarbon
HDS	Hydrodesulphurization
HDN	Hydrodenitrogenation
HYD	Hydrogenation
HVGO	Heavy vacuum gas oil
FAC	Fluid coke
GC	Gas chromatograph
H_2S	Hydrogen sulfide gas
KB	KetjenBlack

KOH	Potassium hydroxide
LHSV	Liquid hourly space velocity
L-H	Langmuir-Hinshelwood
MS	Mass spectroscopy
NiMo/γ-Al_2O_3	Nickel molybdenum supported on alumina
NiMo/AC	Nickel molybdenum supported on active carbon
NiMo/AAC	Nickel moly supported on alumina-active carbon
NTA	Nitrilotriacetic
Petcoke	Petroleum coke
S	Sulphur
THDBT	Tetrahydrodibenzothiophene
XRD	X-ray diffraction
XPS	X-ray photoelectron spectroscopy

Subscripts

exp	Experimental
pred	Model predicted
j	Reaction *j*
i	Chemical species *i*
cat	Catalyst
tot	Total

Acknowledgements

I would like to express my sincere gratitude to Prof. Kevin Smith for his tremendous and continued support and guidance throughout this project and for sharing his knowledge with me. Prof. Smith truly expanded my knowledge in the area of catalysis and in scientific research in general.

I also would like to pay very special gratitude to my loving and affectionate parents and to my grandfather for their continuous support and for being on my side through their heart-felt words at the times of difficulty despite being thousands of miles away from me. It is their support that made uncertainty and challenges look easy.

In addition, I would like to thank Mr. Ali Alzaid, Dr. Ross Kukard, and the rest of the catalysis group for sharing their knowledge and expertise with me and for their guidance and their time in teaching and familiarizing me with the equipment that I used throughout my research.

Lastly, I would like to thank the Royal Saudi Government for the scholarship that they have granted me for the opportunity to study at UBC and explore another side of the world. I would also like to thank NSERC and Royal Dutch Shell for the funding they have provided for this project.

Without the help of the aforementioned people and parties, this work would have not been possible.

Chapter 1: Introduction

1.1 Background

The demand for cleaner fuels in the transportation sector is growing rapidly. At the same time, the supply of aromatic, heavier and more contaminated crude oil is also increasing. The U.S. EPA is proposing that the S content of gasoline be limited to < 10 part per million (ppm) on a yearly average basis by 1 January 2017, down from the present 30 ppm. Furthermore, the EPA is considering whether to either keep the present 80-ppm refinery gate and 95-ppm downstream S caps or reduce them to 50 and 65 ppm, respectively as described in Table 1[1]. Moreover, according to Figure 1, the current S content in diesel fuel in North America is 20 ppm, and this is expected to decline to 10 ppm by 2025[2]. Therefore, for health and environmental reasons, the refractory species containing S must be removed from the crude oil. An improvement in existing catalyst hydrotreating technology to achieve the removal of S and N from heavier refractory components is needed.[3]

Hydrodesulphurization (HDS) and hydrodenitrogenation (HDN) are the major processes used to remove S and N, respectively, from oil feed stocks. They are both categorized as a hydrotreating process, defined as a catalytic chemical process used to remove impurities from natural gas, gasoline, or oil feedstock by reacting it with hydrogen. Several studies have indicated that S removal from refractory components such as dibenzothiophene (DBT) and 4,6-dimethyldibenzothiophene (4,6-DMDBT) is difficult to achieve[4] because of the C-S bond strength and steric hindrance effects in the case of 4,6-DMDBT. Many studies conducted to address this issue, show that high activity for HDS can be achieved using sulfided nickel and molybdenum (NiMo) supported on activated carbon or pretreated petcoke[3,5,6], but these

measurements were made at the laboratory scale, whereas the catalysts may deactivate over extended operation times which has a significant impact on the overall cost of operations.

Table 1: Gasoline Sulfur Standards for the USA[1]

Standard	Cap Option 1		Cap Option 2	
	Limit	Effective	Limit	Effective
Refinery annual average standard	10 ppm	1 Jan 2017	10 ppm	1 Jan 2017
Refinery gate per-gallon cap	80 ppm	Already	50 ppm	1 Jan 2020
Downstream per-gallon cap	95 ppm	Already	65 ppm	1 March 2020

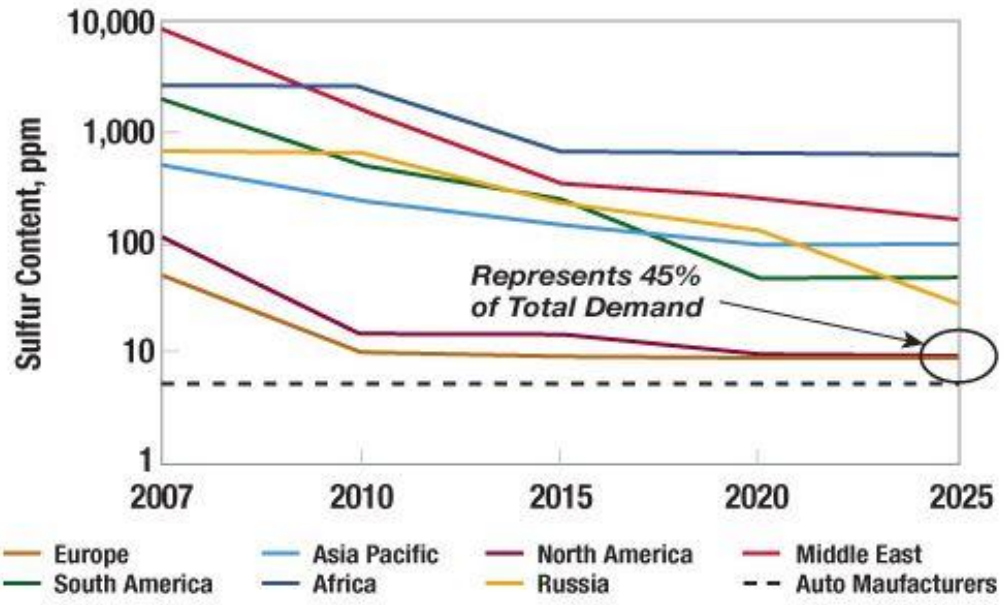

Figure 1: Sulphur content in diesel fuel - trend for all the continents[2]

1.2 Hydrodesulphurization Process

In industry, hydrodesulphurization reactions occur in fixed bed reactors at temperatures ranging from 300 to 400 ^{o}C and pressure from 3 to 13 MPa, with Ni-Mo or Co-Mo catalysts supported on γ-Al_2O_3. The image shown in Figure 2 is a process flow diagram of a hydrodesulphurization unit.

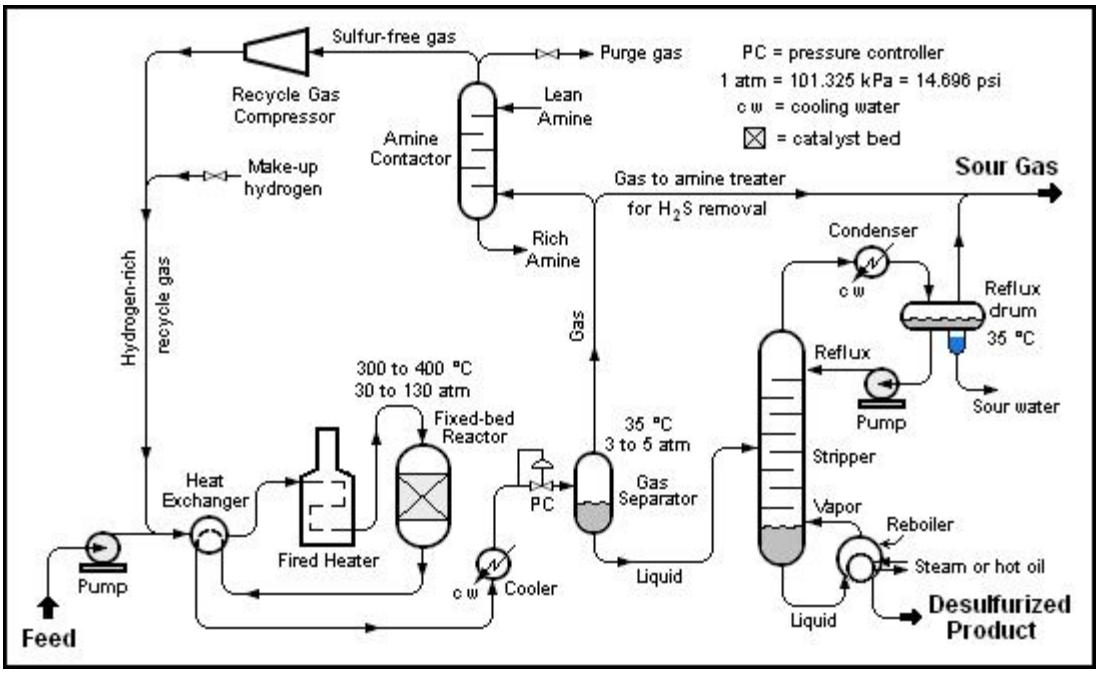

Figure 2: Schematic diagram of a typical HDS unit in a petroleum refinery[7]

As shown in Figure 2, the liquid feed is pumped to the desired pressure and mixed with recycled hydrogen-rich gas. The mixture of liquid-gas feed, flows to the heat exchanger to be preheated. The resulting feed passes through a fuel fired heater to be fully vaporized and heated to the desired temperature, prior to entering the reactor and passing through the packed bed of catalysts where the HDS reaction occurs. The heated products from the reactor are cooled by

passing through a heat exchanger and a water-cooled heat exchanger prior to passing through a pressure controller (PC) which lowers the pressure to approximately 0.3 to 0.5 MPa. The product mixture then passes to the gas separator vessel at 35 ^{o}C and 0.3 - 0.5 MPa pressure.

The majority of the hydrogen-rich gas that comes from the gas separator vessel is directed to an amine contactor in order to remove the hydrogen sulfide gas (H_2S). The resulting S free gas is recovered for recycle. Some S gas from the gas separator is blended with sour gas from the distillation column.

The liquid from the gas vessel is directed to the distillation column. The stripped liquid products in the bottom are the desired desulfurized products.

Ethane, methane, propane and H_2S as well as some heavier compounds are the major components of the sour gas from the distillation stripper. The sour gas is directed to a central gas processing plant in the refinery to remove H_2S using an amine gas treating unit through a series of distillation columns to recover the heavy components such as propane, butane, and pentane. The H_2S extracted by the amine treating unit is then converted to S in a Claus unit[7].

1.3 Canadian Oil Sands, Petroleum Coke and Activated Carbon:

The Canadian oil sands in Alberta produce about 1.8 million barrels of oil per day. The oil sands is a major source of energy for North America. The Canadian oil sands contain about 10% bitumen. Bitumen undergoes upgrading to a synthetic crude. As a result of this process, petroleum coke (petcoke) is produced as a byproduct in large amounts, ranging between 5-6 million tonnes per year. There are two different types of coke generated in oil sand upgrading: delayed coke which is generated by Suncor and fluid coke which is generated by Syncrude. Delayed coke differs from fluid coke in its properties[8]. As shown in Table 2[9], the coke yield

from the delayed coker process is 33 wt% whereas from the fluid coker it is 20 wt%. Fluid coke contains 9 wt% of S which is higher than the delayed coke S content of 7 wt%. Since the S content in the coke is high, it needs to undergo pretreatment processes to be purified for use in other processes such as the iron, cement, aluminum, and thermoelectric industries. The limitations to petcoke use are caused by the high S content of 4-9%, and the presence of other metals such as Ni and V. Petcoke also has a low surface area < 5 m^2/g[8-10]. On the other hand,petcoke has a low volatile matter content which results in a high combustion temperature which makes petcoke safe to handle. In addition, petcoke is superior in heat content compared to coal due to a lower ash content of ~7 wt%, and it is not an explosive hazard[11]. Since petcoke contains many impurities (S, N, V, Ni, and other heavy metals) it must undergo treatment processes to be purified. The present study is aimed at utilizing petcoke as a catalyst support. Since petcoke has a very low surface area (~5 m^2/g), it must be processed to increase the surface area. The pre-treating process can also increase the porosity of the petcoke which makes it effective for use in hydrotreating catalysts.[5,12-16]

Activated carbon is a highly porous material and contains large surface area ranging between 1000-3000 m^2/g and pore volumes of 0.8 - 1.2 cm^3/g. Activated carbon is an effective adsorbent if it has a high surface area, but if it has a lower surface area and mesopores it could be used as a catalyst or catalyst support. The carbon structure consists of segments of graphene sheets with different sizes and dimensions bonded to each other in an unlimited number of ways. The applications of activated carbon depend on its physical and chemical properties. The activated carbon can also be used as a catalyst support that aids in the dispersion of active phase due to its large surface area and weak polarity[17]. For metal sulfide supported on activated carbon, the formation of (Ni,Co)-Mo-S phases are an expected result of the weak interactions between the

metal and the support in the case of carbon[17]. Activated carbons also contain a high number of micropores, but they are usually not effective in hydrotreating processes.[18]

In the current study, Ni-Mo catalysts were supported either on commercial activated carbon or petcoke. There have been several studies showing that cobalt-molybdenum (Co-Mo) or Ni-Mo supported on activated carbon have promising hydrotreatment activities for removing S from oil feedstocks[5,19,20]. As aforementioned, there is a large amount of petcoke that has been produced from bitumen upgrading. In the current study, petcoke will be assessed experimentally for use as a support of NiMoS catalysts. The catalysts will be assessed by measuring the conversion and product distribution over a range of conditions and hence the HDS reaction kinetics will be determined.

Reaction mechanisms of HDS of DBT have been explored in many studies showing that the reaction occurs by two routes; the direct desulphurization reaction route (DDS) and the hydrogenation reaction route (HYD)[3-6,21-23]. In the DDS route, the reaction starts by extracting the S from the DBT reactant producing biphenyl (BP). The hydrogenation of BP to form cyclohexylbenzene (CHB) is very slow compared to the other steps and therefore it can be ignored in the kinetic model[22]. In the HYD route, the reaction starts with the hydrogenation of the DBT to produce tetrahydrodibenzothiophene (THDBT), followed by S removal from the THDBT to produce CHB. Further hydrogenation of CHB leads to bicyclohexyl (BCH).

Table 2: Product yield from Delayed coke and Fluid coke processing of Alberta bitumen[9]

Component /Coke type	Delayed Coke	Fluid coke
H_2S (wt%)	1.1	0.7
Light Ends (wt%)	11.1	11.6
Naphtha (vol%)	25.66	20.7
Middle distillate (vol%)	26.4	15.8
Gas Oil (vol%)	13.8	32.5
Coke (wt%)	33	20
S content (wt%) of the coke	7.35	9

1.4 Literature Review

Many previous studies have been conducted on the HDS of model compounds such as DBT as well as real oil feedstock. A variety of feeds, types of catalyst, reactors, and reaction conditions have been investigated[3-6,21-23] in academic research and industrial processes, reflecting the commercial importance of HDS processes. In this chapter, studies related to the current research are reviewed and discussed.

1.4.1 Comparison of Carbon Supported Catalysts with other Supports

Shi et al.[5] studied the effect of different types of support on heavy vacuum gas oil (HVGO) upgrading. The activated carbon used as a support was obtained from Alberta oil sand petroleum coke, either delayed coke or fluid coke. The coke needs to undergo a chemical process to be purified as well as to improve its physical properties. The BET surface area of the coke after chemical treatment was 2194 m^2/g for the fluid coke and 2357 m^2/g for the delayed coke, and their pore volumes were as high as 1.2 cm^3/g. Both supports had a large number of micropores. Ni-Mo was loaded onto the supports by impregnation of $Ni(NO_3)_2$ and

$(NH_4)_6Mo_7O_{24}$ followed by calcination in N_2 at 773 K. For comparison, two types of catalysts were synthesized using the same aforementioned procedures but using commercial activated carbon and highly porous γ-Al_2O_3 supports. The catalysts were sulphided and a magnetically stirred (400 rpm) autoclave reactor along with HVGO feedstock were used to evaluate the hydrotreatment performance of the catalysts at 643 K and 3.45-5.50 MPa, after 2 h of reaction. In addition to the prepared catalysts, two commercial catalysts were also examined and compared under the same aforementioned conditions. As shown in Figures 3 and 4, the catalysts supported on delayed and fluid coke had better hydrotreating performance when compared with the other supports. The higher hydrotreating activity of the catalyst supported on either delayed coke or fluid coke was as a result of high surface area and pore volume of these supports when compared with other supports.

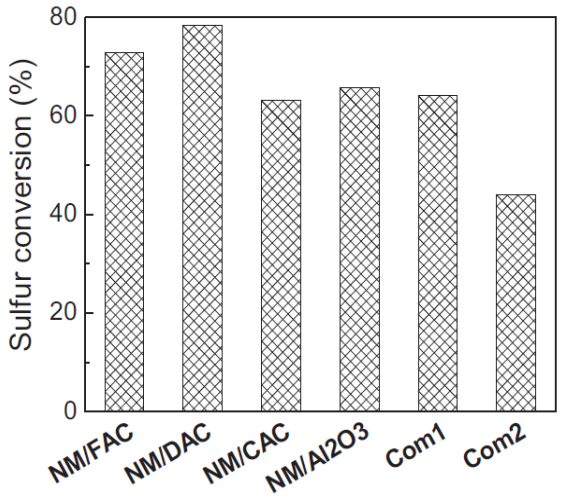

Figure 3: HDS activites obtained with different catalysts (FAC:fluid coke, DAC:delayed coke,CAC: commercial activated carbon) under 643 K,3.45 MPa, and 2 hours reaction time. Copyright © 2012, Elsevier[5]

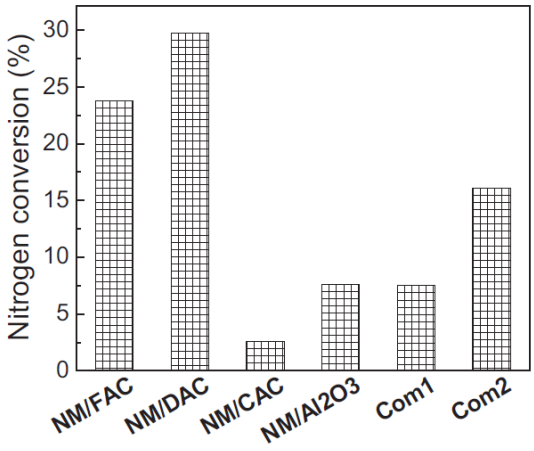

Figure 4: HDN activities obtained with different catalysts (FAC: fluid coke, DAC: delayed coke, CAC: commercial activated carbon) under 643 K,3.45 MPa, and 2 hours reaction time. Copyright © 2012, Elsevier[5]

Liu et al.[24] studied the composite alumina-activated carbon (AAC) as a support of Ni-Mo catalyst for HDS of DBT and compared the results with Ni-Mo supported on alumina (NiMoS/γ-Al_2O_3) and Ni-Mo supported on activated carbon (NiMoS/AC). The three catalysts were prepared by incipient wetness impregnation with a loading of 7 wt% Ni and 14 wt% Mo. A trickle-bed reactor was used to study the catalyst activity for DBT hydrodesulphurization. The catalysts were sulfided in-situ. The feed contained 1 wt% of DBT in decalin and the reaction was conducted at 260-300 ^oC with 3 MPa pressure along with 500 Nm^3/m^3 H_2/feed ratio and 0.3-0.6 h^{-1} LHSV. The investigators showed that the catalyst activity for DBT hydrotreating was significantly increased using the AAC as a support. As shown in Figure 5, 90% DBT conversion was achieved at 260 ^oC compared with only 58% achieved on the NiMoS/AC and 32% conversion on the NiMoS/γ-Al_2O_3. The activation energies for the catalysts were estimated from the data of Figure 5 to be 143 kJ/mol for NiMoS/γ-Al_2O_3, 105 kJ/mol for NiMoS/AC, and 89 kJ/mol for NiMoS/AAC (refer to Appendix A for detailed calculation). The significant impact of the aforementioned catalytic activity was due to the higher dispersion of Ni and Mo on the alumina-activated carbon support versus the other supports as shown in Figure 6. The MoO_3 (+) disappears from the NiMoS/AAC diffractogram whereas it is present for the NiMoS/γ-Al_2O_3, implying that a higher dispersion of Mo occurred on the surface of the alumina-activated carbon than the γ-Al_2O_3.[24]

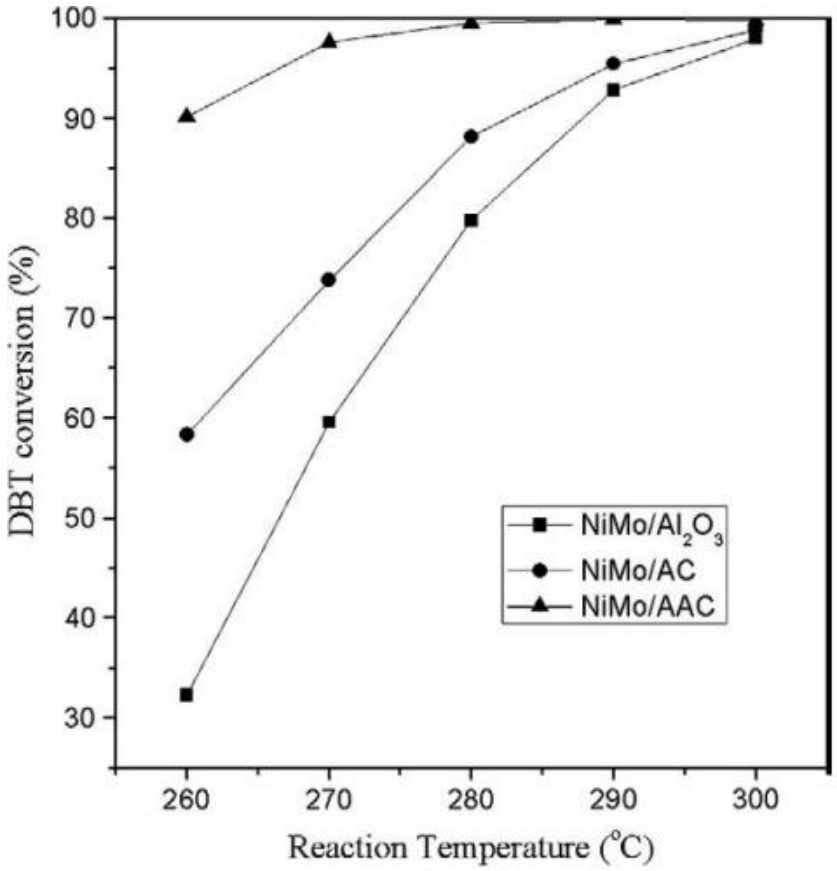

Figure 5: The conversion of DBT over presulfided catalysts NiMoS/γ-Al_2O_3, NiMoS/AC and NiMoS/AAC as a function of reaction temperature. Copyright © 2011, Elsevier[24]

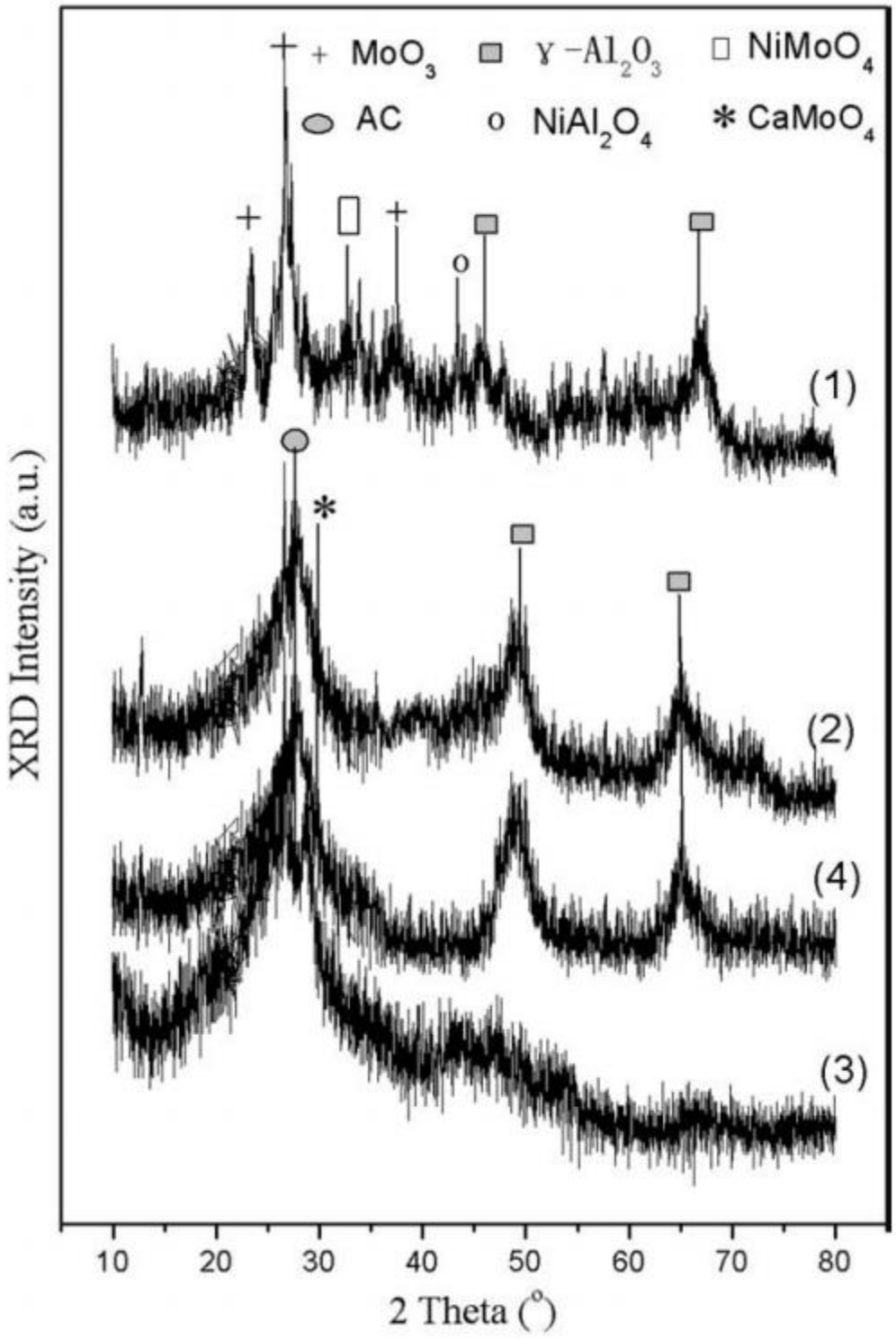

Figure 6: The XRD patterns of NiMoS/γ-Al_2O_3 (1), NiMoS/AAC (2) NiMoS/AC (3), and AAC (4).Copyright © 2011, Elsevier[24]

Shi et al.[6] studied how mesoporous carbon as a support for Co-Mo and Ni-Mo catalysts affects the HDS of 4,6-DMDBT and DBT. Mesoporous carbons (CMC) have larger surface area (1400–2000 m^2/g), pore diameter (3–7 nm) and pore volume (1.44–2.72 cm^3/g) compared to activated carbons (AC) with 936 m^2/g surface area, 3.8 nm pore diameter, and 0.34 cm^3/g pore volume. An impregnation method was used to prepare the catalysts using different types of chelating agents such as citric acid, tetraacetic acid ethylenediamine, ethylenediamine, and nitrilotriacetic acid (NTA). NTA was found to be the best chelating agent for the preparation of Co-Mo/CMC and Ni-Mo/CMC. Co-Mo/CMC and Ni-Mo/CMC showed better surface area and pore volume than the AC supported catalysts. Consequently, those catalysts which were supported on CMC exhibited much better activity than the AC supported catalysts in the HDS of organic S, as most of the micropores of the CMC were converted to mesopores[25] and hence the diffusion rate of the Ni-Mo or Co-Mo species on CMC were faster during the impregnation. According to Figure 7, Co-Mo/CMC showed higher activity than the commercial Co-Mo/ γ-Al_2O_3 in the HDS of thiophene. Moreover, as shown in Figure 8, Ni-Mo/CMC was significantly more active than the commercial Co-Mo/γ-Al_2O_3 in the HDS of DBT.[6]

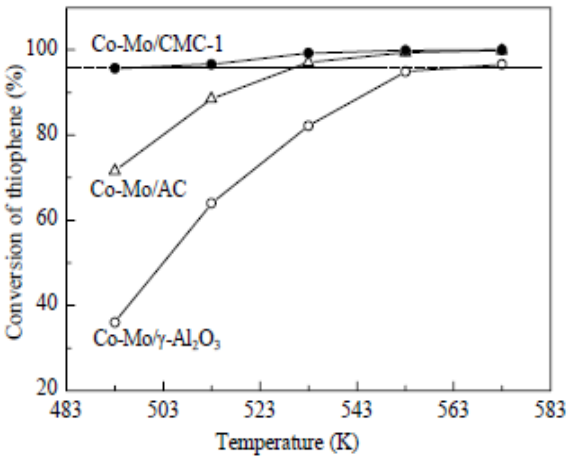

Figure 7: Activity of Co-Mo/CMC-1, Co-Mo/AC, and commercial Co-Mo/γ-Al_2O_3 for the HDS of thiophene in a model gasoline. Reaction conditions: 1.5 MPa, LHSV = 2 h^{-1}, H_2/feed volume ratio = 300. The model gasoline contained 0.05% sulfur from thiophene and 20% 1-hexene, and the balance was *n*-heptane. Copyright © 2010, Elsevier[6]

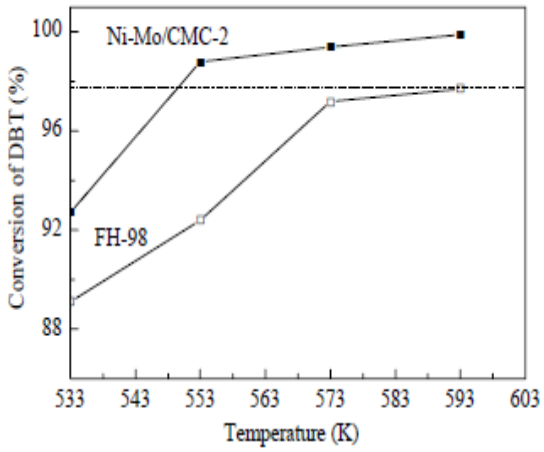

Figure 8: Activity of Ni-Mo/CMC-2 and the commercial catalyst FH-98for the HDS of dibenzothiophene (DBT) in a model diesel. Reaction conditions: 3.1 MPa, LHSV = 2 h^{-1}, H_2/feed volume ratio = 500. The model diesel contained 0.3% sulfur from DBT, 0.02% N from quinolone 5% and 0.5% *n*-octane as an internal standard. Copyright © 2010, Elsevier[6]

Shu and Oyama[21] studied the hydrotreating activity of carbon-supported transition metal phosphides. Ni_2P/C, MoP/C, and WP/C were synthesized through temperature-programmed reduction. BET surface area, CO uptake, extended X-ray absorption fine structure (EXAFS) measurements, and X-ray diffraction (XRD) were used to characterize the above samples. The hydrotreating activity of these catalysts was measured at 613 K and 3.1 MPa and carried out in three different sets of experiments using a packed-bed reactor for HDS and HDN with a liquid feed consisting of (i) 3000 ppm S as CH_3SSCH_3, (ii) 500 ppm S as 4,6-DMDBT and (iii) 200 ppm N in the form of C_9H_7NO. The best activity based on a constant number of CO chemisorption sites (70 µmol) in the reactor, was found to be the Ni_2P/C catalyst. This study found that the best Ni loading for both HDS and HDN was 1.656 mmol/g (11 wt% Ni_2P) which

contributed significantly to raising the HDN conversion to 100% and HDS to 99% at a molar space velocity of 0.88 h^{-1}. The aforementioned conversion results illustrated that the carbon support played a major role for high HDS and HDN activities in comparison with the commercial Ni-Mo-S/γ-Al_2O_3 and Ni_2P/SiO_2 catalysts, which obtained only 68%-94% conversions. Some exceptional features that make carbon better than silica as a support, include smaller metal phosphide particle size, higher CO uptake, less retention of P on the support, and reduced sulfur deposition.[21]

Kouzu et al.[23] prepared four types of activated carbon, differing in surface area from 916 m^2/g to 3075 m^2/g, as support for NiMo-sulfide (NiMoS/AC) catalysts to study the effect of properties of supported carbon on the HDS of 4,6-DMDBT. The study was carried out at 320 ^oC using an autoclave reactor. They reported that an increase in HDS activity was observed as the surface area of the AC increased. By increasing the area, the dispersion of catalytic active components increased. Oxygen functional groups that were present in the activated carbon, restricted the dispersion of the catalytic component. To improve the dispersion, oxygen groups of the activated carbon were reduced, which resulted in an enhancement of dispersion and, hence, the HDS activity. After the reduction treatment, NiMoS was prepared and supported on the reduced AC which catalyzed the hydrogenation reaction path of HDS of 4,6-DMDBT and DBT more than the commercial alumina supported catalysts (NiMoS/γ-Al_2O_3). A tubular reactor was also used to carry out the reaction with a real-feedstock under H_2 and 5 MPa pressure in 250 nL/L volumetric ratio of H_2/Oil. The best result achieved by NiMoS/AC catalyst at 337 ^oC was a product with 10 ppm-S, whereas for NiMoS/γ-Al_2O_3 catalyst even at the highest HDS temperature of 350 ^oC, the catalyst could not achieve the same result as the NiMoS/AC catalyst, as shown in Figure 9.

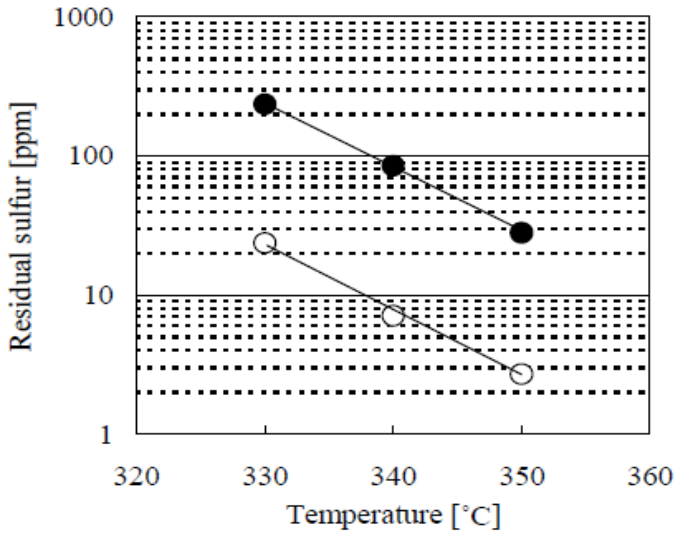

Figure 9: Temperature vs. residual sulfur content in HDS reaction of real gas–oil feedstock using down-flow tubular reactor, with LHSV of 1.5 h^{-1} under hydrogen pressure of 5MPa in volumetric hydrogen/oil ratio of 250 nl l^{-1}. (○) Over the best Ni-Mo/Activated carbon catalyst (k at 330 ºC = 1.59 h^{-1}), (●) over the conventional Ni-Mo/γ-Al_2O_3 catalyst (*k* at 330◦C = 0.68 h^{-1}) Copyright © 2004, Elsevier[23].

Sakanishi et al.[3] studied the kinetics and mechanism of 4,6-DMDBT HDS over NiMo/C. To establish the kinetics and mechanism of HDS, the feed containing 4,6-DMDBT in decane was hydrodesulfurized (NiMoS/C) using a 50-ml autoclave, equipped with a sampling apparatus, under hydrogen pressure of 3 to 15 MPa. Ni-Mo salts were dissolved in aqueous CH_3OH to impregnate the carbon support by simultaneous impregnation. After impregnation, the oxides on the carbon were presulfided at 360 ºC for 2 h .The study compared alumina and carbon as support for NiMo. NiMo/C catalysts showed higher activity than the commercial NiMo/γ-Al_2O_3 for HDS of 4,6-DMDBT in the temperature range 613-653 K. It was found that the DDS reaction was dominant in this temperature domain. The study also showed that the HYD route of HDS was the dominant pathway at temperature < 573 K. Another aspect of this study was to show the

effect of H_2S on the catalyst activity. Despite the effect of temperature, H_2S extensively inhibits the DDS route, but on the other hand, H_2S significantly enhances the HYD route of the HDS of 4,6-DMDBT.

Sakanishi et al.[26]studied Ketjen Black (KB) as a support for NiMo catalysts for hydrogenation of 1-methylnaphthalene and compared it in activity and conversion with a commercial NiMo/γ-Al_2O_3 catalyst. KetjenBlack (KB) has unique properties such as high surface area >1000 m^2/g and low specific gravity around 115 g/L. The reaction was carried out using a 50-mL magnetically-stirred autoclave reactor under the standard conditions of 380 ^oC, 40 min, and 9.5 MPa of H_2 reaction pressure. The catalyst was prepared from $[CH_3COCH=C(O)CH_3]_2MoO_2$ and $Ni(CH_3CO_2)_2$ in CH_3OH solution using successive impregnations of Mo (10 wt %) and Ni (2 wt %), respectively. The catalyst exhibited the highest conversion of 84% to methyltetralins as shown in Figure 10. It is worth mentioning that the merging of organic soluble metal salts with methanol may have great impact on suppressing the agglomeration of KB ultrafine carbon particles due to the balanced hydrophobic nature of the solvent matrix. The study found that NiMo supported on KB is more active than the commercial NiMo/γ-Al_2O_3.

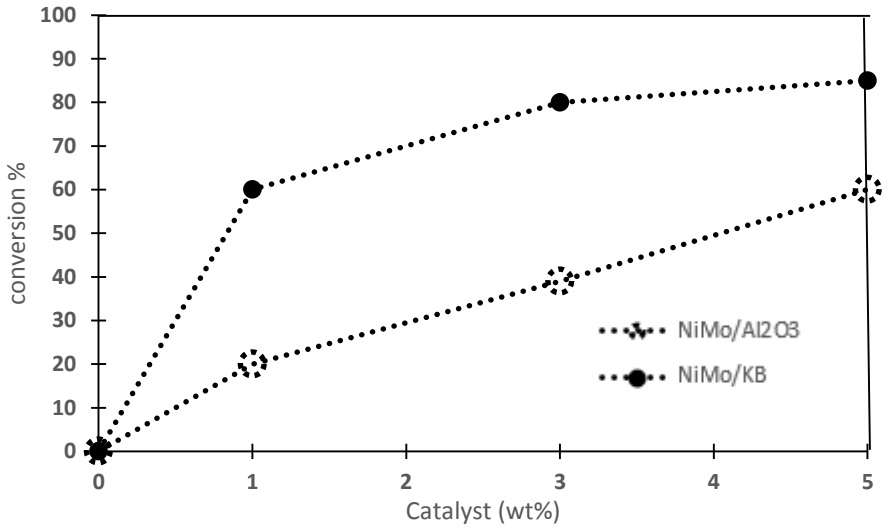

Figure10: Effect of catalyst amount on the hydrogenation conversion of 1-methylnaphthalene with NiMo/KB or NiMo/γ-Al_2O_3. Reaction conditions: 1-Methylnaphthalene/decalin= 1/9; reaction temperature 380 ºC; reaction pressure 9.5 MPa; reaction time 40min; catalyst NiMo/KB or NiM/γ-Al_2O_3, 1-5wt% addition to 1-Methylnaphthalene.Adapted from [26].Copyright © 1995, American Chemical Society [26]

1.4.2 Reaction Kinetics

Egorova and Prins[22] studied the HDS of DBT and 4,6-DMDBT over sulfided CoMo/γ-Al_2O_3, NiMo/γ-Al_2O_3 and Mo/γ-Al_2O_3. The NiMo/γ-Al_2O_3 results were obtained from elsewhere.[27,28] Since the DBT results are related to the current study, they will be discussed here. The feed in the gas phase contained 130 kPa toluene, 8 kPa dodecane as a reference for DBT and their derivates, 1 kPa DBT , 4 MPa H_2 and 0-100 kPa H_2S. A continuous fixed- bed Inconel reactor was used to carry out the reactions.[27,28] The Ni and Co promoters effectively contributed to the activity of the Mo metal catalyst especially through the DDS route of the HDS of DBT, while the HYD route was to a much lower extent promoted. Several experiments were conducted at 340 ºC and 35 kPa H_2S with different space velocities over Mo/γ-Al_2O_3 and CoMo/γ-Al_2O_3 as

shown in Figures 11 and 12. Adding Co as a promotor significantly enhanced the DDS reaction route but the HYD route was not enhanced to any great extent.

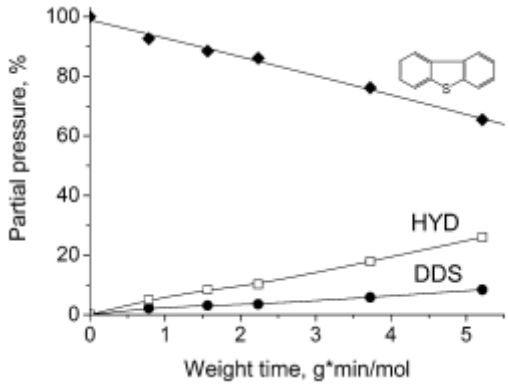

Figure 11: Relative partial pressures of the products in the HDS of dibenzothiophene at 340 ºC and 35 kPa H_2S over Mo/γ- Al_2O_3 as function of weight time.Copyright © 2004, Elsevier [22]

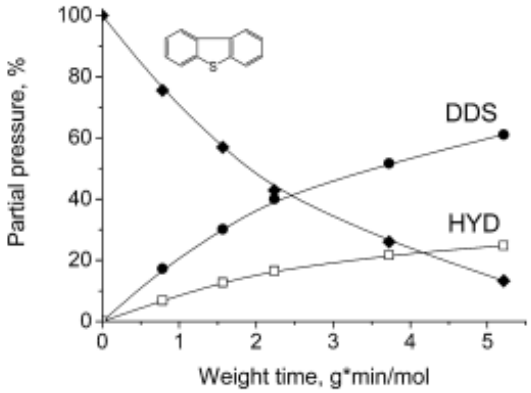

Figure 12: Relative partial pressures of the products in the HDS of dibenzothiophene at 340 ºCand 35 kPa H_2S over CoMo/γ-Al_2O_3 as function of weight time. Copyright © 2004,Elsevier [22]

Egorova and Prins proposed the following reaction sequence for the HDS of DBT

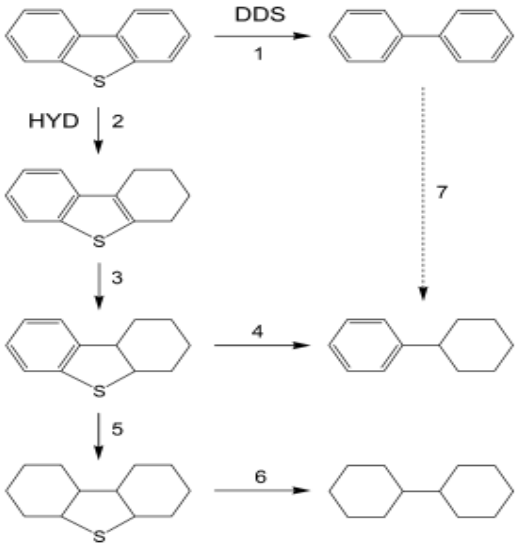

Figure 13: Proposed reaction pathway for HDS of DBT. Copyright © 2004, Elsevier [22]

It was found that the HDS of DBT over CoMo/γ-Al_2O_3 and NiMo/γ-Al_2O_3 catalysts proceeded through steps 1, 2, 3 and 4 of the reaction pathway, whereas over Mo/γ-Al_2O_3 catalyst the reaction occurred through steps 1, 2, 3, 4, 5, 6 and 7. Reaction 7, which was the hydrogenation of BP to CHB, was found to occur over the Mo and NiMo catalysts, but not over the CoMo catalysts. This suggests that the active sites aiding HDS over the NiMo and Mo catalysts are not quite the same as those over the CoMo catalysts. The difference was explained by DFT analysis which showed that the active sites of the Co are at the edge of the S slab of MoS_2, whereas the active sites of Mo and NiMo catalysts are at the Mo atom edge[29,30]. The active phase of MoS_2 is always promoted by Ni or Co. As shown in Figure 14, the layered structure of an MoS_2 particle results in rim and edge sites. It is reported in the literature[31] that the DDS reaction in the HDS of DBT takes place at edge sites, while the HYD reaction takes place on rim sites. In order to improve S removal, it is suggested to increase the height of the MoS_2 particle to allow for more DDS reactions to occur[31]. Moreover, the structure of MoS_2 is significantly sensitive to the support where the metal support interaction plays a significant role in MoS_2 dispersion. According to Hensen et al.[32] a γ-Al_2O_3 support results in a lower dispersion of MoS_2 compared to other supports such as silica and AC.

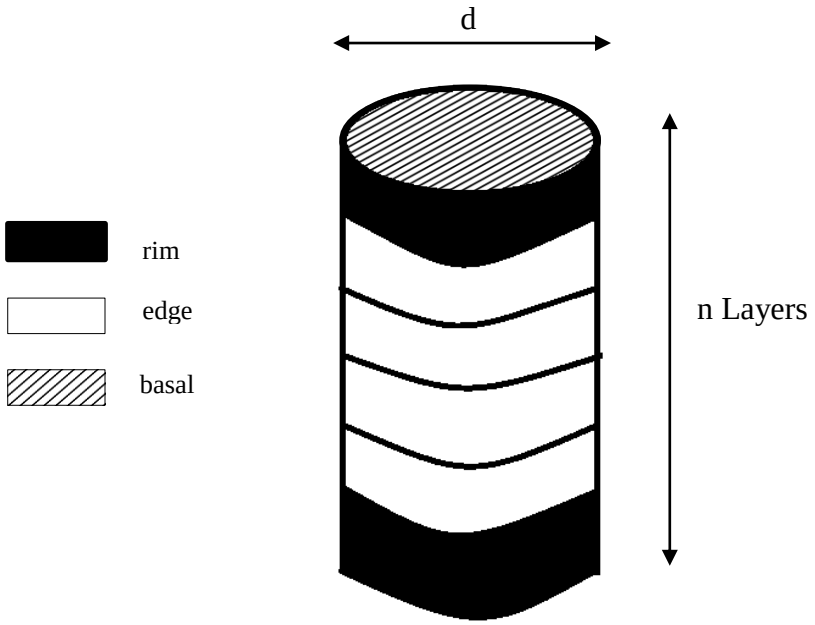

Figure 14: Rim/edge model of MoS_2 particle adapted from [31]. Copyright © 1994Academic Press[31].

Egorova and Prins[22] also studied the effect of different H_2S partial pressures on the HDS of DBT over the three aforementioned catalysts (CoMo/γ-Al_2O_3, NiMo/γ-Al_2O_3, Mo/γ-Al_2O_3,). H_2S partial pressures of 0, 10, 35, and 100 kPa were used in the study at 340 ^oC. In the absence of H_2S, the hydrotreatment activities were fast and conversion reached 100% at only τ=(W/F)= 1.9 g.min/mole over both NiMo/γ-Al_2O_3 and CoMo/γ-Al_2O_3 catalysts, and 55% conversion over Mo/γ-Al_2O_3 at τ=3.7 g.min/mol. The DBT conversion was strongly inhibited by H_2S on the three types of catalyst. The conversion reduced to 53% over CoMo/γ-Al_2O_3, 60% over NiMo/γ-Al_2O_3 and only 24% over Mo/γ-Al_2O_3 at τ=3.7 gmin/mol and 100 kPa H_2S. The pseudo-first-order kinetics was used to describe the observed kinetics in this study. Mo/γ-Al_2O_3 catalyst was found to be in an agreement with first order kinetics showing that changing the initial pressure does not affect the conversion, whereas over the other two catalysts the conversion changed with initial pressure. The behavior of HDS activity was described by the following equation:

$$r = \frac{kK_{DBT}\,P_{DBT}}{(1+K_{DBT}\,P_{DBT}+K_{H_2S}P_{H_2S})}$$

For further simplification, the authors assumed that P_{H_2S} dominated the surface and the equation was reduced to $r = k'P_{DBT}$ where $k' = \frac{kK_{DBT}}{(K_{H_2S}P_{H_2S})}$. The pseudo rate constant includes the effect of P_{H_2S}. Table 3 shows the estimated rate constants for all partial pressures. The product distributions were analyzed at different H_2S partial pressures, the rate constants of both routes DDS and HYD (k_{DDS}, k_{HYD}) were measured from k_{tot} and the selectivities at low space velocity.

Table 3: Rate constants of the total, DDS and HYD (desulfurization) of DBT and of the desulfurization of tetrahydrodibenzothiophene over NiMo//γ-Al_2O_3, CoMo//γ-Al_2O_3, and CoMo//γ-Al_2O_3 catalysts at different initial partial pressures of H_2S and a fixed temperature of 340 °C. Adopted from [22] Copyright © 2004, Elsevier [22]

Catalyst	Rate constant, mol/(g min)	P_{H_2S} (init), kPa			
		0	10	35	100
NiMo	k_{tot}	2.33	1.06	0.39	0.25
	k_{DDS}	2.05	0.90	0.32	0.17
	k_{HYD}	0.28	0.16	0.07	0.08
	k_{DESULF}^{HYD}	36	15	5.3	2.7
CoMo	k_{tot}	1.42	0.42	0.36	0.20
	k_{DDS}	1.31	0.34	0.28	0.14
	k_{HYD}	0.11	0.08	0.08	0.06
	k_{DESULF}^{HYD}	29	9.1	5.1	3.3
Mo	k_{tot}	0.25	0.09	0.08	0.08
	k_{DDS}	0.19	0.05	0.03	0.03
	k_{HYD}	0.06	0.04	0.05	0.05
	k_{DESULF}^{HYD}	4.7	1.3	0.70	0.50

In Table 3, k_{DDS} is the rate constant of the DDS route in Figure 13, k_{HYD} is the rate constant of the HYD reaction route in Figure 13, k_{Desulf}^{HYD} is the rate constant for the HYD reaction followed by the desulphurization reaction pathway (2, 3, and 4) in the case of the NiMo or CoMo catalysts and in the case of the Mo catalyst the reaction follows the pathway (2, 3, 4, 5, and 6) in Figure 13, k_{tot} is the summation of k_{DDS} and k_{HYD}. Based on the values of rate constants reported in Table 3, the total rate constant k_{tot} of Mo was the least affected by the H_2S pressure changes as it follows the pseudo-first order behavior with only 68% reduction compared with the initial rates at zero H_2S pressure. The CoMo rate constant was reduced by 85% and the NiMo total reaction rate was the most affected rate constant with 89% reduction. For more illustration, Figure 15 indicates the effect of H_2S partial pressure on the estimated rate constants for each of the catalysts studied.

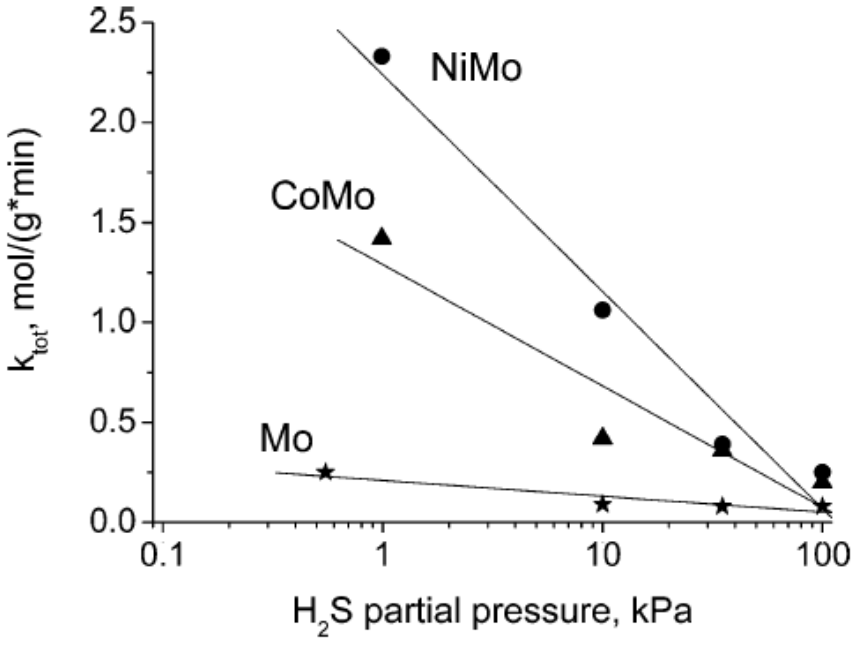

Figure 15: Pseudo first-order rate constants of the total conversion of DBT over CoMo/γ-Al_2O_3, NiMo/γ-Al_2O_3, and Mo/γ-Al_2O_3 catalysts at different partial pressures of H_2S and a fixed temperature of 340 °C. Copyright © 2004, Elsevier[22]

Vanrysselberghe and Froment[33] studied the kinetics of the HDS of DBT over a commercial CoMo/γ-Al_2O_3 catalyst. The feed contained 2 wt% of DBT which has 0.35 wt% S content dissolved in Parapur. Parapur is a mixture of paraffin consisting of 33.66 wt% $CH_3(CH_2)_{10}CH_3$, 48.42 wt% $CH_3(CH_2)_9CH_3$, 5.23 wt% $CH_3(CH_2)_8CH_3$, 12.52 wt% $CH_3(CH_2)_{11}CH_3$, and 0.19 wt% $CH_3(CH_2)_{12}CH_3$. Experiments were conducted in a multiphase continuous reactor under a range of 5-8 MPa total pressure and between 513-573 K temperature, the DBT molar flow rate F_{DBT}^{o} was between 1.74x10^{-6} and 4.04x10^{-6} kmol/h and the molar H_2 to HC (hydrocarbon) ratio was varied between 1.1-4.1. The molar hydrogen to methane ratio was set to be 6.4 for all the experiments. Methane acted as an internal standard for online analysis of the reactor effluent. A commercial CoMo/γ-Al_2O_3 catalyst was used with 5-30 wt% MoO_3, 0-6 wt% SiO_2 1-10 wt% CoO , and 0-10 wt% P_2O_5 on γ-Al_2O_3 support. $\frac{W}{F_{DBT}^{o}-F_{DBT}^{g}}$ kg_{cat}hr/kmol was defined as the space time where F_{DBT}^{o} is the DBT molar flow rate and F_{DBT}^{g} is the evaporated fraction of DBT. Different space times influenced the HDS of DBT to its products at fixed 553 K and 6 MPa condition. Figure 16 shows that the DBT was mostly and rapidly desulphurized to BP but the hydrogenation of BP to CHB was slow. Also, DBT was hydrogenated to THDBT and other partially hydrogenated DBT intermediates, but they were all instantly converted to CHB. The aforementioned observation is in agreement with the study by Egorova and Prins[22]. A prime example to explain the above observation is at 600 kg_{cat} hr/kmol: the DBT conversion was 39%, the conversion to BP was 27%, and the conversion to CHB was 8% whereas at 1200 kg_{cat} hr/kmol, the conversion was promoted for DBT, BP and CHB to 58%, 48%, and 14% , respectively as shown in Figure 16. At the same space time, the temperature variations significantly enhanced the conversion of DBT as illustrated in Figure 17. For instance, at 600

kg_{cat} hr/kmol and 513 K, DBT conversion was 17% whereas at the same space time of 600 kg_{cat} hr/kmol and 573 K, DBT conversion was 72%. The highest conversion was 87% achieved at 1000 kg_{cat} hr/kmol and 573 K.

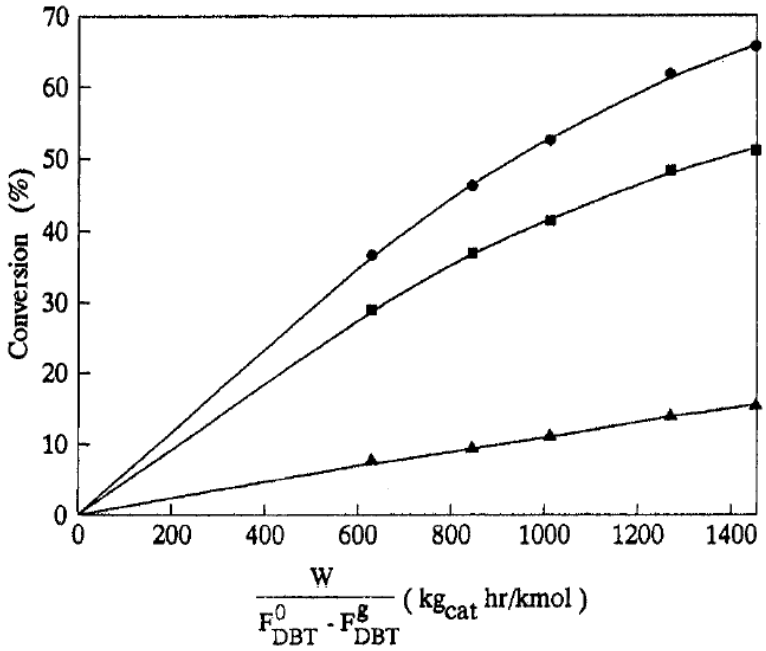

Figure 16: Conversion as function of space time (●) total conversion of DBT,(■) conversion of DBT into BP,(▲) conversion of DBT into CHB. Reaction conditions=553K, Pt=60 bar, H_2/CH_4=6.39.Copyright © 1996 American Chemical Society[33]

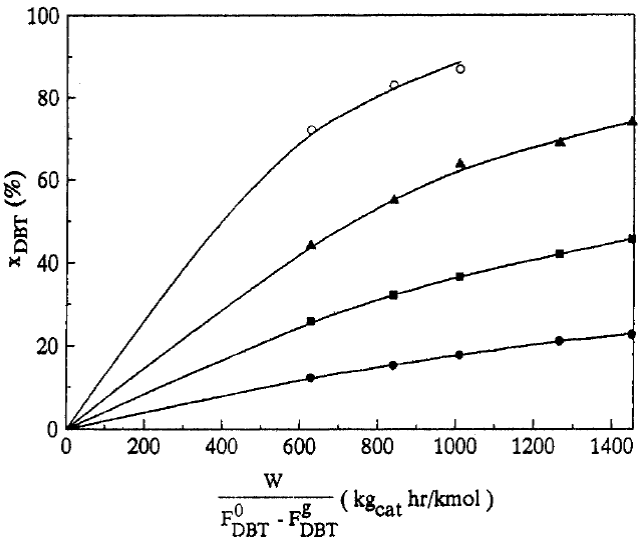

Figure 17: Total conversion of DBT as a function of space time at various temperature: (●) 513, (▲)533, (■) 553,and (○) 573K under Pt=80 bar H_2/CH_4=6.38, and H_2/HC=1.33.and H_2/HC=1.10 reaction conditions. Copyright © 1996 American Chemical Society[33]

In order to study the reaction kinetics, the authors deduced the following reaction pathway

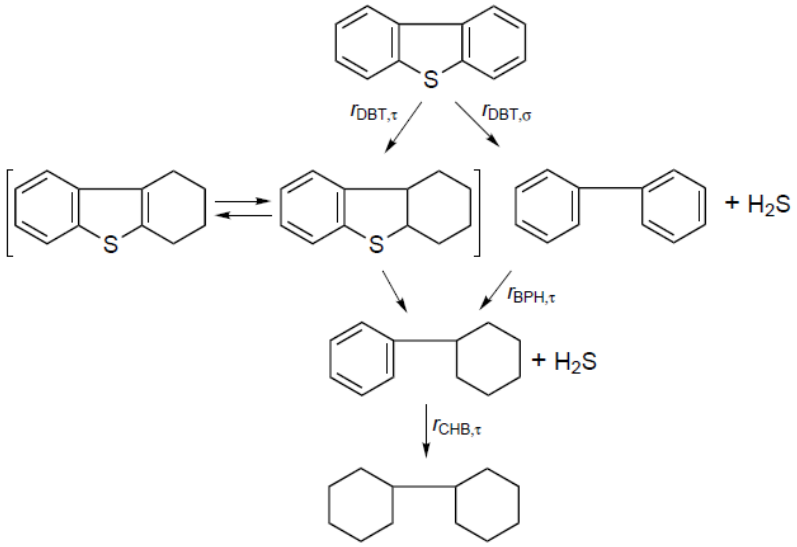

Figure 18: Proposed reaction network, note that here BPH refers to biphenyl (BP)). Copyright © 1996 American Chemical Society[33].

A kinetic model for HDS was developed based on σ and τ, the two different types of active sites for hydrogenolysis and hydrogenation reactions, consistent with the idea of rim-edge sites in the Daage and Chianelli[31] model. A Langumir-Hinshelwood mechanism was developed for both types of reactions as described below, the rate determining step for all the reactions was the surface reaction step. For instance, the hydrogenation of BP into CHB on the τ sites, the rate determining step was the surface reaction step BP.τ + 2H.τ ↔PHCHD.τ+ 2τ (The model description and rate expression are provided in Appendix B).

In addition, the adsorption equilibrium constants and rate coefficients at 573K were estimated and are reported in the following table.

Table 4: Adsorption equilibrium constants and rate coefficients at 573K. Adopted from [33] Copyright © 1996 American Chemical Society[33]

$K_{DBT,\sigma} = 7.56868 \times 10^{1}$	m^3/kmol
$K_{H,\sigma} = 7.01679 \times 10^{-1}$	m^3/kmol
$K_{H_2S,\sigma} = 6.27912 \times 10^{1}$	m^3/kmol
$K_{BP,\sigma} = 9.53728$	m^3/kmol
$k_{DBT,\sigma} = 1.58251 \times 10^{-1}$	kmol(kg_{cat} h)
$K_{DBT,\tau} = 2.52021$	m^3/kmol
$K_{H,\tau} = 1.41658 \times 10^{-2}$	m^3/kmol
$K_{BP,\tau} = 1.41256$	m^3/kmol
$k_{DBT,\tau} = 3.08384 \times 10^{-1}$	kmol(kg_{cat} h)
$k_{BP,\tau} = 1.69206$	m^3/(kg_{cat} h)
$k_{CHB,\tau} K_{CHB,\tau} = 3.38631 \times 10^{-1}$	

Based on the results above, the adsorption rate constants of DBT, hydrogen (H), and BP on σ active site $K_{DBT,\sigma}$, $K_{H,\sigma}$, $K_{BP,\sigma}$, with values of 75.7, 0.7 ,and 9.54 m^3/kmol were significantly higher than the adsorption constants on τ sites $K_{DBT,\tau}$, $K_{H,\tau}$, and $K_{BP,\tau}$ with values of 2.52, 0.0141, and 1.412 m^3/kmol, which explains why HDS of DBT prefers the DDS route over the HYD route. Another observation was that the adsorption of DBT, BP and hydrogen is weaker

on the τ sites than on the σ sites. Moreover, the apparent activation energy for DBT hydrodesulphurization was estimated as 122 kJ/mol which is in good agreement with the results listed in the literature and summarized in the following table.[24,33-37]

Table 5: Comparison of activation energies for HDS of DBT from several literature studies

The authors	Reaction conditions	Catalyst	Ea kJ/mol
Broderick et al[34]	548-598 K, 3.4-16.2 MPa H_2	Co-Mo/γ-Al_2O_3	125
Vrinat et al[36]	473-520 K, 0.5-5 MPa H_2	Co-Mo/γ-Al_2O_3	96
O'Brien et al[37]	540-695 K 3.4-12.2 MPa H_2	Co-Mo/γ-Al_2O_3	138
Vanrysselberghe and Froment[33]	513-573 K 0.5-0.8 MPa H_2	Co-Mo/γ-Al_2O_3	122
Liu et al[24]	533-573 K 3 MPa H_2	Ni-Mo/γ-Al_2O_3	145

Broderick et al.[34] Vrinat et al.[36] and O'Brien et al.[37] used a Langmuir-Hinshelwood (L-H) kinetic model to estimate the activation energy. Broderick et al.[34], Vanrysselberghe and Froment[33] reaction conditions are close to each other as a result they obtained more or less the same activation energies. Liu et al[24] obtained a high activation energy compared to others but a different catalyst NiMo/γ-Al_2O_3 was used in this study. It is observed that the activation energies appear to depend on the reaction temperature and pressure.

1.5 Literature Review Summary

As described in the literature review, several studies have discussed HDS reactions of DBT using different types of catalyst support. DBT has been used as a reactant with decalin as a solvent in many of the reports[4,21,24,26]. Continuous flow reactors as well as stirred batch reactors were used in previous studies to assess catalyst activity and selectivity.

Reaction mechanisms of HDS of DBT reported in many studies show that the reaction occurs by two routes - DDS and HYD[3-6,21-23]. In the DDS route direct extraction of the S from the DBT occurs to produce BP. The subsequent hydrogenation rate of BP to form CHB is very slow compared to the other steps and therefore, it can be ignored in kinetic models.[22] For the HYD route, where double bonds and phenyl species are hydrogenated prior to S removal to produce CHB, further hydrogenation will result in BCH.

Incipient wetness impregnation is the most common HDS catalyst preparation method[38]. Many catalysts and supports have been reported in previous studies,[3-6,21-23] with the most active catalysts for the HDS of DBT being bimetallic NiMo and CoMo sulfides [5,19,20]. Ni or Co play a significant role as promoters in enhancing the activity of MoS_2. γ-Al_2O_3 is widely used as a support for many catalysts. However, γ-Al_2O_3 has a lower surface area than AC. AC has a large surface area and pore volume but it contains a large fraction of micropores which are not utilized in HDS as the diffusion rate of reactants and products are very low through micropores. Moreover, in terms of conversion and selectivity, the best catalyst loading was reported by Kouzu et al.[23] to be 15wt% Mo and 3wt% Ni. Nevertheless, NiMo catalysts were inhibited by H_2S pressures changes as reported in the study by Egorova and Prins[22], but they were chosen for the present research due to their high HDS activity towards DBT.

1.6 Study Objectives

The aim of the present study is to investigate and compare the HDS activity of Ni-Mo-sulfided catalysts on carbon supports, including petcoke, to the known HDS activity of a conventional γ-Al_2O_3 supported catalyst. A major goal of the study is to demonstrate that the petcoke can be converted to a useful support for catalysts in hydrotreating processes. Consequently, hydrotreating technology might be able to use petcoke as a promising alternative support for catalysts instead of commercial γ-Al_2O_3. In addition, it is expected that the petcoke may contain promoters or other contaminants which may be beneficial for catalysis. The kinetics of the HDS reaction over the different carbon supports will be evaluated and compared to the known kinetics of Ni-Mo on γ-Al_2O_3 supports. The experiments have been performed in a novel slurry-phase batch microreactor. The Levenberg-Marquardt method was used to estimate the kinetic parameters from the measured data.

Chapter 2: Experimental

2.1 Catalysts Preparation

Two types of carbon support were used to prepare the Ni-Mo catalysts. Activated carbon (DARCO®, −100 mesh particle size, powder, Sigma Aldrich) has a surface area of 1332 m^2/g and 0.35 cm^3/g pore volume. The petroleum coke (petcoke) was obtained from Canadian oil sands in Alberta, and subjected to a chemical activation process using KOH, to be more effective for the hydrotreating process[5]. The raw coke was ground and sieved to match the particle size of the commercial activated carbon of 125-149 μm. The ground coke sample was mixed with KOH with mass ratio of KOH/coke = 3/1. The sample was placed in an oven at 393 K and dried for 2 h. Then, the mixture was transferred into a ceramic boat that was inserted into a horizontal furnace with N_2 gas flow at 50 mL/min. Subsequently, the mixture was heated to the desired temperature of 1073 K at a ramp rate of 5 K/min and kept at that temperature for 9 h. After the activation process the sample was cooled to room temperature and the product was washed with 1 M diluted HCl and distilled water through filtration paper until a pH of 7 of the product was achieved.[5,39] The recovered coke was heated at 393 K overnight in ambient air. The resulting activated coke had a surface area of 1100 m^2/g and a pore volume of 0.7 cm^3/g.

The Ni-Mo was added to the carbon support by wetness impregnation. Mo with 15 wt% loading was added from a solution of $(NH_4)_6Mo_7O_{24}\cdot 4H_2O$ (Sigma Aldrich 81.0-83.0% MoO_3 basis), and Ni at 3 wt% loading was added from a solution prepared from $Ni(OCOCH_3)_2\cdot 4H_2O$ (99.998% trace metal basis,Sigma Aldrich). The impregnation was done using 10 g of either the activated carbon or the petcoke as support. The incipient wetness impregnation method requires that the volume of the metal used in the preparation be the same as the pore volume of the support. The pore volume of the carbon supports was measured by N_2 adsorption at 77 K, as

described in Section 2.2. The pore volume of the activated carbon was 0.35 cm^3/g so the required solution impregnation volume was 3.5 cm^3. The required amount of Mo salt was 4.11 g. Since the Mo salt was not soluble at this concentration, the Mo salt was impregnated three times as only 1.37 g of Mo salt was soluble in 3.5 $cm^3$of H_2O at a pH of 6.52. For each impregnation step, the sample was kept away from sunlight and aged overnight followed by drying at 393 K for 3 h. In the same manner, the desired amount of Ni was obtained from two impregnations using 0.75 g of Ni salt in 3.5 cm^3 of distilled water at a pH of 7. As before, after each impregnation step the sample was aged overnight and dried at 393 K for 3 h. The same procedures were followed to prepare the catalysts supported on petcoke. In this case, 1.4 g of support with a pore volume of 0.7 cm^3/g was prepared. One impregnation step was needed for the Mo as 0.58 g was soluble in 1 cm^3 distilled water. The sample was aged overnight and dried at 393 K for 3 h. One impregnation step was also needed for Ni since 0.22 g of the Ni salt was soluble in 1 cm^3 distilled water. Again the sample was aged overnight and dried at 393 K for 3 h.

The sulfidation of the NiMo catalyst was completed ex-situ in a 300 mL autoclave stirred reactor with 1400 mg catalyst, 1358 mg DBT, 66544 mg decalin, and 697 mg CS_2 at 573 K and 4 MPa for 3 h to yield the NiMoS/AC and NiMoS/PC catalysts.

2.2 Catalyst Characterization.

The total BET surface area, average pore width, and pore volume of the carbon supports and the prepared catalysts were measured using a Micromeritics ASAP 2020 Accelerated Surface Area and Porosimetry analyzer. Prior to the analysis the sample was degassed at 1.33 kPa/s while heating at a ramp rate of 10 ^oC/min until 0.04 kPa and 393 K. The temperature was kept at 393 K for 120 min. After degassing, the sample was moved to the analysis section and the

N_2 adsorption/desorption isotherm was measured at 77 K. (Further details are provided in Appendix C).

The catalysts were also characterized by X-ray diffraction (XRD) using a Siemens D500 instrument with Co Kα radiation (λ=0.1789 nm). The XRD patterns for all the samples were scanned from 10-90^o with a scan step size of 0.04^o. The XRD pattern was used to calculate the crystallite size using the Scherrer formula which relates crystal size to peak width at half maximum height.

X-ray photoelectron spectroscopy (XPS), a surface catalyst characterization technique, was done using a Leybold MAX200 instrument with an Al Kα achromatic X-ray source. XPS was used to confirm the presence of metals on the support. A survey scan with a pass energy of 192 eV, as well as a narrow scan, with a pass energy of 48 eV, were used to analyze the catalyst samples from which the presence of Ni, Mo, and S elements was confirmed.

2.3 Catalyst Activity Measurements

The HDS reaction was conducted in a stirred batch microreactor in the presence of pure hydrogen as well as a measured amount of catalyst. Figure 19 shows a process flow diagram of the novel slurry-phase batch hydroconversion micro-reactor that was used in this study. The novelty of this reactor is represented in a micro scale size and the ability to mix the feed at that scale. The reactor consists of a glass insert of height 250 mm with an internal diameter of 4 mm, placed inside a stainless steel shell with glass beads placed inside the shell to keep the insert in the desired heating zone. Kukard has shown that the reactor operates isothermally.[40] A vortex mixer placed at the bottom of the reactor was used to mix the feed and limit the effects of

external mass transfer. The reaction temperature was monitored by a thermocouple placed co-axially in the glass insert.

In order to study the HDS reaction kinetics on the NiMoS catalysts on both the AC and petcoke supports, the effects of reaction time and temperature were examined for each of the different catalyst supports. The reactions were performed for 30, 60, 90 and 120 min at temperatures of 588, 603, 623, and 638 K. Pressure was fixed at a target of 4.8 MPa. At each temperature, two types of supports were examined with different reaction times as aforementioned to determine the activity for the HDS of DBT.

At the beginning of each run, the glass insert was loaded with 150 µL of the total feed consisting of 2 wt% of the model compound (DBT), 95 wt% of decalin, 0.99 wt% carbon disulphide and 2 wt% of catalyst, and a total feed weight of 1 g. The insert was placed inside the reactor and sealed, the micro-reactor was purged three times in H_2 to insure the removal of air from the system. After purging, the reactor was pressurized to the target pressure using H_2 to 4.28 MPa at room temperature. Prior to the start of the temperature ramp, the system was subjected to a leak test using a leak detector to insure that the system was well sealed. The micro-reactor was then heated to the desired temperature, and kept for the desired reaction time. At the end of the run, the system was depressurized and cooled to room temperature. The liquid products were recovered and stored at 2 ^{o}C. To identify the liquid products recovered from the reaction, a Shimadzu QP-2010S GC/MS equipped with Restek RTX5 30 M x 0.25 mm capillary column was used. The calibration curves were constructed by analyzing known concentrations of the DBT and BP. The GCMS reported different corresponding areas of known DBT and BP concentrations. The GCMS area for the unknown sample were determined and the concentration

was calculated using the aforementioned calibration curve (refer to Appendix D for more details).

To minimize internal and external diffusion, the catalyst particle size was kept between 125 - 150 μm and the vortex mixer speed was set at 2000 rpm, as it was suggested that the short diffusion length and the dynamic mixing in the micro batch reactor promotes the HDS of DBT free of internal and external mass transfer effects.[41] In other words, the mixing and the reduced wall effect enhance mass transfer which allows us to measure the intrinsic rate of reaction, as the mass transfer resistance is reduced.

The carbon balance was determined by measuring the model compound DBT and all the products (BP, DBT, 1, 2, 3, 4-THDBT, CHB, and BCH) and the closure was better than 95%. To be consistent with the modeling, DBT conversion was calculated from the product measurements. The reproducibility of the micro-reactor was endorsed by repeating several selected runs and the results obtained showed ±11% error in the DBT conversion along with ±10 % of BP selectivity, ±10 % of THDBT selectivity, ±10 % CHB selectivity, and ±10 % BCH selectivity (refer to Appendix E for more details).

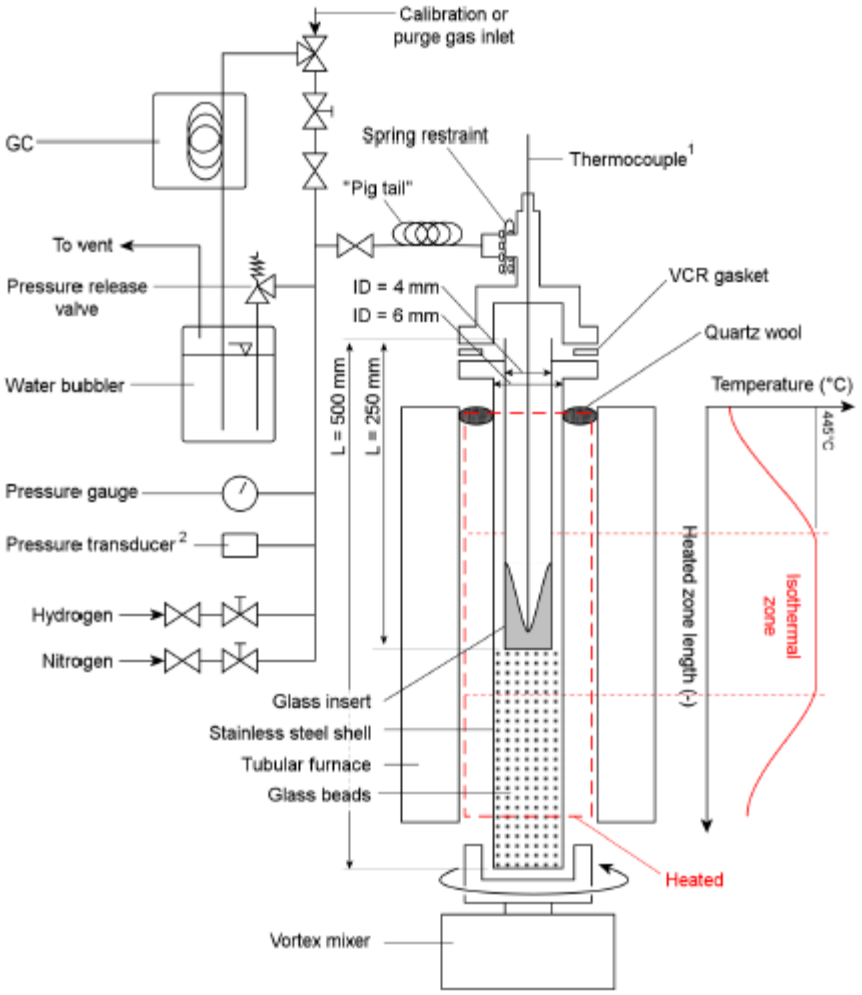

Figure 19: Process flow diagram of a novel slurry-phase batch hydroconversion micro-reactor. Copyright ©2015 American Chemical Society.[41]

Chapter 3: Results and Discussion

3.1 Catalyst Characterization

Table 6 reports the BET surface area, pore volume and pore size of the carbon supports and the sulphided catalysts used in this study. Activated carbon is known to have a high surface area[5] but contains a large number of micropores and some mesopores. The micropores are not necessarily useful for HDS of DBT because of their small diameter (< 2nm). After doping the Ni-Mo onto the supports and following sulphidation, the average pore size of the NiMoS/AC catalyst increased significantly because the very small micropores were filled. There was also a corresponding decrease in the surface area by ~90% and pore volume by ~37%. In the case of petcoke, the average pore size decreased by ~15% and the surface area and pore volume decreased by ~97%. The loss in porosity of the NiMoS/PC catalyst compared to the support is likely due to NiMoS that blocks and fills the pores causing the pore volume and surface area to decline, as well as due to the thermal treatments that likely collapse the pore structure of the carbon supports. Both effects result in loss of micropore and mesopore volume. The surface area of the non-sulphided commercial NiMo/γ-Al_2O_3 is also reported since the activity of this catalyst will be discussed in Section 3.3.1

Table 6: BET surface area, pore volume, and pore size for the catalysts and their supports

Supports and supported Catalyst	Specific Surface Area (m^2/g)	Pore volume (cm^3/g)	Pore size (nm)	Metal content (wt%)
Activated carbon(AC)	1323	0.35	2.21	-
Petcoke (Petcoke)	1140	0.67	2.40	-
NiMoS/AC	145	0.22	5.91	15Mo-3Ni
NiMoS/PC	37	0.019	2.03	15Mo-3Ni
NiMo/γ-Al_2O_3	71	-	-	8Mo-3Ni

Figure 20 shows the XRD patterns of the activated carbon support, the NiMoS/AC catalyst, and the NiMoS/PC catalyst. The lack of peaks corresponding to MoS_2 at $2\theta = 40^o$ and $2\theta = 60^o$ for the (103) and (110) planes of MoS_2, suggests high dispersion of Ni-Mo on the support. The peaks at 2θ=23 to 36^o are associated with graphite and SiO_2 in the activated carbon. For the NiMoS/PC catalyst, high dispersion of the Ni-Mo on the support is also suggested by the lack of MoS_2 peaks.

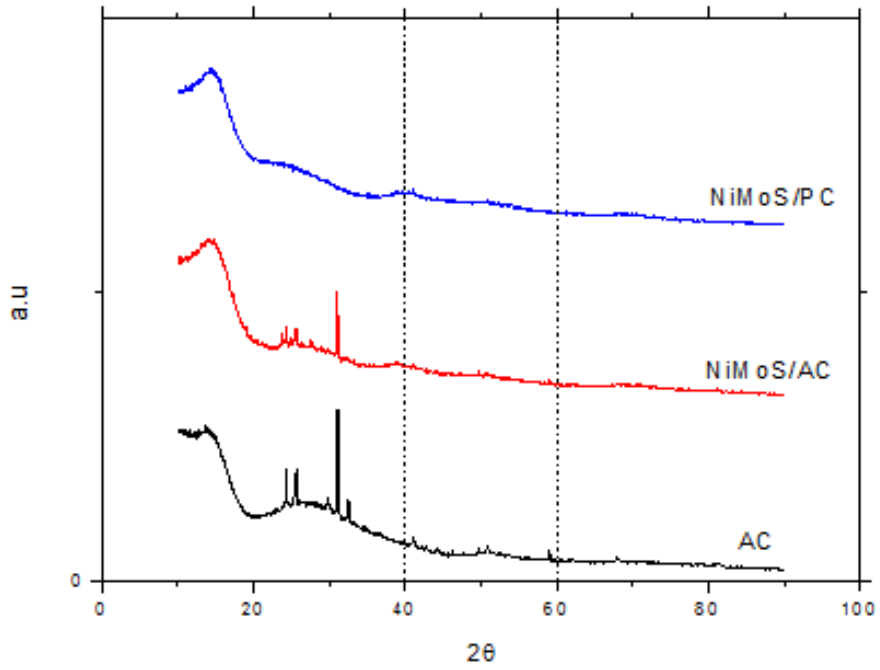

Figure 20: XRD pattrens for AC, NiMoS/AC, NiMoS/PC

The XPS survey scan data of Table 7 show that the Mo/C and Ni/C surface atom ratio was higher on the petcoke than the AC, indicative of a higher dispersion on the petcoke than the AC. As shown by the narrow scan data of Figures 21, 22, 23, and 24 there were no apparent chemical shifts for the Mo and S species on the AC versus the petcoke. When deconvoluting the peaks in both supports for Mo 3d, MoS_2, MoO_2, and MoO_3 species were identified (Tables 8, 9 and Figures 21, 23). Similarly, as a result of deconvoluting the S peaks for both supports (Tables 10, 11 and Figures 22, 24), a number of compounds were identified such as MoS_2, DBT, SO_x, dihydrothiophene/Mo, and S. Their binding energies are close to or mostly the same as that reported in the literature.[42] The data in Table 8, 9, 10 and 11 show that the most abundant species is MoS_2 which could not be identified by the XRD analysis. Some oxide species were also identified by XPS likely because of the exposure of the catalyst to air during sample handling procedures associated with the XPS analysis.

Table 7: Surface composition as defined by XPS of carbon supports NiMoS

Support/Element	Mo At%	S At%	Ni At%	C At%	Mo/C %	Ni/C %	Mo/S %
Activated carbon	1.29	2.87	0.19	87.96	1.467	0.22	0.45
Petcoke	2.13	6.37	0.8	78.68	2.707	1.02	0.33

Table 8: Chemical states of Mo on activated carbon support from Mo 3d XPS narrow scan

Mo	Mo $3d_{3/2}$ B.E.	Mo $3d_{5/2}$ B.E.	B.E. Area%
MoS_2	232.3	229.1	51
MoO_2	232.8	229.6	11
MoO_3	235.8	232.5	38

Table 9: Chemical states of Mo on petcoke support from Mo 3d XPS narrow scan

Mo	Mo $3d_{3/2}$ B.E.	Mo $3d_{5/2}$ B.E.	B.E. Area %
MoS_2	232.1	229.1	55
MoO_2	233	230	18
MoO_3	236.1	233.1	27

Table 10: Chemical states of S on activated carbon support from S 2p XPS narrow scan

Compound	$2p_{1/2}$ B.E.	$2p_{3/2}$ B.E.	2p B.E.	S 2s B.E.	B.E.Area%
MoS_2	163.8	162.2	-	-	24
S or S_8	164.7	163.1	-	-	12
SO_x	-	-	169	-	36
dihydrothiophene/Mo	162.8	161.7-161.6	-	-	27
S	-	-	-	226.4	0

Table 11: Chemical states of S on petcoke support from S 2p XPS narrow scan

Compound	$2p_{1/2}$	$2p_{3/2}$	2p	S 2s	Area %
MoS_2	163.8	162.2	-	-	23
$S(C_6H_5)_2$	164.6	163	-	-	15
SO_x	-	-	169	-	41
dihydrothiophene /Mo	162.8	161.7	-	-	21
S	-	-	-	226.4	0

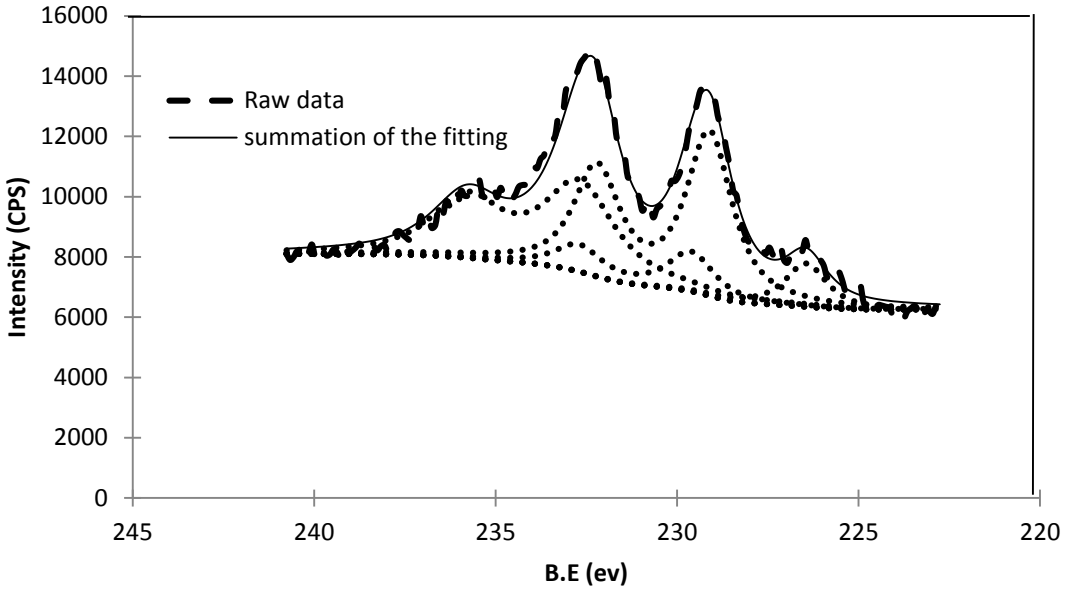

Figure 21: Narrow scan with peak deconvolution for Mo 3d on activated carbon

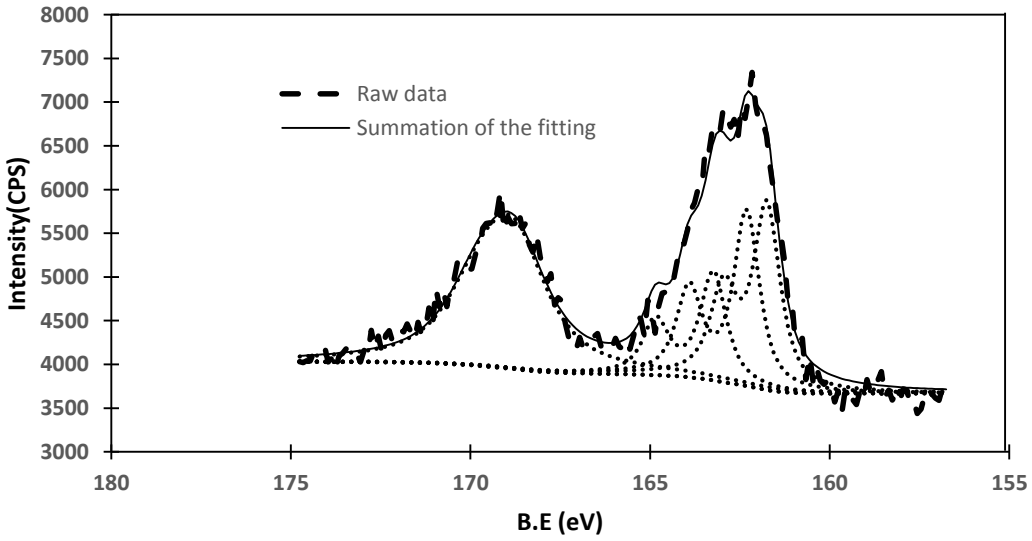

Figure 22: Narrow scan with peak deconvolution for S 2P on activated carbon

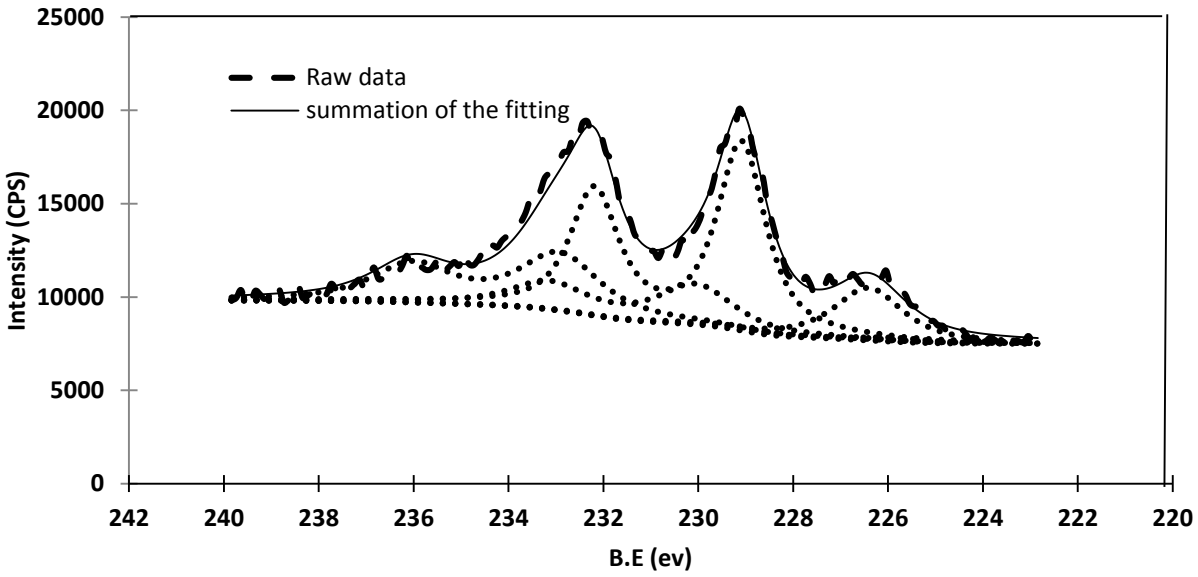

Figure 23: Narrow scan with peak deconvolution for Mo 3d on petcoke

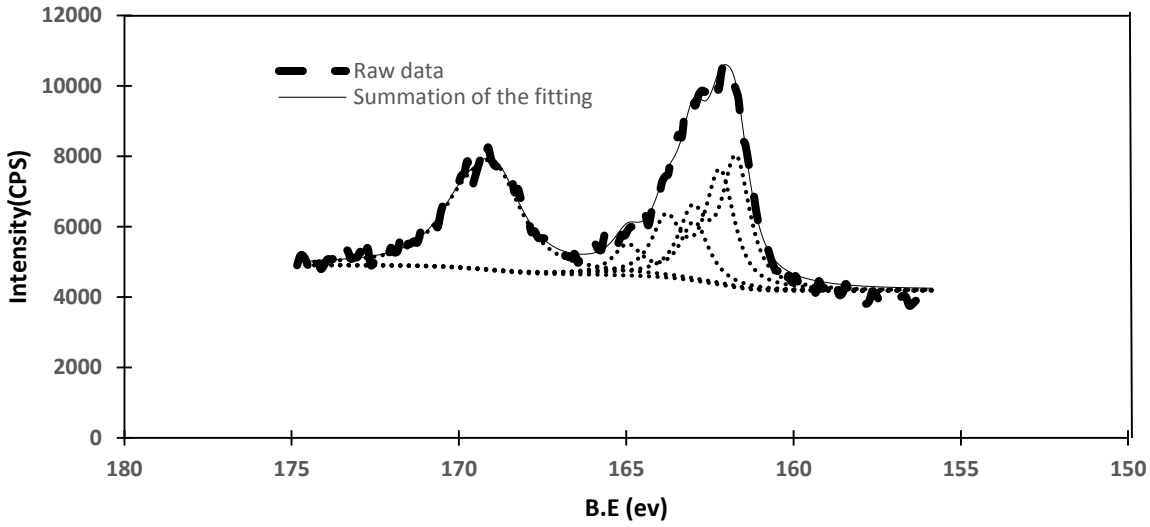

Figure 24: Narrow scan with peak deconvolution for S 2P on Petcoke

3.2 Catalyst Characterization Summary

There was a loss in surface area and pore volume of the AC and petcoke supports after doping with NiMoS. XRD analysis did not show peaks attributable to MoS_2, indictive of a high dispersion of this species on both the petcoke and AC support. XPS analysis indicated a higher dispersion of the Ni and Mo metals on the petcoke support compared to the AC support. It was also found that there were no differences in the chemical states of both Mo and S on the supports, based on similar binding energies of these species on both supports.

3.3 Catalytic Activity

3.3.1 Preliminary Studies to Test the Activity of Different Catalysts

Three types of catalysts were examined at the same reaction conditions in the first part of this study. The NiMoS/PC and NiMoS/AC were compared with a commercial NiMo/γ-Al_2O_3 catalyst. An activity test was also done without catalyst to determine the extent of reaction due to thermal reactions and/or reactions catalyzed by the components present in the stainless-steel thermocouple. The HDS reaction was carried out at 623 K and 4.8 MPa at different reaction times. As shown in Figure 25, the NiMoS/PC activity, as reflected in the DBT conversion was promising when compared with the optimized commercial catalyst. Even though the activated carbon has higher surface area than the commercial NiMo/γ-Al_2O_3 and the NiMoS/PC catalyst, it showed the lowest DBT conversion activity. This is likely because of inaccessible active sites in the micropores of the AC. In addition, the commercial NiMo/γ-Al_2O_3 catalyst contains some other components such as phosphorus to optimize activity. Moreover, the surface composition shows that the low activity of the activated carbon corresponds to a lower Mo/C and Ni/C of the NiMoS/AC compared to the NiMoS/PC catalyst. Other temperatures for the NiMoS/AC and

NiMoS/PC catalysts were also examined and the data are shown in the Section 3.3.2 and 3.3.3, while the thermal run data are summarized in Appendix F.

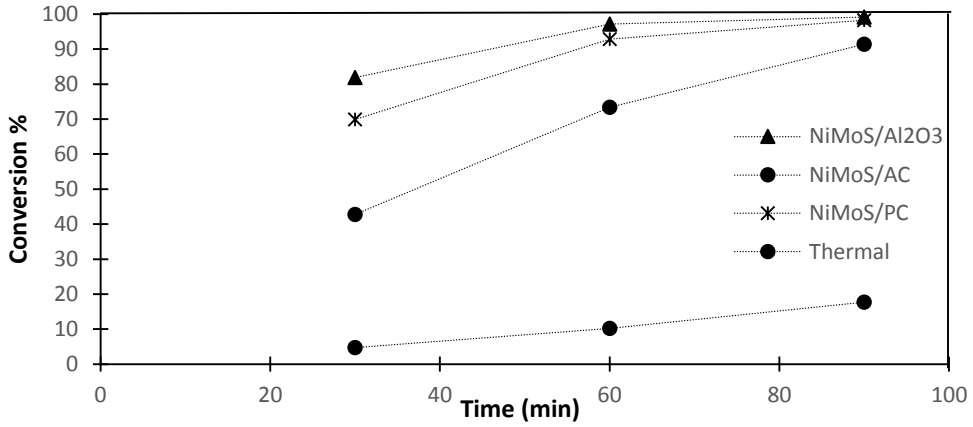

Figure 25: Comparison of DBT conversion between catalysts, NiMoS/γ-Al_2O_3, NiMoS/AC, NiMoS/PC and thermal reaction at 623 K and 2000RPM at different times

In terms of selectivity of the three catalysts, Figures 26(a-d) show that the NiMoS/PC has almost as high selectivity towards BP as the commercial NiMoS/γ-Al_2O_3. This indicates that NiMoS/PC is not only an active catalyst but also highly selective towards BP via the DDS route.

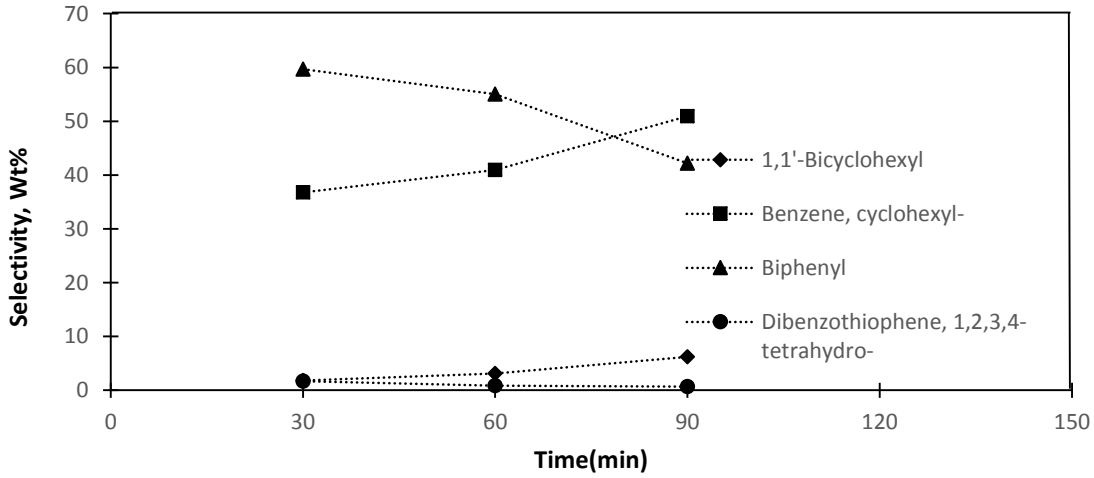

Figure 26(a): Selectivity of NiMoS/γ-Al_2O_3 catalysts at 623 K and 2000RPM at different time

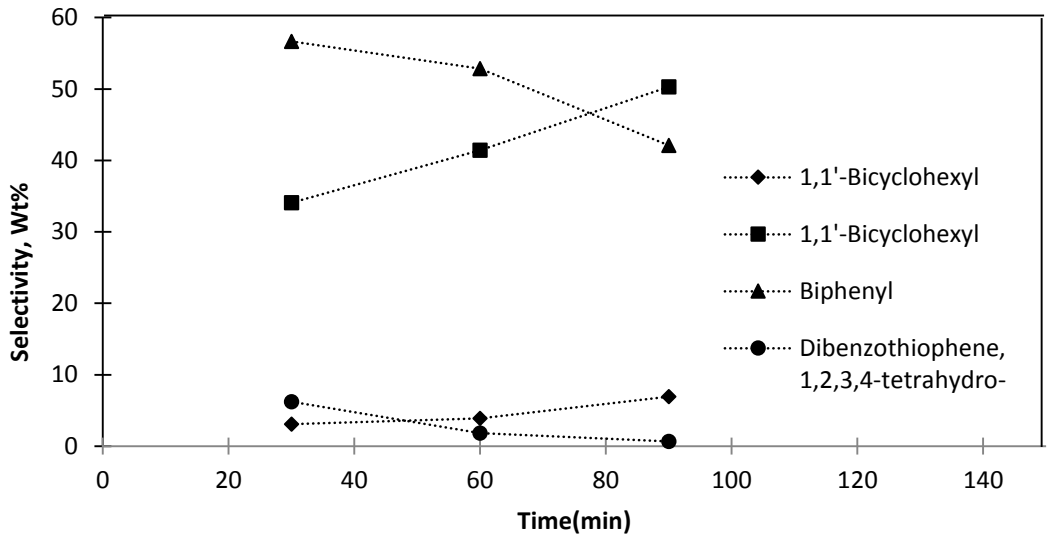

Figure 26(b): Selectivity of NiMoS/ PC catalysts at 623 K and 2000RPM at different time

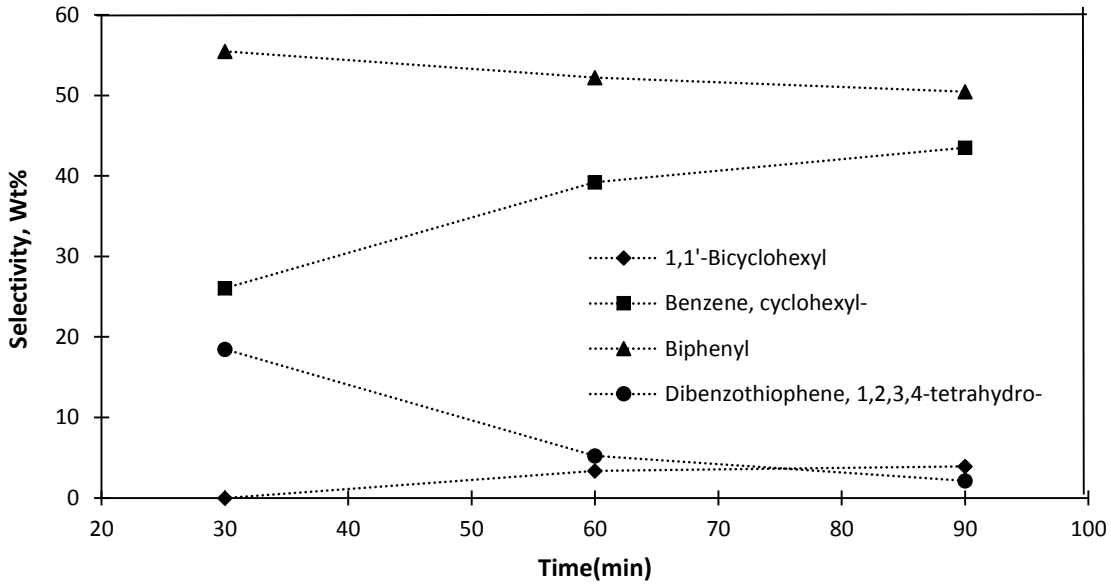

Figure 26(c): Selectivity of NiMoS/AC catalyst at 623 K and 2000RPM at different time

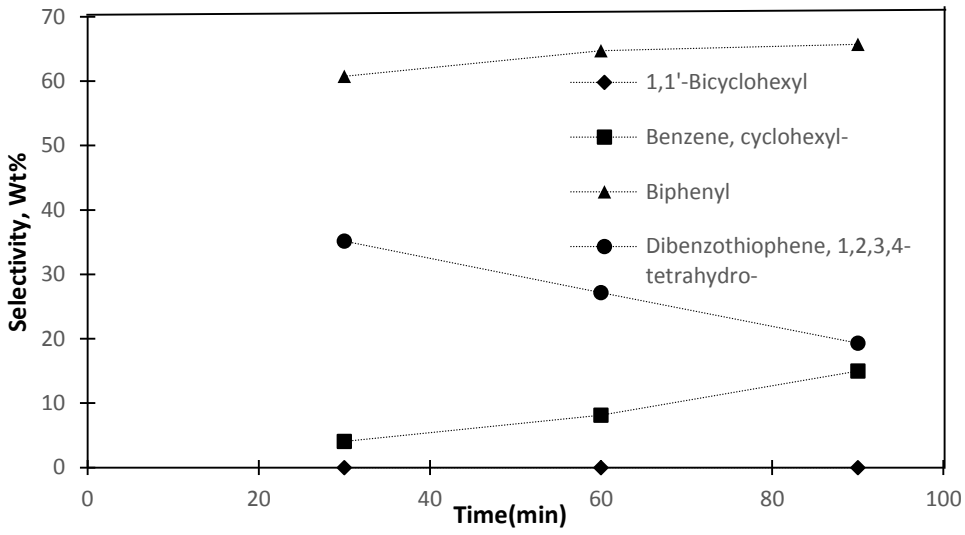

Figure 26(d): Selectivity of the thermal reaction at 623 K and 2000RPM at different time

3.3.2 Activity of the NiMoS/AC Catalyst for the HDS of DBT

Reactions were conducted at different temperatures and reaction times with temperatures varying between 588-638 K and reaction times of 30-120 minutes at fixed pressure of 4.83 MPa. The experiments were designed to obtain the highest conversion in the most optimal reaction times. As shown in Figure 27, as the temperature increased the activity of NiMoS/AC catalyst for the hydrotreating of DBT increased and therefore the DBT conversion increased.

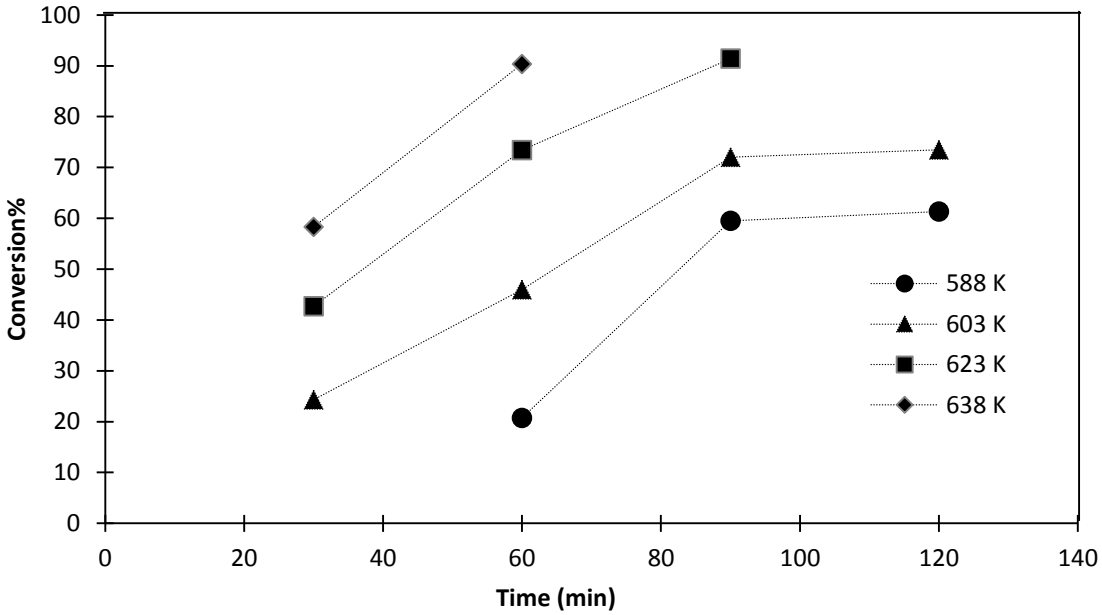

Figure 27: Effect of reaction temperature on the DBT conversion with respect to time over NiMoS/AC

3.3.3 Activity of NiMoS/PC Catalyst for HDS of DBT

At the same reaction conditions and procedures stated above, experiments were conducted on the NiMoS/PC catalyst. As expected, the DBT conversion increased as temperature of reaction increased as shown in Figure 28. Interestingly, the highest DBT conversion was achieved at 623 K which indicated that petcoke is a promising support for the hydrotreating process because of the high dispersion of Ni and Mo on the petcoke support. No data could be obtained at 638 K because all the DBT was converted in less than 30 min.

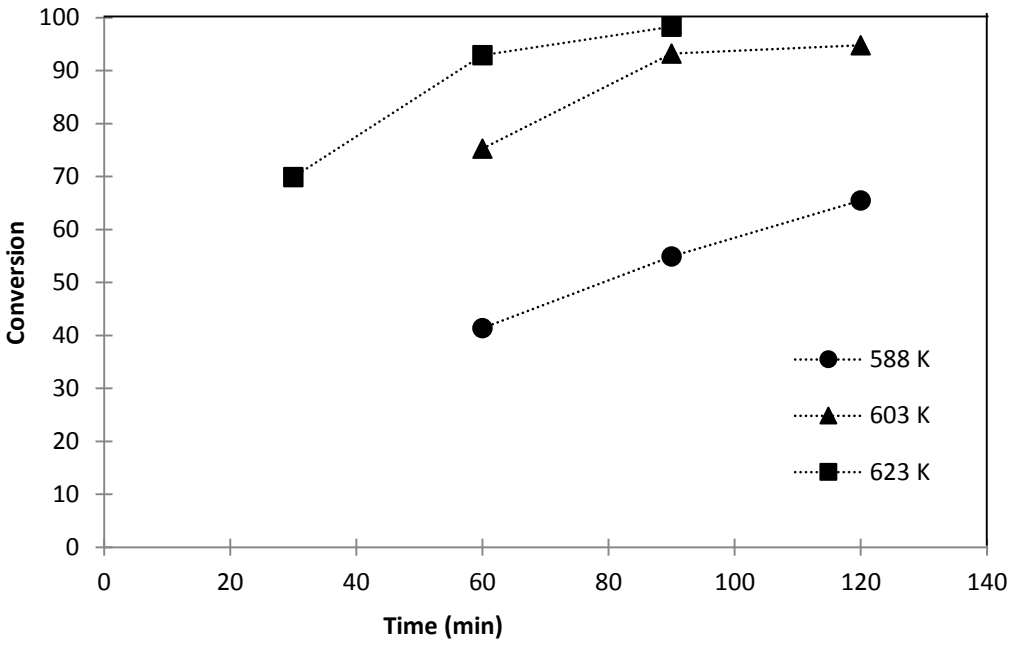

Figure 28: Effect of reaction temperature on the DBT conversion with respect to time over NiMoS/PC

3.3.4 Comparison Between the Activity of NiMoS/AC and NiMoS/PC

Figures 29 and 30 show the HDS of DBT for both catalysts at 603 K and 623 K. In both figures, NiMoS/PC has higher activity than NiMoS/AC for the HDS of DBT, as reflected in the DBT conversion. This is in agreement with the chemical surface compositions since the Ni/C and Mo/C atom ratio on petcoke is higher than on the AC support.

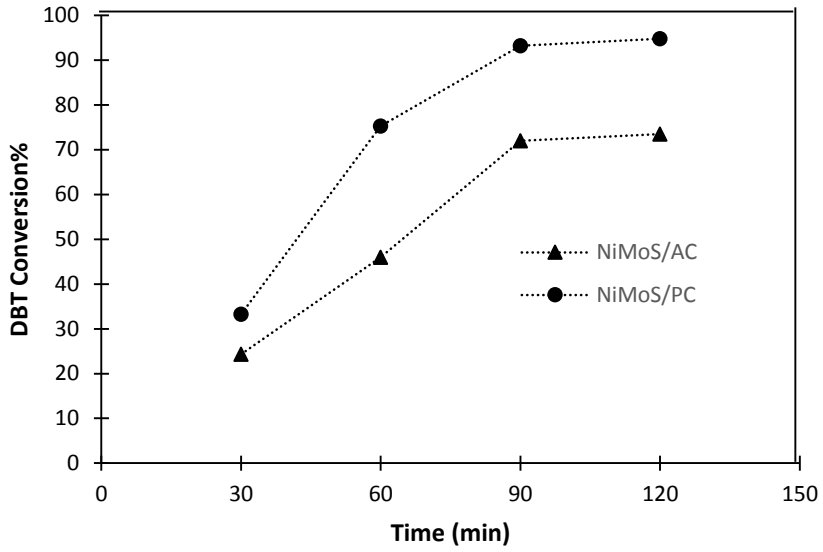

Figure 29: Comparison between NiMoS/AC and NiMoS/PC for HDS of DBT at 603 K and 4.8 MPa reaction condition

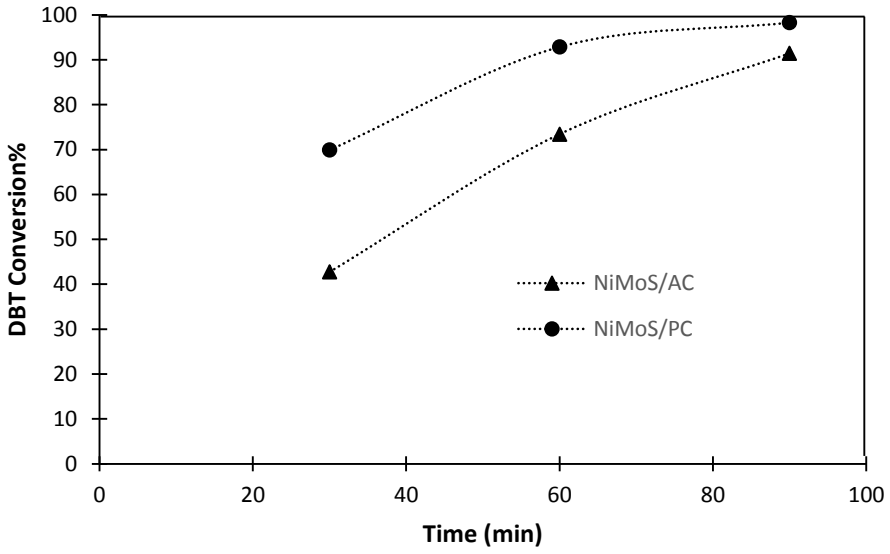

Figure 30: Comparison between NiMoS/AC and NiMoS/PC for HDS of DBT at 623 K and 4.8 MPa reaction condition

3.4 Product Distribution

The major DBT products were BP, THDBT, CHB, and BCH. Although other products were identified their quantities were < 10 ppm and are not considered further. The following section discusses the product distribution for the different supports.

3.4.1 Product Distribution over the NiMoS/AC Catalyst

Figures 31-34 illustrate the product distribution of the HDS of DBT over NiMoS/AC at different temperatures. The selectivity to BP, which represents the DDS of DBT, varies between 43 wt% and 60 wt% at different reaction times and temperatures. At all temperatures the the selectivity to BP remained high as a function of reaction time, with only a small decline. In contrast, the selectivity towards 1, 2, 3, 4-THDBT significantly declined while there was a correspondingly significant increase in the selectivity to CHB with reaction time. These results are indicative of the hydrogenation of 1, 2, 3, 4-THDBT leading to the formation of CHB as shown, for instance, in Figure 34, with an insignificant hydrogenation of BP to CHB. This finding is in agreement with Figure 13 presented by Egorova and Prins[22]. The data also show that 1,1-bicyclohexyl was a minor product, requiring long reaction times (120 min) and higher temperature to be observed in the product. The maximum bicyclohexyl formation was 4 wt% at 638 K.

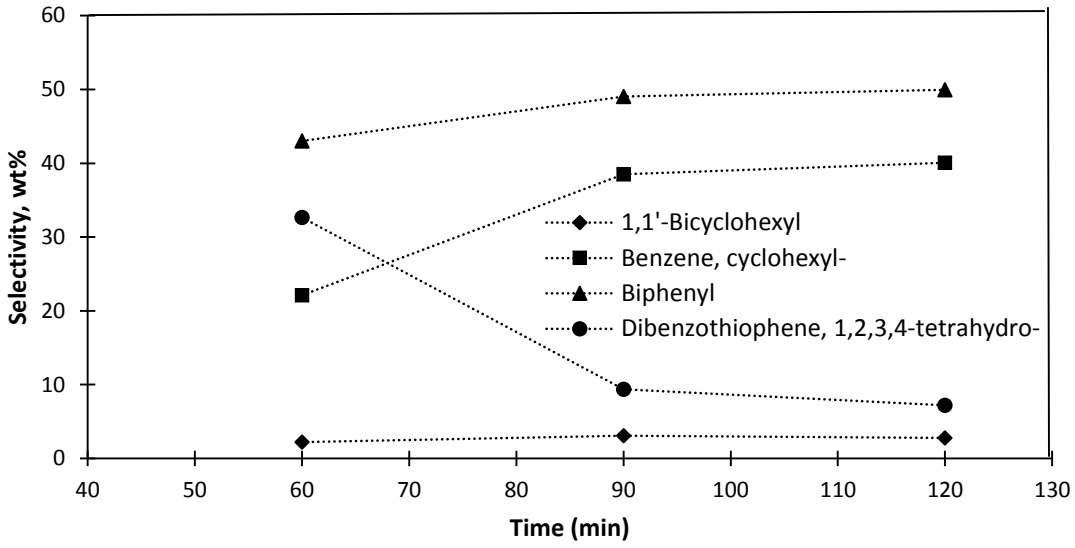

Figure 31: Selectivity of the product in HDS of DBT at 588K over NiMoS/AC as function of time

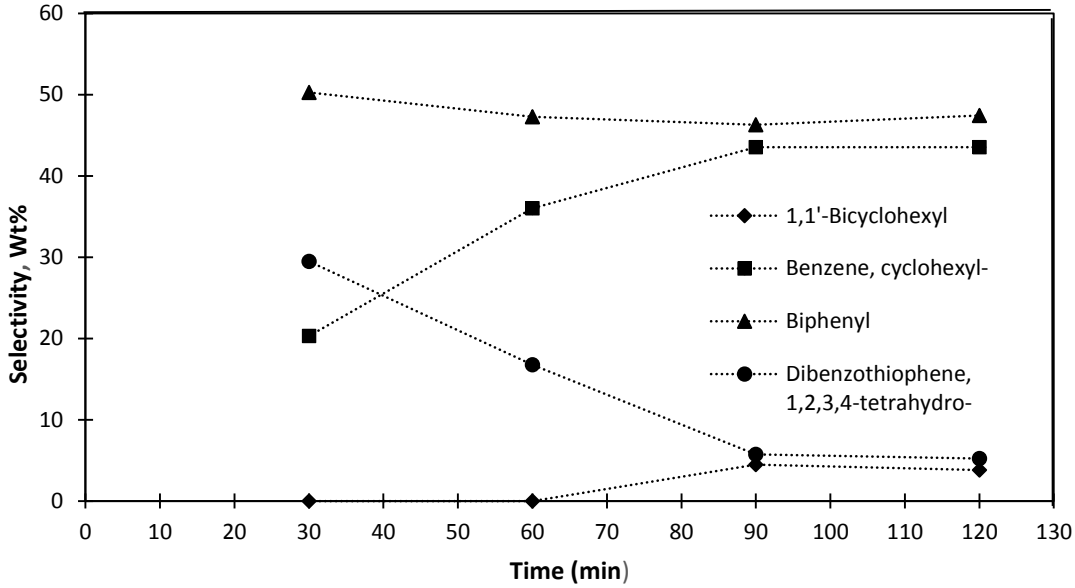

Figure 32: Selectivity of the product in HDS of DBT at 603K over NiMoS/AC as function of time

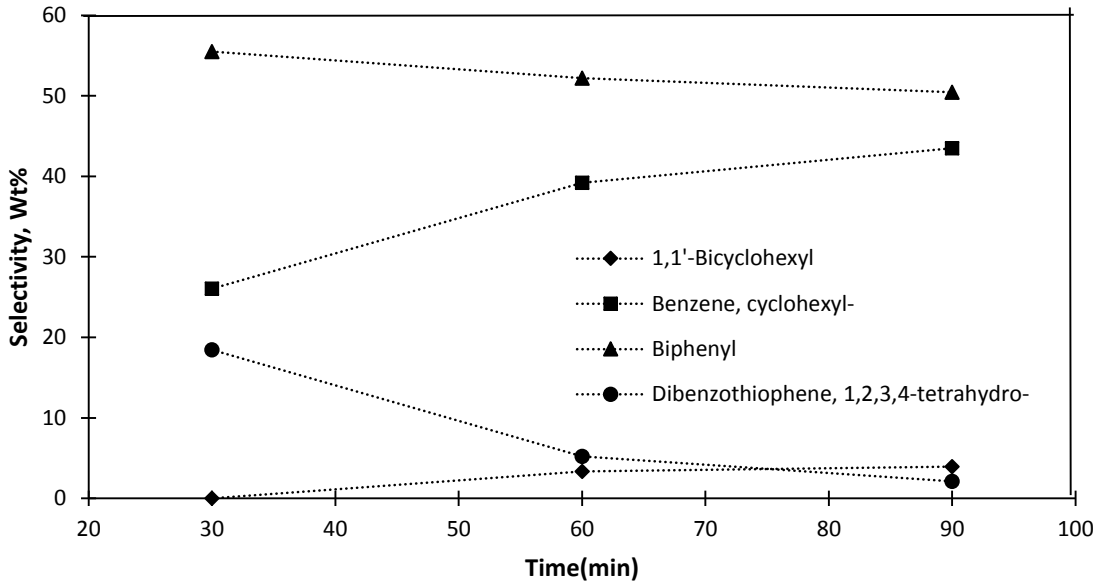

Figure 33: Selectivity of the product in HDS of DBT at 623K over NiMoS/AC as function of time

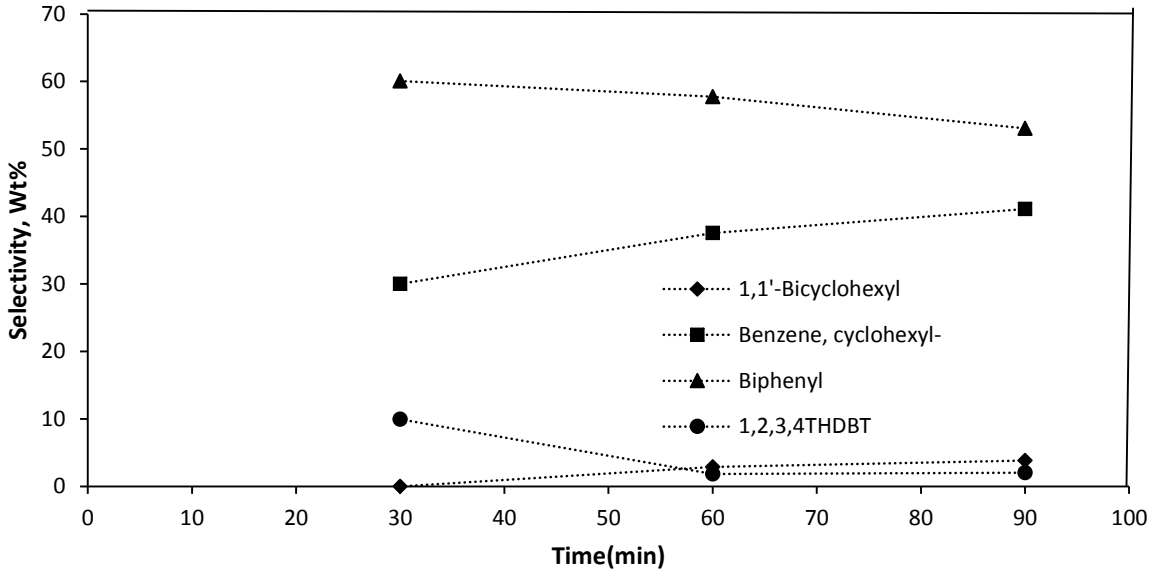

Figure 34: Selectivity of the product in HDS of DBT at 638K over NiMoS/AC as function of time

3.4.2 Product Distribution over NiMoS/PC

Figures 35-38 illustrate the product distributions of the HDS of DBT over NiMoS/PC at different temperatures. The results are very similar to those obtained for the NiMoS/AC catalyst. The selectivity to BP changes between 40 wt% and 60 wt% at different reaction times and temperature. As before, the selectivity towards 1, 2, 3, 4-THDBT dramatically decreased while the selectivity to CHB increased, consistent with the view that the formation of CHB is primarily from the hydrogenation of 1, 2, 3, 4-THDBT. This finding is in agreement with Figure 13 in the literature review. BCH was difficult to observe, requiring more than 120 min reaction time and higher temperature to be observed in the product. The maximum BCH formation was 6.8 wt% at 638 K.

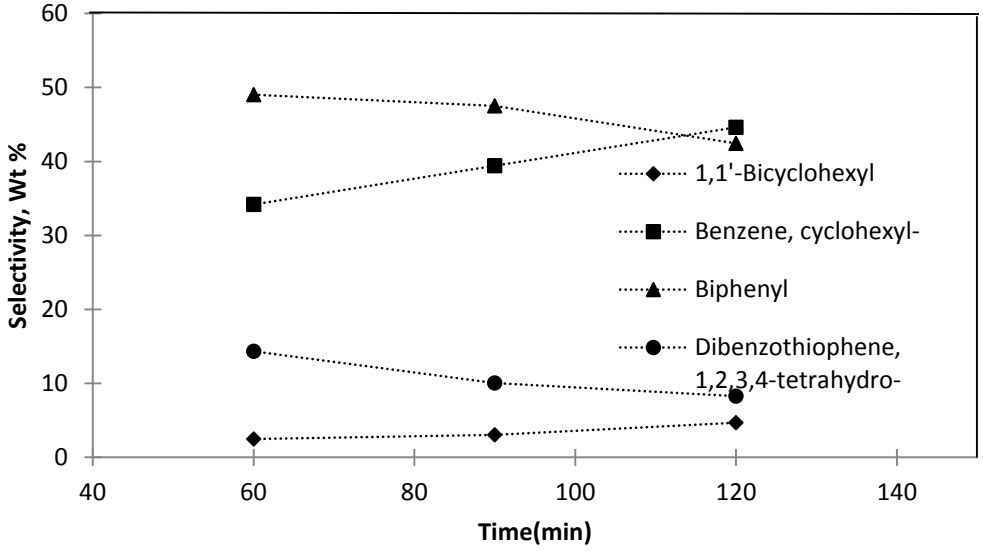

Figure 35: Selectivity of the product in HDS of DBT at 588 K over NiMoS/PC as function of time

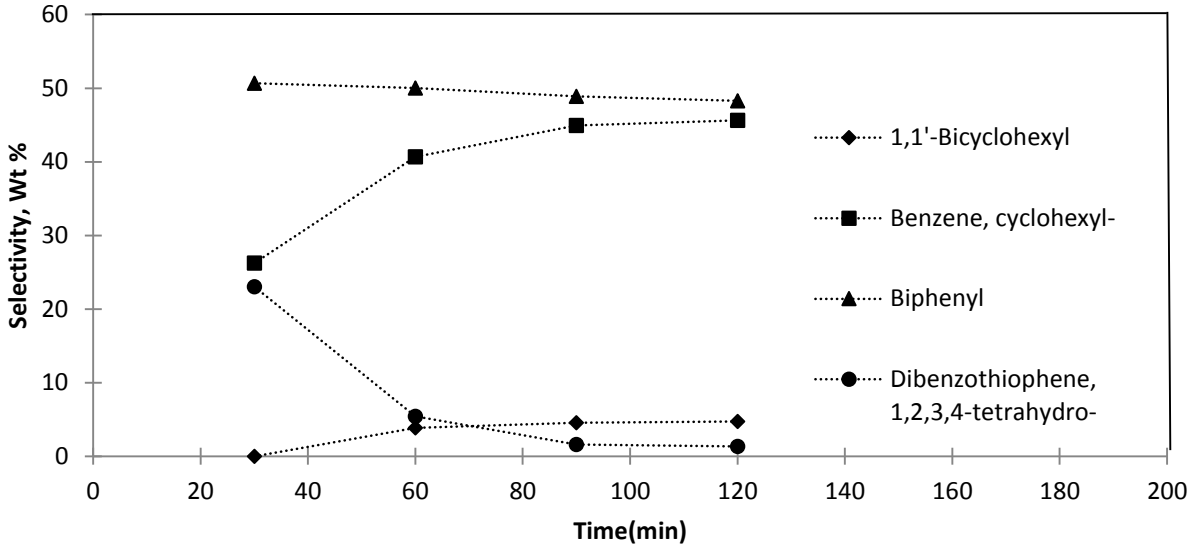

Figure 36: Selectivity of the product in HDS of DBT at 603 K over NiMoS/PC as function of time.

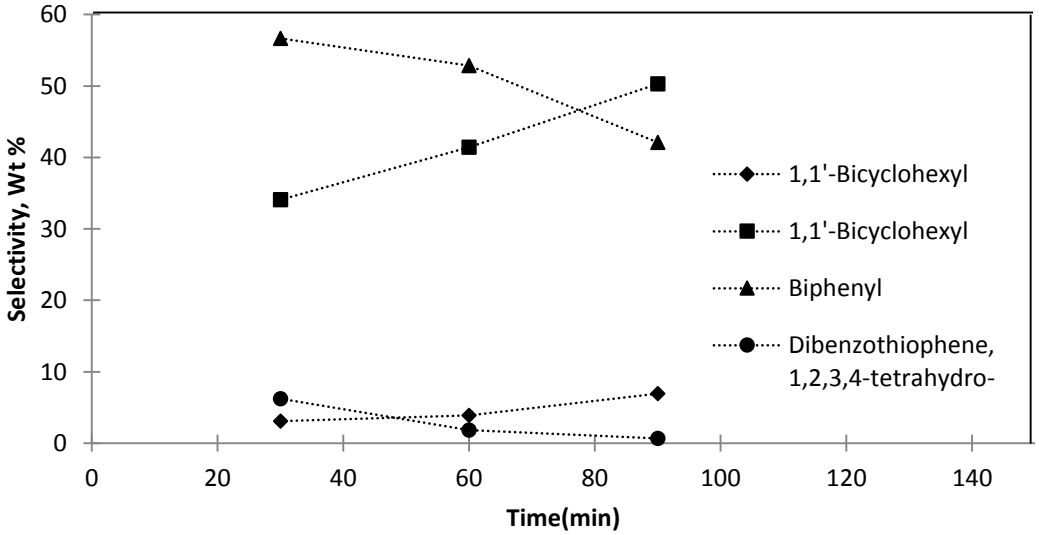

Figure 37: Selectivity of the product in HDS of DBT at 623 K over NiMoS/PC as function of time.

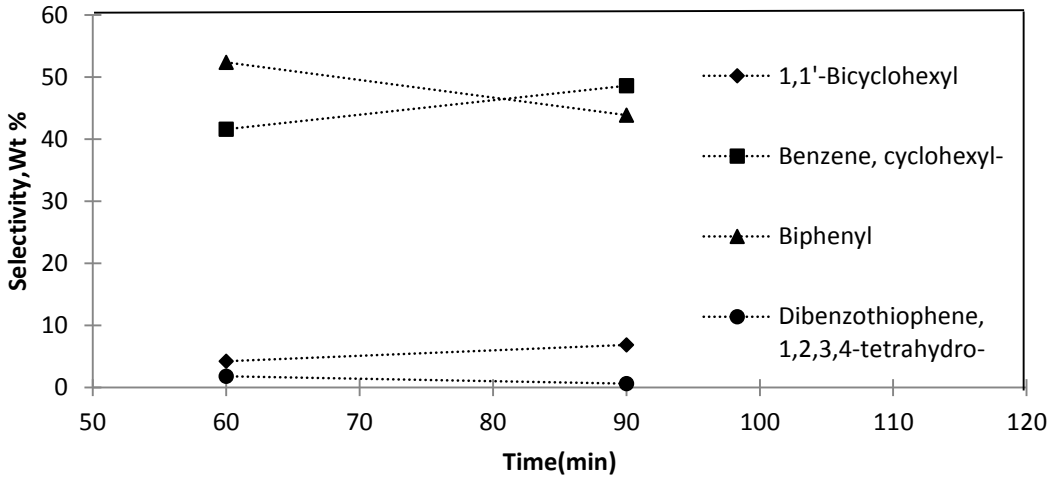

Figure 38: Selectivity of the product in HDS of DBT at 638 K over NiMoS/PC as function of time.

3.4.3 Comparison Between the Selectivity of NiMoS/AC and NiMoS/PC

Figures 39 and 40 show the selectivity of HDS of DBT reaction for both catalysts at 603 K and 623 K. Taking account of the experimental error associated with the measured selectivities (Appendix E), one concludes that there is minimal difference in selectivity between the NiMoS supported on petcoke versus the AC.

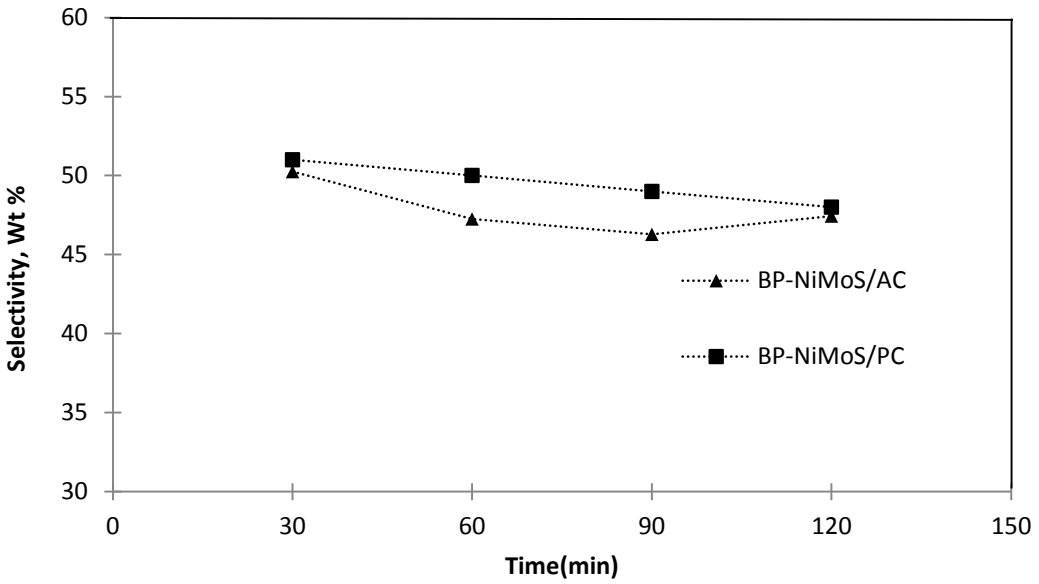

Figure 39: Comparison between NiMoS/AC and NiMoS/PC in term of selectivity towards DDS route at 603 K

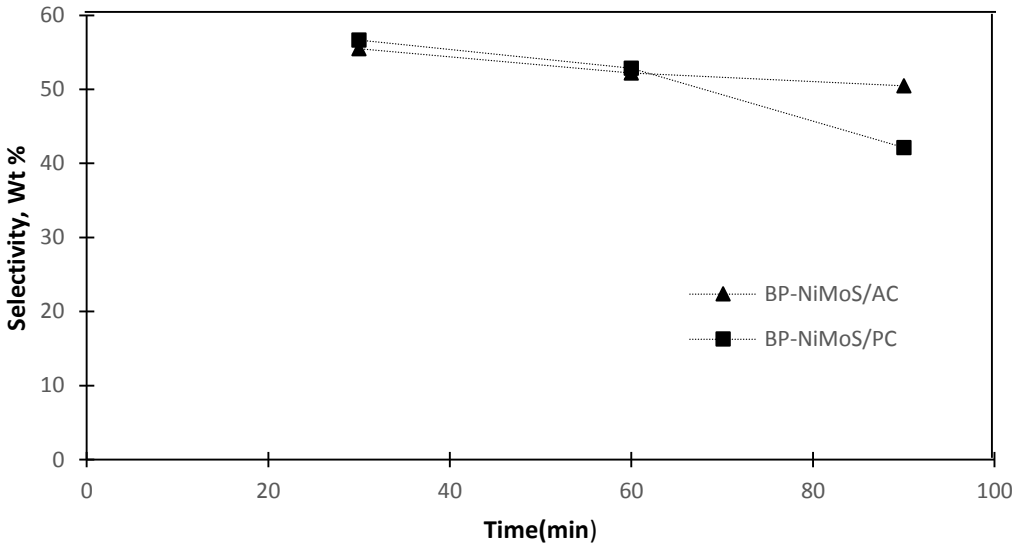

Figure 40: Comparison between NiMoS/AC and NiMoS/PC in term of selectivity towards DDS route at 623 K

3.5 Summary of Findings

Among the two catalysts prepared on either the AC or the pretreated petcoke, the NiMoS/PC catalyst showed higher HDS activity, although product selectivities were the same. Both catalysts had about 50% selectivity to DDS products.

In terms of properties of the different supports, the XPS narrow scan analysis showed that the petcoke exhibited the highest concentration of metal on the surface, corresponding with the higher hydrotreating activity of the NiMoS/PC catalyst towards DBT, achieving 90% conversion at 623K compared with NiMoS/AC, which achieved 90% conversion at 638 K. In terms of selectivity, both catalysts showed comparable trends over the reaction times, with NiMoS/PC resulting in ~20% higher formation of CHB than the catalyst supported on NiMoS/AC at 638 K. The selectivity of the HDS of DBT measured in the current study are in an agreement with the literature.[22]

Chapter 4: HDS Reaction Kinetics of DBT over NiMoS/AC and NiMoS/PC

4.1 Reaction Mechanism

From Figure 25-40 along with the discussion of the results in the previous chapter, it is concluded that the HDS of DBT proceeds by two routes, the DDS route and the HYD route. In the DDS route, the reaction starts by extracting S from DBT to produce BP which may then undergo further hydrogenation to form CHB. However the product selectivity data suggest the hydrogenation of BP is relatively slow and it can therefore be ignored in the kinetic model.[22] In the HYD route, the reaction starts with the hydrogenation of DBT to produce THDBT, followed by S removal from the THDBT to produce CHB. Further hydrogenation of CHB leads to BCH. The aforementioned conclusion is in agreement with several studies in the literature.[3-6,21-23]. The reaction pathways for the HDS of DBT are illustrated in Figure 41.[43]

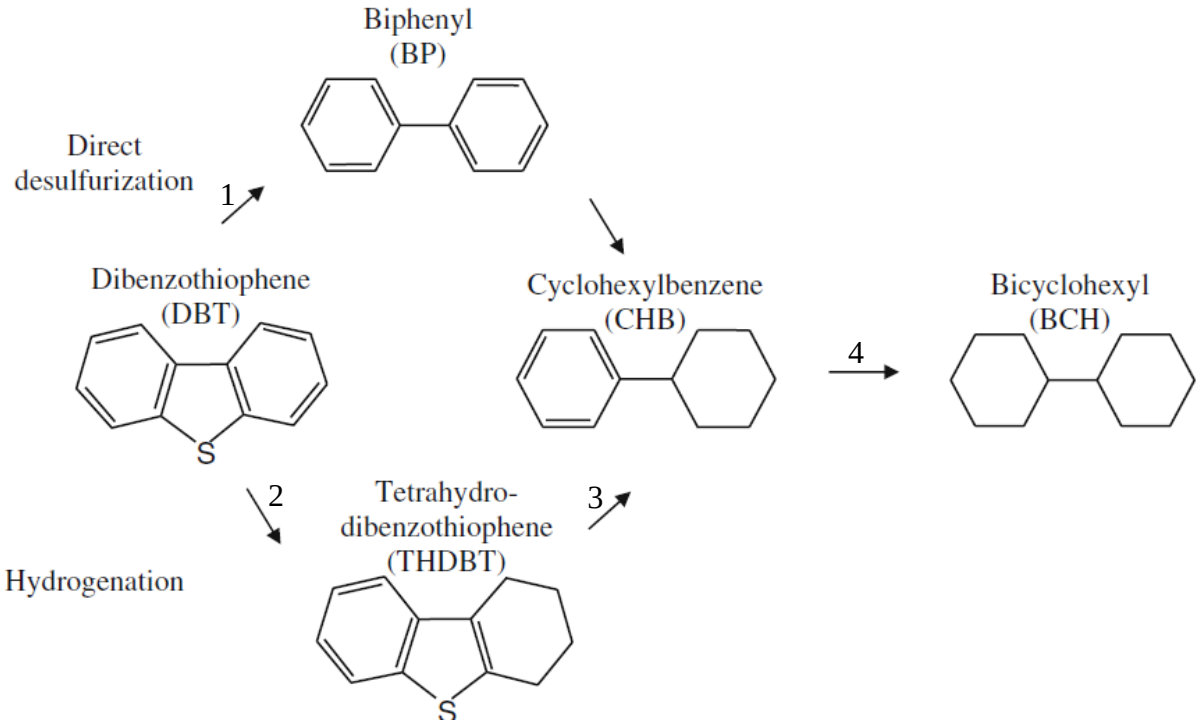

Figure 41: Proposed reaction pathway of HDS of DBT. Copyright © 2006, Springer Science Business Media, Inc.[43]

4.2 Kinetic Development

From the liquid sample analysis, the concentrations of the model compound DBT and reaction products BP, CHB, THDBT, and BCH as shown in Figure 41 were determined as a function of time. Based on the reaction studies of Tye and Smith[20] and Egorova and Prins [22,43], the rate constants for each step can be determined using a power law model assuming the reaction is 1st order and accounting for both the catalytic and non-catalytic reactions. The rate constant for the formation of CHB from BP through the DDS reaction route was eliminated as it is relatively slow and can be ignored.[22] Hence for each of the reaction steps of Figure 41 we can write:

$$r_1 = (k_1' C_{cat} + k_1)\, C_{DBT} \qquad (1)$$

$$r_2 = (k_2' C_{cat} + k_2)\, C_{DBT} \quad (2)$$

$$r_3 = (k_2' C_{cat} + k_2)\, C_{DBT} + (k_3' C_{cat} + k_3)\, C_{THDBT} \quad (3)$$

$$r_4 = (k_4' C_{cat} + k_4)\, C_{CHB} \quad (4)$$

The rate of reaction has units of r_n=mol/(cm^{3}s), where k_j' is the catalytic rate constant with units of cm^3/(g$_{cat}$s) and k_n is the thermal or non-catalytic rate constant with unit of s^{-1}. C_{cat} is the catalyst concentration in the reaction fluid (g/cm^3) defined as the mass of the catalyst inside the reactor divided by the liquid volume (V).

4.3 Mole Balance

The general mole balance equation for any system is

$$\begin{bmatrix}\text{rate of flow of}\\ \text{A into the system}\end{bmatrix} - \begin{bmatrix}\text{rate of flow of}\\ \text{A out of the}\\ \text{system}\end{bmatrix} + \begin{bmatrix}\text{rate of generation}\\ \text{of A by chemical reaction}\\ \text{within the system}\end{bmatrix} = \begin{bmatrix}\text{rate of}\\ \text{accumulation}\\ \text{of A within the}\\ \text{system}\end{bmatrix}$$

$$\{[v_i\ C_i]\text{-}[\ v_f\ C_{if}]\} + [\textstyle\sum_{j=1}^{N} \delta_{ji}\ \Omega\ a_j\ r_j] = [\mathrm{V}\ \frac{dC_i}{dt} + C_i \frac{dV}{dt}] \quad (5)$$

where is v_i the influent volumetric flow rate, v_f is the effluent volumetric flow rate. V is the total volume, C_i is the concentration of species i, δ_i is the stoichiometric coefficient of species i in reaction j, Ω is the overall effectiveness factor, a_j is the catalyst activity, r_j is rate of generation of component j, and N is the number of reactions. The mole balance equation can be simplified for the current study with the following assumptions:

- There is no input and output: $\{[v_i\ C_i]\text{-}[\ v_f\ C_{if}]\} = 0$ because the unit is operated in batch mode.

- A catalyst effectiveness of Ω = 1 since the catalyst particles are very small.
- No catalysts deactivation: a_j=1
- Liquid density changes are negligible: $\frac{dV}{dt}$ = 0

After applying the above assumptions the general mole balance equation is reduced to

$$\frac{dC_i}{dt} = \sum_{j=1}^{N} v_{ji}\, r_j \qquad (6)$$

After combining the mole balance equations with the reaction rate equations we obtain:

$$\frac{dC_{DBT}}{dt} = -(k_1' C_{cat} + k_1)\, C_{DBT} - (k_2' C_{cat} + k_2)\, C_{DBT} \qquad (7)$$

$$\frac{dC_{BP}}{dt} = (k_1' C_{cat} + k_1)\, C_{DBT} \qquad (8)$$

$$\frac{dC_{THDBT}}{dt} = (k_2' C_{cat} + k_2)\, C_{DBT} - (k_3' C_{cat} + k_3)\, C_{THDBT} \qquad (9)$$

$$\frac{dC_{CHB}}{dt} = (k_3' C_{cat} + k_3)\, C_{THDBT} - (k_4' C_{cat} + k_4)\, C_{CHB} \qquad (10)$$

$$\frac{dC_{BCH}}{dt} = (k_4' C_{cat} + k_4)\, C_{CHB} \qquad (11)$$

4.4 Parameter Estimation

The parameters of the kinetic equations were estimated by minimizing the objective function using the sum of least-squares method. The objective function was defined as the sum of squares of the difference between the experimental concentrations and the model calculated concentration for each chemical species *i* at each reaction time *t* as shown in Equation 12:

$$\text{OBJ} = \sum \sum (C_{exp,i,t} - C_{pred,i,t})^2 \qquad (12)$$

The above equation was minimized using the Levenberg-Marquardt method implemented in MATLAB. At each iteration, the ordinary differential equations (ODEs) obtained in equations

7-10 were solved simultaneously using a Runge-Kutta 4th order numerical integration, except Equation 11 which was replaced by mass balance, in order to estimate the model calculated concentrations C_{DBT}, C_{THDBT}, C_{BP}, C_{CHB}, and C_{BCH}. A series of thermal experiments were conducted at each reaction temperature and their data were collected to estimate k_1- k_4 for the non-catalytic reaction using the aforementioned numerical method. The same procedures were followed to calculate the catalytic rate constants $k_1' - k_4'$ for NiMoS/AC and NiMoS/PC catalysts. (Refer to appendix G for ODE MATLAB codes)

According to Figure 25 and 26 (d) the thermal reaction becomes significant after 60 min at 623 K with the DDS reaction and HYD reactions most significant. Hence the thermal rate constants k_1 and k_2 in equation 1 and 2 were estimated for these data sets. Due to the low concentrations and selectivity of the other reactions and the significant error associated with the low concentration measurements, the model parameters k_3 and k_4 were ignored and set to zero.After determining the rate constants for the thermal reaction, the catalytic rate constants $k_1' - k_4'$ in equations 7-11 were estimated. The Arrhenius equation was used to obtain the reaction apparent activation barrier energy as follows:

$$k_j = A_j * \exp\left(\frac{-E_{aj}}{R*T}\right) \qquad (13)$$

The pre-exponential factors A_j as well as the activation energy E_{aj} can be determined from the intercept and the slope of $\ln(k_j)$ versus $\left(\frac{1000}{T}\right)$ (Detailed calculations are given in Appendix H).Table 12 and 13 report the fitted parameter values of the thermal reactions. Table 14 - 17 report the parameter estimates for the NiMoS/AC and NiMoS/PC catalysts. The fit of the kinetic model is shown in Figures 42 and 43, with the degree of explanation (R^2) determined to be 0.92 for both catalysts. This result is acceptable and the reaction fits the pseudo first order

reaction assumption. The Arrhenius plots are given in Figure 44 - 46. Note that k_4' is not plotted in the Arrhenius diagram of NiMoS/AC and NiMoS/PC (Figures 45, 46, respectively) because of the large parameter errors, a consequence of the low concentration of the product BCH and few experimental data points where the concentration of this component was significant.

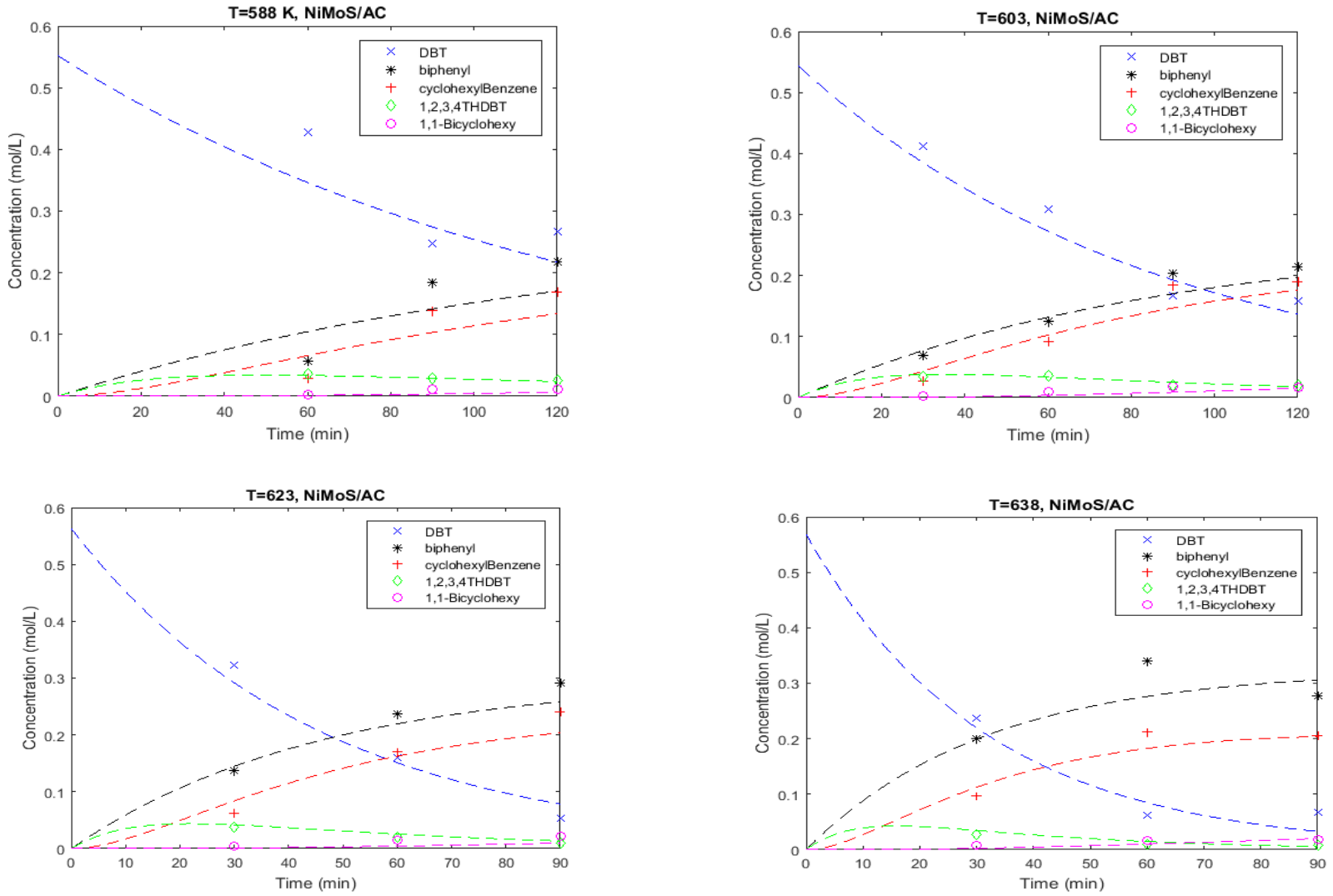

Figure 42: Measured (points) and model predicted (line) concentrations as function of time for NiMoS/AC catalyst at different temperatures.

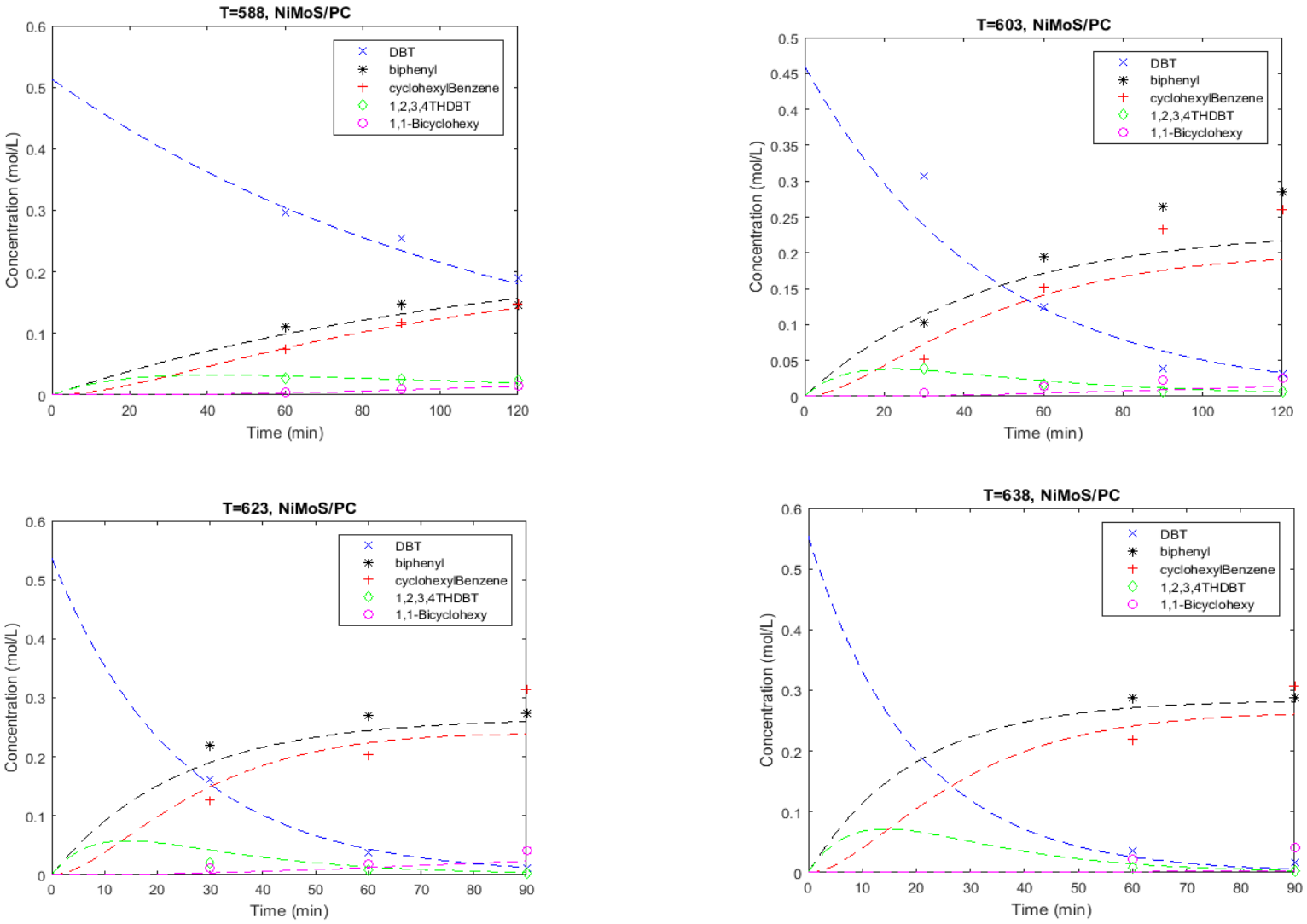

Figure 43: Measured (points) and model predicted (line) concentrations as function of time for NiMoS/PC catalyst at different temperatures.

Table 12: Estimated reaction rate constants for the thermal reaction of HDS of DBT

Parameter	Reaction temperature, K							
	588 K		603 K		623 K		638 K	
	Value	Std. error	Value	Std. error	Value	Std. error	Value	Std. error
k_1, 1/s	4.6E-04	1.08E-04	4.5E-04	2.9E-05	1.37E-03	7.6E-05	1.50E-03	8.058E-05
k_2, 1/s	2.47E-04	1.31E-04	2.65E-04	3.52E-05	6.33E-04	9.12E-05	6.05E-04	9.71E-05

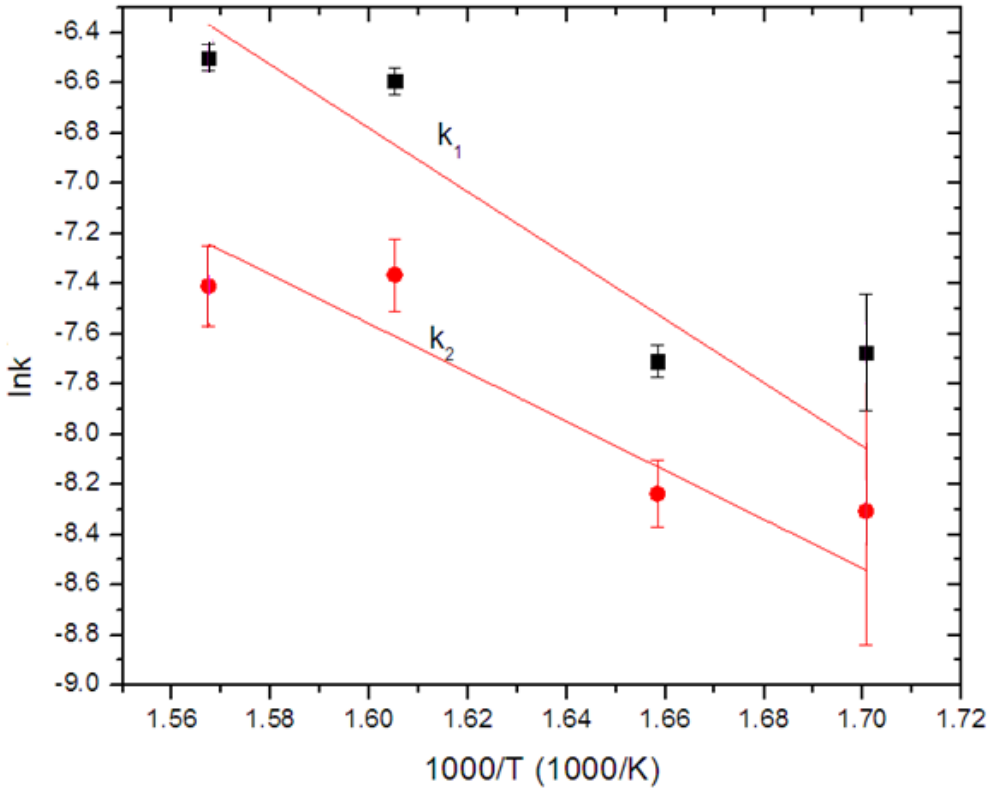

Figure 44: Arrhenius plot of ln (k_j) versus(1000/T) for the thermal HDS of DBT

Table 13: The pre-exponential factors A_j and activation energies for all k_1 at the thermal reaction

Parameter	ln(A_j), 1/s Value	Std. err	E_{aj}, kJ/mol	std.err
k_1	13.5	±6	105	±32
k_2	8	±5.3	81	±27

Table 14: Estimated reaction rate constants for the HDS of DBT over NiMoS/AC at tested temperature

Parameter	Reaction temperature, K							
	588K		603K		623K		638K	
	Value	Std. error	Value	Std. error	Value	Std. error	Value	Std. error
k_1', cm^3/g_{cat}*s	1.7E-01	5.9E-04	2.6E-01	3.5E-04	5.2E-01	7.1E-04	8.3E-01	1.4E-03
k_2', cm^3/g_{cat}*s	1.8E-01	7.4E-04	2.8E-01	4.4E-04	4.8E-01	8.4E-04	6.5E-01	1.4E-03
k_3', cm^3/g_{cat}*s	1.783	2.6E-02	2.493	1.5E-02	3.36	2.4E-02	4.811	4.9E-02
k_4', cm^3/g_{cat}*s	4.3E-02	3.4E0-3	6.81E-02	1.2E-03	4.54E-02	1.3E-03	8.337E-02	1.5E-03

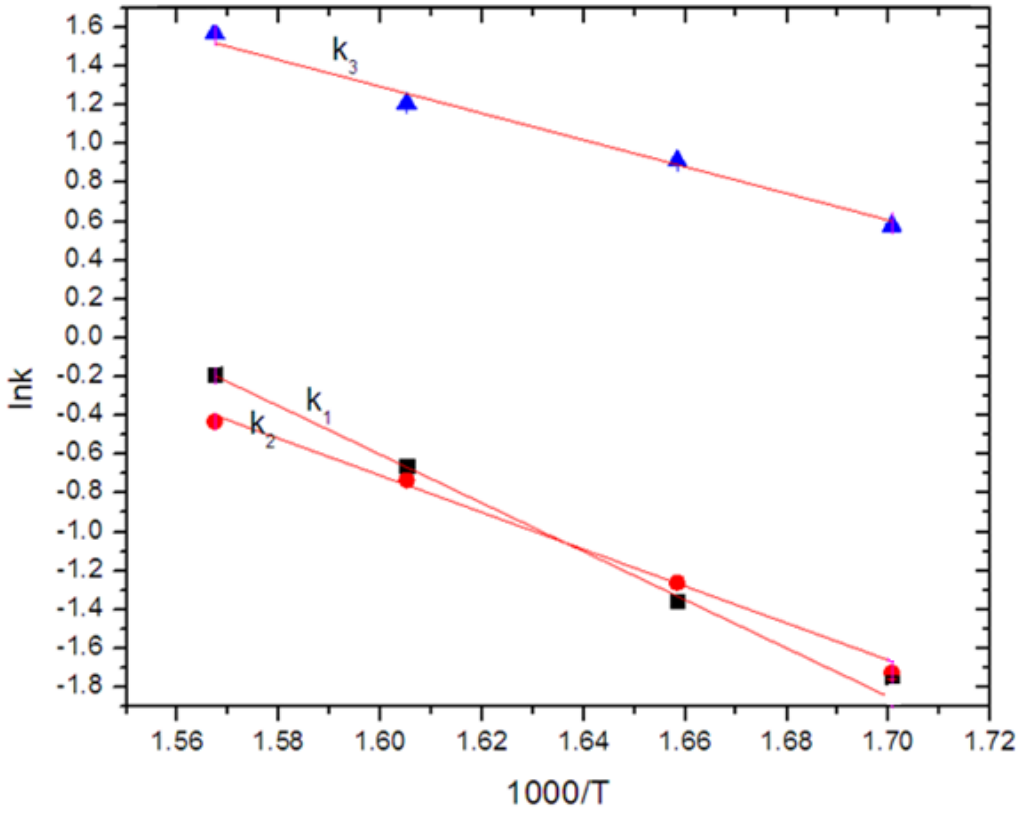

Figure 45: Arrhenius plot of ln (k_j') versus (1000/T) for all reaction temperature using NiMoS/AC catalyst.

Table 15: The pre-exponential factors A_j and activation energies for all k'_j at NiMoS/AC catalysts

Parameter	ln(A_j), cm^3/g_{cat}*s Value	Std. err	E_{aj}, kJ/mol	std. err
k'_1	19.37	±0.92	104	±5
k'_2	14.5	±0.71	79	±4
k'_3	12.3	±1.1	57	±6

Table 16: Estimated catalytic reaction rate constants for reaction of HDS for DBT over NiMoS/PC at tested temperature

Parameter	Reaction temperature, K					
	588 K		603 K		623 K	
	Value	Std. err	Value	Std. err	Value	Std. error
k_1', cm^3/g_{cat}*s	1.822E-01	1.437E-04	5.40E-01	7.704E-04	9.65E-01	2.16E-03
k_2', cm^3/g_{cat}*s	2.17E-01	1.842E-04	5.40E-01	9.079E-04	1.02E+00	2.48E-03
k_3', cm^3/g_{cat}*s	2.212	7.206E-03	3.534	2.486E-02	4.72	4.27E-02
k_4', cm^3/g_{cat}*s	8.305E-02	6.905E-04	5.201E-02	8.074E-04	0	1.10E-03

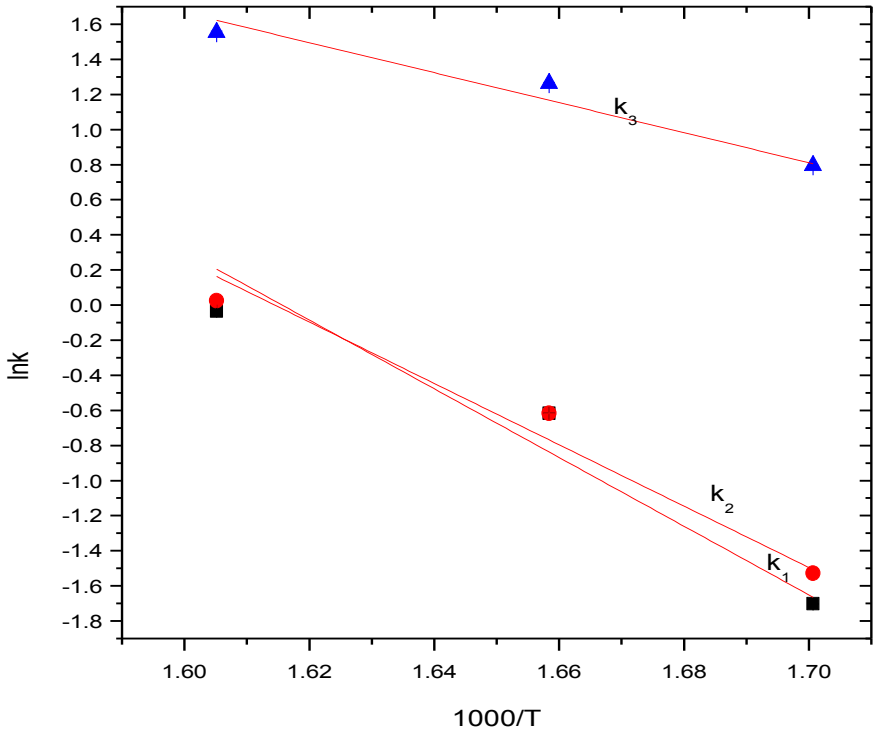

Figure 46: The Arrhenius plot of ln (k_j') versus (1000/T) for all reaction temperature using NiMoS/PC catalyst.

Table 17: The pre-exponential factors A_j and activation energies for all k'_j at NiMoS/PC catalysts

Parameter	ln(A_j), cm^3/g_{cat}*s Value	std. err	E_{aj}, kJ/mol	std. err
k'_1	31.6	±7.3	163	±36
k'_2	28.22	±4.5	146	±22
k'_3	15.3	±2.5	71	±13

The H_2S partial pressure in the reactor of the current study is between 150 – 300 kPa. Hence we can compare the rate of consumption of DBT (r_{DBT}) in Table 3 at P_{H_2S} = 100 kPa with the r_{DBT} in Tye's work[44] along with the r_{DBT} in the current study as shown in Table 18. It is concluded that the r_{DBT} in this study is lower by a magnitude of 10 compared to Prins's work. The lower rate observed in the present study is likely due to the fact the present study was conducted in the liquid phase at relatively high H_2S partial pressure (>100 kPa) which significantly inhibits the DBT consumption rate of DBT according to Figure 15 (Appendix I provides detailed calculations of the phases present during reaction and the H_2S partial pressure in the reactor). On the other hand r_{DBT} for the current study is higher by a magnitude of 100 compared to Tye's work. This difference is likely due to the significant effect of the promoter and the support used in the current study whereas Tye's catalysts were neither promoted nor supported.

Table 18: Comparison of DBT rates for the total DBT conversion at 623 K and 4.8 MPa with P_{H_2S}= 100 kPa with literature data

Literature	Catalysts	r_{DBT}, mol/(g Mo s)
Prins's work[22]	NiMoS/γ-Al_2O_3	0.05
Tye's work[44]	Unsupported MoS_2	8.00E-05
Current study	NiMoS/AC	0.004
	NiMoS/PC	0.008

According to Table 19, the HDS of DBT reaction in Prins's work prefers the DDS route over the HYD route as indicated by the rate constants. Whereas, in both catalysts in the current study, the relative rates of HYD versus DDS are approximately equal. The metal support interaction is a suggested reason for these findings. Since the support used in Prins's work was γ-Al_2O_3, with a known ability to interact with the metal and form a different MoS_2 stacking structure. In addition, a strong metal support interaction results in the precursor being converted to MoO_x that is not easily reduced. In contrast, the carbon support is known to have a weak metal support interaction resulting in a uniform dispersion and hence better MoS_2 formation along with reduced MoO_x.[31,32] XPS data showed good dispersion of NiMo on AC and petcoke indicating that the MoS_2 are well dispersed, indicative of a high and probably equal distribution of edge and rim sites. Hence the rate constants in both catalysts of both routes are statistically the same.

Table 19: Comparison of rate of reaction for DBT total, DDS, HYD conversion at 623 K and 4.8 MPa

Rates	Prins's work NiMoS/γ-Al_2O_3	Current work NiMoS/AC	Current work NiMoS/PC
r_{tot}, mol/(g Mo s)	0.05	0.004	0.008
r_{DDS}, mol/(g Mo s)	0.035	0.002	0.004
r_{HYD}, mol/(g Mo s)	0.016	0.0018	0.0038

The activation energy is defined as the barrier energy between the reactants and products of each rate step. From Table 15 and 17, it is concluded that for the NiMoS/AC catalyst, the activation energy of the DDS route is significantly higher (>20 kJ/mol) than the activation energy for the HYD route. In the case of the NiMoS/PC catalyst, both routes have similar activation energy, taking account of the error associated with the activation energy estimates for these two routes.

The activation energy for NiMoS in this study can be compared to the data from Liu et al.[24] and Tye and Smith[44] for the HDS of DBT reaction at the same assumptions and conditions, by extracting the activation energy of Liu's work from Figure 47 as reported in Table 20.

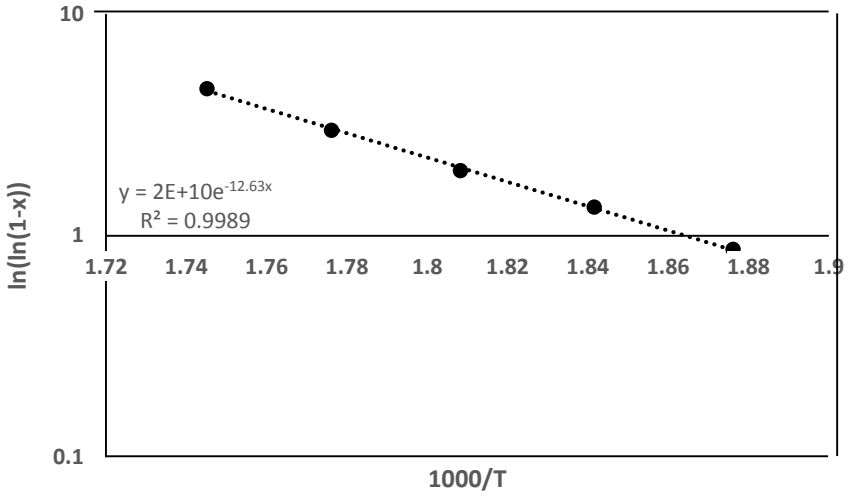

Figure 47: Arrhenius plot to calculate Ea from Liu et al. work on NiMo/AC

Table 20: Comparison of activation energies for the total DBT conversion

Authors	Type of Catalyst	E_a (kJ/mol)
Current work	NiMoS/AC	83
	NiMoS/PC	90
Liu et al.[24]	NiMo/AC	105
Tye and Smith[44]	Unsupported MoS_2	149

Tye and Smith catalyst was unsupported and unpromoted but Liu et al. and the current study catalysts were all supported on activated carbon and petcoke: NiMo/AC, NiMoS/AC, NiMoS/PC respectively. The activation energies for the current study are the lowest (refer to Appendix A for detailed calculation) indicative that the NiMoS/AC and NiMoS/PC catalysts

that were prepared in the current study have the lowest activation barrier, which means NiMoS/AC and NiMoS/PC have higher activity at lower temperature.

Broderick et al.[34] Vrinat et al.[36], Liu et al[24], and O'Brien et al[31] reported the activation energies for the same reaction mechanism used in this study, using Co-Mo/γ-Al_2O_3 and NiMo/AC catalysts for Liu et al.[24] as indicated in Table 5 in the literature review section. By comparing the values with the current study activation energies, it can be concluded that the present study's activation energies are in agreement with the literature values in Table 5. This shows that the reaction mechanism developed in the current study fits the pseudo first order assumption.

Chapter 5: Conclusion and Recommendations

5.1 Conclusion

Petcoke, which was obtained from Canadian Oil sand from Alberta, was successfully treated in this study using KOH reagent. Petcoke after treatment has a surface area of 1140 m^2/g and a pore volume of 0.67 cm^3/g. The treated petcoke was used as a support for the NiMoS catalysts. Hence, the HDS activity and selectivity of 3 catalyst supports were compared: NiMoS/AC, NiMoS/PC, and NiMo/γ-Al_2O_3 using DBT as a model compound reactant. The reactions were conducted in a novel slurry-phase batch microreactor at different reaction times (30-120 min) and temperatures (588-638 K) and a fixed H_2 pressure of 4.8 MPa.

The NiMoS catalysts used in this study showed higher dispersion on petcoke compared to AC. The results also showed that NiMoS/PC had a promising activity and selectivity when compared with the optimized NiMo/γ-Al_2O_3 catalyst, indicative that petcoke can be used as a promising support for catalysts. The HDS of DBT proceeded by two routes: the DDS reaction route and the HYD reaction route.

The pseudo 1^{st} order kinetic power law provided a suitable approximation of the reaction kinetics of the HDS reactions. The rate constants for both DDS and HYD routes showed similar magnitude on both NiMoS/AC and NiMoS/PC catalysts, whereas for the apparent activation energy, the DDS route activation energy was higher than the HYD route activation energy on the NiMoS/AC catalyst, but they were statistically equal on the NiMoS/PC catalyst.

The key contributions of this study are firstly, demonstrating that raw petcoke can be converted into a useful catalyst support for hydroteating processes. Secondly, after examining the catalyst supported on petcoke for S removal from DBT and obtaining a relatively high

activity, we can conclude that the treated petcoke is a promising support for hydrotreating catalysts.

5.2 Recommendations

The experiments reported herein were done at relatively high concentrations of H_2S, which is known to suppress catalytic activity. Additional experiments are needed using both NiMoS/AC and NiMoS/PC catalyst at lower H_2S partial pressure and in the gas phase to assess the performance of these catalysts at conditions comparable to literature reports.
The carbon supported catalysts need to be assessed using a real feedstock for a period of at least one month to observe how the catalysts behave in terms of activity, selectivity, and deactivation under industrial conditions.

The present study limited the catalyst activity measurements to the HDS of DBT. Use of more refractory model compounds such as 4,6-DMDBT will provide further clarification as to the relative activity and selectivity of the catalysts.

The petcoke support properties can be influenced by varying the pretreatment processes and conditions, which in turn will impact the catalyst performance. Further studies with petcoke prepared under different conditions to control pore volume, pore size and surface area are needed.

The kinetic modeling can be improved by using CHB as a reactant over both catalysts to produce BCH. Data form the present study showed that it is difficult to form BCH at the reaction conditions studied.

Bibliography

1. greencarcongress. EPA proposes tier 3 standards for gasoline sulfur content and vehicle emissions; harmonized with california LEV III
. http://www.greencarcongress.com/2013/03/tier3-20130329.html. Accessed October/22, 2015.

2. UOP Honeywell company. Sulphur content in diesel fuel. http://www.honeywell-uop.cn/more-diesel-reflect-changing-market. Updated 2015. Accessed 11/01, 2015.

3. Sakanishi K, Nagamatsu T, Mochida I, Whitehurst DD. Hydrodesulfurization kinetics and mechanism of 4,6-dimethyldibenzothiophene over NiMo catalyst supported on carbon. *J Mol Catal A: Chem*. 2000;155(1-2):101-109.

4. Ali SA, Ahmed S, Ahmed KW, Al-Saleh MA. Simultaneous hydrodesulfurization of dibenzothiophene and substituted dibenzothiophene over phosphorus modified CoMo/γ-Al_2O_3 catalysts. *Fuel Process Technol*. 2012;98:39-44.

5. Shi Y, Chen J, Chen J, MacLeod RA, Malac M. Preparation and evaluation of hydrotreating catalysts based on activated carbon derived from oil sand petroleum coke. *Appl Catal , A*. 2012;441-442:99-107.

6. Shi G, Zhao Y, Huang Y, Shen J. Mesoporous carbon supported Co-Mo and Ni-Mo catalysts for hydrodesulfurization. *Cuihua Xuebao*. 2010;31(8):961-964.

7. Milton Beychok. Hydrodesulfurization. http://www.eoearth.org/view/article/171121/. Updated 2013. Accessed Nov. 22, 2014.

8. Hill JM, Karimi A, Malekshahian M. Characterization, gasification, activation, and potential uses for the millions of tonnes of petroleum coke produced in canada each year. *The Canadian Journal of Chemical Engineering*. 2014;92(9):1618-1626.

9. R. Murray Gray. Upgrading petroleum residues and heavy oils. . 1994:244.

10. DiPanfilo R, Egiebor NO. Activated carbon production from synthetic crude coke. *Fuel Process Technol*. 1996;46(3):157-169.

11. PEC Consulting Group. Comparative properties of bituminous coal and petroleum coke as fuels in cement kilns. http://pecconsultinggroup.com/newsflash/comparative-properties-of-coal-and-petcoke. Accessed october/8, 2015.

12. PEC Consulting Group. Comparative properties of bituminous coal and petroleum coke as fuels in cement kilns. http://pecconsultinggroup.com/newsflash/comparative-properties-of-coal-and-petcoke. Updated 2015. Accessed March, 03, 2015.

13. Liang C, Li Z, Dai S. Mesoporous carbon materials: Synthesis and modification. *Angew Chem , Int Ed*. 2008;47(20):3696-3717.

14. Shen WZ, Zheng JT, Zhang YL, Wang JG, Qin ZF. Preparation of mesoporous carbon by steam activation of commercial activated carbon in the presence of yttrium oxide. *Studies in Surface Science and Catalysis*. 2003;146:767-770.

15. Marsh H, Yan DS, O'Grady TM, Wennerberg A. Formation of active carbons from cokes using potassium hydroxide. *Carbon*. 1984;22(6):603-611. doi: http://dx.doi.org/10.1016/0008-6223(84)90096-4.

16. Karimi A, Thinon O, Fournier J, Hill JM. Activated carbon prepared from canadian oil sands coke by CO_2 activation: I. trends in pore development and the effect of pre-oxidation. *The Canadian Journal of Chemical Engineering*. 2013;91(9):1491-1499.

17. Rodríguez-reinoso F. The role of carbon materials in heterogeneous catalysis. *Carbon*. 1998;36(3):159-175.

18. Marsh H, Rodríguez-Reinoso F. Chapter 2 - activated carbon (origins). In: Rodríguez-Reinoso HM, ed. *Activated carbon.* Oxford: Elsevier Science Ltd; 2006:13-86. http://dx.doi.org/10.1016/B978-008044463-5/50016-9.

19. Glasson C, Geantet C, Lacroix M, Labruyere F, Dufresne P. Beneficial effect of carbon on hydrotreating catalysts. *Journal of Catalysis*. 2002;212(1):76-85.

20. Vázquez P, Pizzio L, Blanco M, et al. NiMo(W)-based hydrotreatment catalysts supported on peach stones activated carbon. *Applied Catalysis A: General*. 1999;184(2):303-313.

21. Shu Y, Oyama ST. Synthesis, characterization, and hydrotreating activity of carbon-supported transition metal phosphides. *Carbon*. 2005;43(7):1517-1532.

22. Egorova M, Prins R. Hydrodesulfurization of dibenzothiophene and 4,6-dimethyldibenzothiophene over sulfided NiMo/γ-Al_2O_3, CoMo/γ-Al_2O_3, and Mo/γ-Al_2O_3 catalysts. *Journal of Catalysis*. 2004;225(2):417-427.

23. Kouzu M, Kuriki Y, Hamdy F, Sakanishi K, Sugimoto Y, Saito I. Catalytic potential of carbon-supported NiMo-sulfide for ultra-deep hydrodesulfurization of diesel fuel. *Appl Catal , A*. 2004;265(1):61-67.

24. Liu F, Xu S, Chi Y, Xue D. A novel alumina-activated carbon composite supported NiMo catalyst for hydrodesulfurization of dibenzothiophene. *Catalysis Communications*. 2011;12(6):521-524.

25. - Huang Y, - Hu S, - Zuo S, - Xu Z, - Han C, - Shen J. - Mesoporous carbon materials prepared from carbohydrates with a metal chloride template. - *J Mater Chem*. (- 41):- 7759.

26. Sakanishi K, Hasuo H, Mochida I, Okuma O. Preparation of highly dispersed NiMo catalysts supported on hollow spherical carbon black particles. *Energy Fuels*. 1995;9(6):995-8.

27. Egorova M, Prins R. Mutual influence of the HDS of dibenzothiophene and HDN of 2-methylpyridine. *Journal of Catalysis*. 2004;221(1):11-19.

28. Egorova M, Prins R. Competitive hydrodesulfurization of 4,6-dimethyldibenzothiophene, hydrodenitrogenation of 2-methylpyridine, and hydrogenation of naphthalene over sulfided NiMo/γ-Al_2O_3. *Journal of Catalysis*. 2004;224(2):278-287.

29. Byskov LS, Nørskov JK, Clausen BS, Topsøe H. DFT calculations of unpromoted and promoted MoS_2-based hydrodesulfurization catalysts. *Journal of Catalysis*. 1999;187(1):109-122.

30. Schweiger H, Raybaud P, Toulhoat H. Promoter sensitive shapes of Co(Ni)MoS nanocatalysts in sulfo-reductive conditions. *Journal of Catalysis*. 2002;212(1):33-38.

31. Daage M, Chianelli RR. Structure-function relations in molybdenum sulfide catalysts: The "rim-edge" model. *Journal of Catalysis*. 1994;149(2):414-427.

32. Hensen EJM, Kooyman PJ, van der Meer Y, et al. The relation between morphology and hydrotreating activity for supported MoS_2 particles. *Journal of Catalysis*. 2001;199(2):224-235.

33. Vanrysselberghe V, Froment GF. Hydrodesulfurization of dibenzothiophene on a CoMo/γ-Al_2O_3 catalyst: Reaction network and kinetics. *Ind Eng Chem Res*. 1996;35(10):3311-3318.

34. Broderick DH, Sapre AV, Gates BC, Kwart H, Schuit GCA. Hydrogenation of aromatic compounds catalyzed by hydrogen sulfide-cobalt(II) oxide-molybdenum oxide/alumina. *J Catal*. 1982;73(1):45-49.

35. Vanrysselberghe V, Le Gall R, Froment GF. Hydrodesulfurization of 4-methyldibenzothiophene and 4,6-dimethyldibenzothiophene on a CoMo/γ-Al_2O_3 catalyst: Reaction network and kinetics. *Ind Eng Chem Res*. 1998;37(4):1235-1242.

36. Vrinat. M.L and de Mourgues. L. Kinetic study of DBT on CoMo/γ-Al_2O_3 catalyst. . 1982;45:79.

37. O'Brien. W, Chen. R, Carr. G. Kinetics study of DBT HDS over CoMo/γ-Al_2O_3. 1979;661:76.

38. Campanati M, Fornasari G, Vaccari A. Fundamentals in the preparation of heterogeneous catalysts. *Catalysis Today*. 2003;77(4):299-314.

39. Kawano T, Kubota M, Onyango MS, Watanabe F, Matsuda H. Preparation of activated carbon from petroleum coke by KOH chemical activation for adsorption heat pump. *Appl Therm Eng*. 2008;28(8–9):865-871.

40. Kukard R. *Catalytic hydroconversion of diphenylmethane with unsupported MoS_2.* [PhD]. university of british columbia; 2014.

41. Kukard RS, Smith KJ. Slurry-phase batch microreactor for hydroconversion studies. *Energy Fuels*. 2015;29(8):5274-5281.

42. Whiffen VML, Smith KJ. Hydrodeoxygenation of 4-methylphenol over unsupported MoP, MoS2, and MoOx catalysts. *Energy Fuels*. 2010;24(9):4728-4737.

43. Tye CT, Smith KJ. Catalytic activity of exfoliated MoS_2 in hydrodesulfurization, hydrodenitrogenation and hydrogenation reactions. *Top Catal*. 2006;37(2-4):129-135.

44. Tye CT, Smith KJ. Catalytic activity of exfoliated MoS_2 in hydrodesulfurization, hydrodenitrogenation and hydrogenation reactions. *Top Catal*. 2006;37(2-4):129-135.

Appendices

Appendix A Calculation of Activation Energies from the Data of Liu et al.[24]

After extracting the conversions from Figure 5 of each catalyst and fitting them with the temperatures, we assume 1st-order kinetics so that k = (1/τ)(-ln(1-X), and hence a plot of lnk versis 1/T will yield a slope proportional to the Ea. the activation energies will be

- NiMoS/γ-Al_2O_3

Table 21: Conversions and corresponding temperature for NiMoS/γ-Al_2O_3

x	ln(1-x)	T	1000/T
0.32	0.385662481	260	1.876173
0.59	0.891598119	270	1.841621
0.78	1.514127733	280	1.808318
0.91	2.407945609	290	1.776199
0.98	3.912023005	300	1.745201

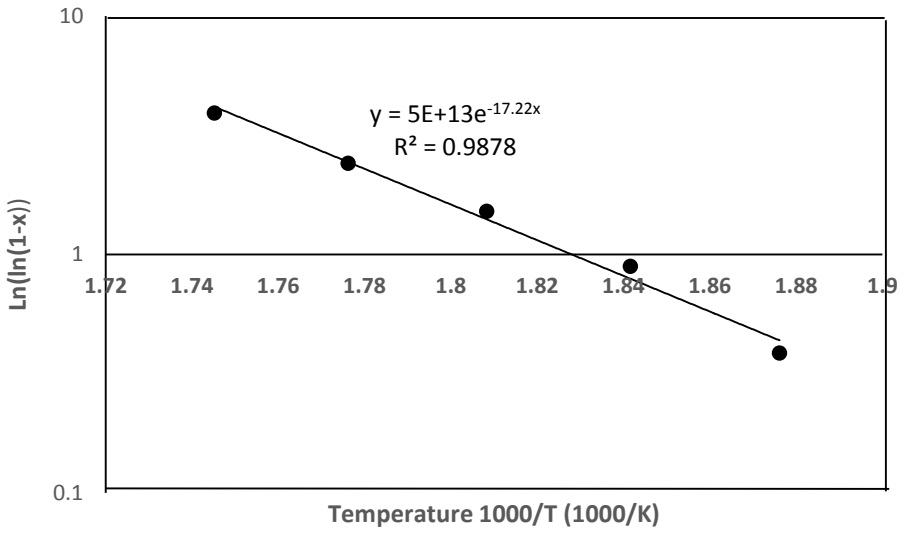

Figure 48: Arrhenius plot to calculate Ea for NiMoS/γ-Al_2O_3 catalyst

Ea = -8.314*-17.22

=143.16 kJ/mol

- NiMoS/AC

Table 22: Conversions and corresponding temperature for NiMoS/AC

x	ln(1-x)	T	1000/T
0.58	0.867500568	260	1.876173
0.74	1.347073648	270	1.841621
0.86	1.966112856	280	1.808318
0.95	2.995732274	290	1.776199
0.99	4.605170186	300	1.745201

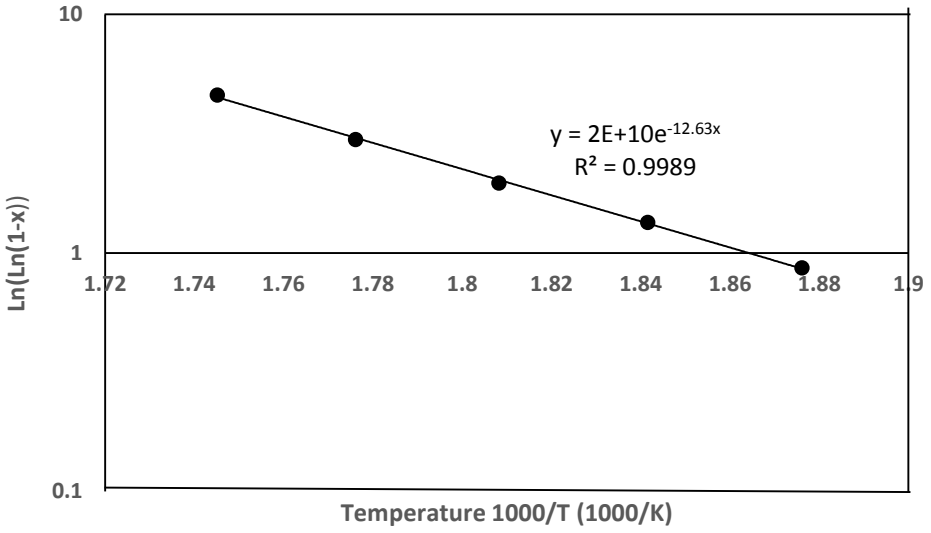

Figure 49: Arrhenius plot to calculate Ea for NiMoS/AC catalyst

Ea = -8.314*-12.63

=105 kJ/mol

- NiMoS/AAC

Table 23: Conversions and corresponding temperature for NiMoS/AAC

x	ln(1-x)	T	1000/T
0.9	2	260	1.9
0.97	4	270	1.8
0.99	5	280	1.8
0.999	7	290	1.8

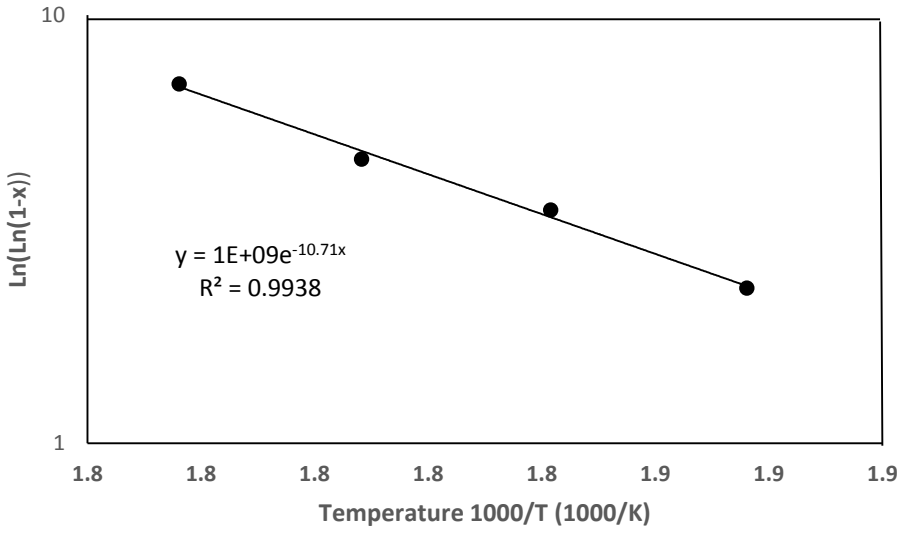

Figure 50: Arrhenius plot to calculate Ea for NiMoS/AAC catalyst

Ea = -8.314*10.71

= 89 kJ/mol

- Current work NiMoS/AC

Table 24: Conversions and corresponding temperature for NiMoS/AC

x	ln(1-x)	1000/T
0.61	0.94	1.70
0.71	1.24	1.66
0.912	2.43	1.61

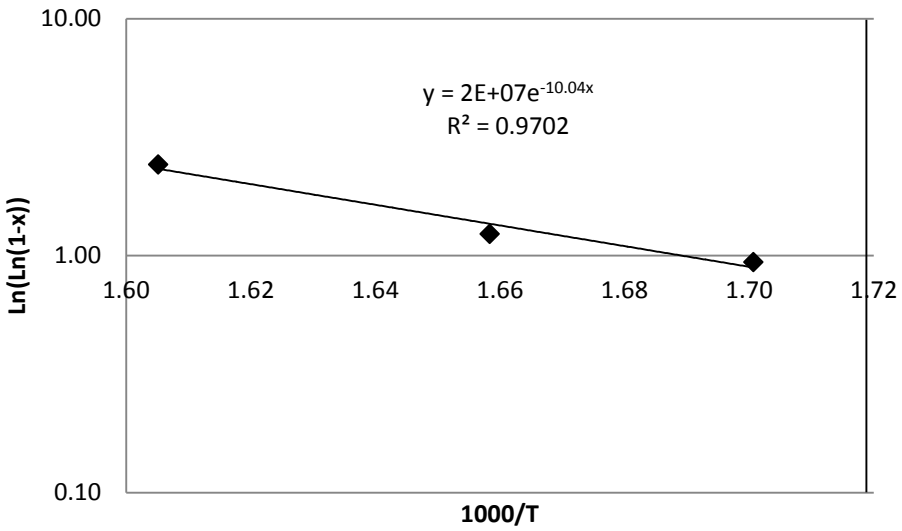

Figure 51: Arrhenius plot to calculate Ea for NiMoS/AC catalyst for the current study

Ea = -8.314*10.04

= 83 kJ/mol

- NiMoS/PC

Table 25: Conversions and corresponding temperature for NiMoS/PC

x	ln(1-x)	1000/T
0.6547	1.063342	1.700
0.97	3.506558	1.605
0.99	4.60517	1.560

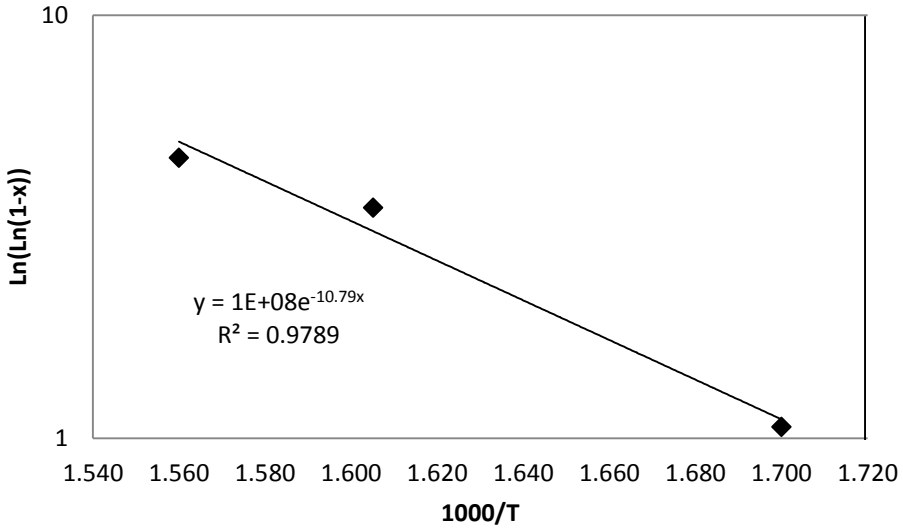

Figure 52: Arrhenius plot to calculate Ea for NiMoS/PC catalyst for the current study

Ea = -8.314*10.79

= 90 kJ/mol

Appendix B The Kinetic Model for HDS in Vanrysselberghe and Froment[33]

The study was developed based on σ and τ, the two different types of active sites for hydrogenolysis and hydrogenation reactions. A Langmuir-Hinshelwood mechanism was developed for both types of reactions as described below:

$$DBT + \sigma \rightleftharpoons DBT.\sigma$$

$$H_2 + 2\sigma \rightleftharpoons 2H.\sigma$$

$$DBT.\sigma + 2H.\sigma \rightarrow BPH.\sigma + S.\sigma + \sigma \qquad \text{(rds)}$$

$$S.\sigma + 2H.\sigma \rightleftharpoons H_2S.\sigma + 2\sigma$$

$$BPH.\sigma \rightleftharpoons BPH + \sigma$$

$$H_2S.\sigma \rightleftharpoons H_2S + \sigma$$

(b) hydrogenation of DBT into THDBT and HHDBT on the τ sites, followed by hydrogenolysis into CHB and

H_2S on the σ sites

$$DBT + \tau \rightleftharpoons DBT.\tau$$

$$H_2 + 2\tau \rightleftharpoons 2H.\tau$$

$$DBT.\tau + 2H.\tau \rightleftharpoons DHDBT.\tau + 2\tau \qquad \text{(rds)}$$

$$DHDBT.\tau + 2H.\tau \rightleftharpoons THDBT.\tau + 2\tau$$

$$THDBT.\tau \rightleftharpoons THDBT + \tau$$

$$THDBT.\tau + 2H.\tau \rightleftharpoons HHDBT.\tau + 2\tau$$

$$HHDBT.\tau \rightleftharpoons HHDBT + \tau$$

$$THDBT + \sigma \rightleftharpoons THDBT.\sigma$$

$$HHDBT + \sigma \rightleftharpoons HHDBT.\sigma$$

$$H_2 + 2\sigma \rightleftharpoons 2H.\sigma$$

$$THDBT.\sigma + 2H.\sigma \rightarrow PHCH.\sigma + S.\sigma + \sigma$$

$$PHCH.\sigma + 2H.\sigma \rightleftharpoons CHB.\sigma + 2\sigma$$

$$HHDBT.\sigma + 2H.\sigma \rightarrow CHB.\sigma + S.\sigma + \sigma$$

$$S.\sigma + 2H.\sigma \rightleftharpoons H_2S.\sigma + 2\sigma$$

$$CHB.\sigma \rightleftharpoons CHB + \sigma$$

$$H_2S.\sigma \rightleftharpoons H_2S + \sigma$$

(c) hydrogenation of BPH into CHB on the τ sites

$$BPH + \tau \rightleftharpoons BPH.\tau$$

$$H_2 + 2\tau \rightleftharpoons 2H.\tau$$

$$BPH.\tau + 2H.\tau \rightarrow PHCHD.\tau + 2\tau \qquad \text{(rds)}$$

$$PHCHD.\tau + 2H.\tau \rightleftharpoons PHCH.\tau + 2\tau$$

$$PHCH.\tau + 2H.\tau \rightleftharpoons CHB.\tau + 2\tau$$

$$CHB.\tau \rightleftharpoons CHB + \tau$$

(d) hydrogenation of CHB into BCH on the τ sites

$$CHB + \tau \rightleftharpoons CHB.\tau$$

$$H_2 + 2\tau \rightleftharpoons 2H.\tau$$

$$CHB.\tau + 2H.\tau \rightarrow CHCHD.\tau + 2\tau \qquad \text{(rds)}$$

$$CHCHD.\tau + 2H.\tau \rightleftharpoons CHCH.\tau + 2\tau$$

$$CHCH.\tau + 2H.\tau \rightleftharpoons BCH.\tau + 2\tau$$

$$BCH.\tau \rightleftharpoons BCH + \tau$$

The rate expressions were obtained as follow

$$r_{\mathrm{DBT},\sigma} = \frac{k_{\mathrm{DBT},\sigma} K_{\mathrm{H},\sigma} K_{\mathrm{DBT},\sigma} C_{\mathrm{DBT}} C_{\mathrm{H_2}}}{\left(1 + K_{\mathrm{DBT},\sigma} C_{\mathrm{DBT}} + \sqrt{K_{\mathrm{H},\sigma} C_{\mathrm{H_2}}} + K_{\mathrm{BPH},\sigma} C_{\mathrm{BPH}} + K_{\mathrm{H_2S},\sigma} C_{\mathrm{H_2S}}\right)^3}$$

$$r_{\mathrm{DBT},\tau} = \frac{k_{\mathrm{DBT},\tau} K_{\mathrm{H},\tau} K_{\mathrm{DBT},\tau} C_{\mathrm{DBT}} C_{\mathrm{H_2}}}{\left(1 + K_{\mathrm{DBT},\tau} C_{\mathrm{DBT}} + \sqrt{K_{\mathrm{H},\tau} C_{\mathrm{H_2}}} + K_{\mathrm{BPH},\tau} C_{\mathrm{BPH}}\right)^3}$$

$$r_{\mathrm{BPH},\tau} = \frac{k_{\mathrm{BPH},\tau} K_{\mathrm{H},\tau} K_{\mathrm{BPH},\tau} C_{\mathrm{BPH}} C_{\mathrm{H_2}}}{\left(1 + K_{\mathrm{DBT},\tau} C_{\mathrm{DBT}} + \sqrt{K_{\mathrm{H},\tau} C_{\mathrm{H_2}}} + K_{\mathrm{BPH},\tau} C_{\mathrm{BPH}}\right)^3}$$

$$r_{\mathrm{CHB},\tau} = \frac{k_{\mathrm{CHB},\tau} K_{\mathrm{H},\tau} K_{\mathrm{CHB},\tau} C_{\mathrm{CHB}} C_{\mathrm{H_2}}}{\left(1 + K_{\mathrm{DBT},\tau} C_{\mathrm{DBT}} + \sqrt{K_{\mathrm{H},\tau} C_{\mathrm{H_2}}} + K_{\mathrm{BPH},\tau} C_{\mathrm{BPH}}\right)^3}$$

Appendix C Catalyst Characterization

C.1 BET Surface Area Calculations

The N_2 adsoprtion isotherm is measured at 77K using the Micromeritics ASAP 2020. The volume of N2 adsorpbed as a function of pressure ratio (P/p0) is measured. Hence, the BET surface area can be estimated through the following equation

$$\frac{{}^{P}/_{P_o}}{V(1-\frac{P}{P_o})} = \frac{C-1}{V_m C}\left(\frac{P}{P_o}\right) + \frac{1}{V_m C}$$

Where

P is the equilibrium pressure

P_o is the saturation pressure of the adsorbate pressure

V is the adsorbed volume

V_m is the adsorbed volume at the monolayer coverage

C is constant

C.2 BET Analysis for Activated Carbon Before Impregnation

Full Report Set

ASAP 2020 V3.01 H | Unit 1 | Serial #: 336 | Page 1

Sample: activated carbon new bottle (again)
Operator: Majed
Submitter: UBC
File: C:\...\MAJED\000-175.SMP

Started:	01/05/2014 6:02:29PM	Analysis Adsorptive:	N2
Completed:	01/05/2014 8:44:23PM	Analysis Bath Temp.:	-195.850 °C
Report Time:	02/05/2014 12:21:33PM	Thermal Correction:	No
Sample Mass:	0.1200 g	Warm Free Space:	28.4000 cm^3 Measured
Cold Free Space:	90.4938 cm^3	Equilibration Interval:	10 s
Low Pressure Dose:	None	Automatic Degas:	Yes

Summary Report

Surface Area

Single point surface area at p/p° = 0.312549128: 1326.0480 m^2/g

BET Surface Area: 1322.5673 m^2/g

t-Plot Micropore Area: 652.5297 m^2/g

t-Plot External Surface Area: 670.0375 m^2/g

BJH Adsorption cumulative surface area of pores
between 1.7000 nm and 300.0000 nm diameter: 436.478 m^2/g

Pore Volume

t-Plot micropore volume: 0.349497 cm^3/g

BJH Adsorption cumulative volume of pores
between 1.7000 nm and 300.0000 nm diameter: 0.241134 cm^3/g

Pore Size

BJH Adsorption average pore diameter (4V/A): 2.2098 nm

Sample: activated carbon new bottle (again)
Operator: Majed
Submitter: UBC
File: C:\...\MAJED\000-175.SMP

Started: 01/05/2014 6:02:29PM
Completed: 01/05/2014 8:44:23PM
Report Time: 02/05/2014 12:21:33PM
Sample Mass: 0.1200 g
Cold Free Space: 90.4938 cm³
Low Pressure Dose: None

Analysis Adsorptive: N2
Analysis Bath Temp.: -195.850 °C
Thermal Correction: No
Warm Free Space: 28.4000 cm³ Measured
Equilibration Interval: 10 s
Automatic Degas: Yes

Isotherm Tabular Report

Relative Pressure (p/p°)	Absolute Pressure (mmHg)	Quantity Adsorbed (cm³/g STP)	Elapsed Time (h:min)	Saturation Pressure (mmHg)
			01:22	755.363525
0.049434026	37.340660	356.1179	01:50	
0.120518469	91.035255	391.4967	01:59	
0.181500324	137.098724	410.8322	02:06	
0.245724202	185.611099	427.4877	02:12	
0.312549128	236.088211	443.1075	02:19	

Full Report Set

ASAP 2020 V3.01 H Unit 1 Serial #: 336
Page 3

Sample: activated carbon new bottle (again)
Operator: Majed
Submitter: UBC
File: C:\...\MAJED\000-175.SMP

Started: 01/05/2014 6:02:29PM
Completed: 01/05/2014 8:44:23PM
Report Time: 02/05/2014 12:21:33PM
Sample Mass: 0.1200 g
Cold Free Space: 90.4938 cm³
Low Pressure Dose: None

Analysis Adsorptive: N2
Analysis Bath Temp.: -195.850 °C
Thermal Correction: No
Warm Free Space: 28.4000 cm³ Measured
Equilibration Interval: 10 s
Automatic Degas: Yes

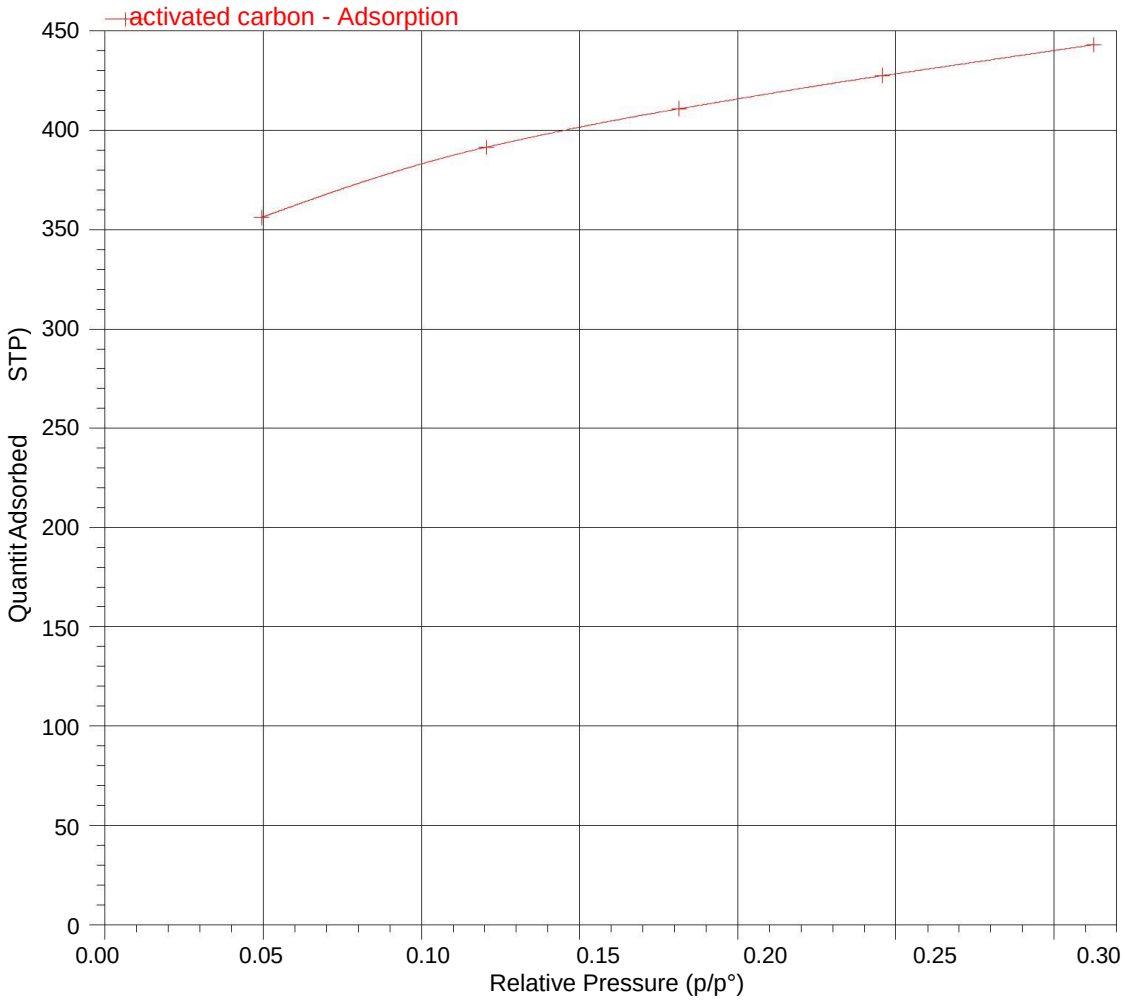

Figure 53: Isotherm Linear Plot

C.3 BET Analysis for Activated Carbon After Impregnation

micromeritics®

ASAP 2020 V3.01 H Unit 1 Serial #: 336 Page 1

Sample: Majed active carrbon with cata.2015
Operator: MAJED oct.2, 2015
Submitter:
File: C:\DATA\MAJED\000-213.SMP

Started: 10/2/2015 8:14:25PM
Completed: 10/3/2015 3:40:00AM
Report Time: 10/3/2015 12:25:48PM
Sample Mass: 0.2532 g
Cold Free Space: 87.7548 cm³
Low Pressure Dose: None

Analysis Adsorptive: N2
Analysis Bath Temp.: 77.332 K
Thermal Correction: No
Warm Free Space: 27.9507 cm³ Measured
Equilibration Interval: 10 s
Automatic Degas: Yes

Summary Report

Surface Area

Single point surface area at p/p° = 0.200429005: 145 .1785 m^2/g

BET Surface Area: 151.5212 m^2/g

Langmuir Surface Area: 210.7268 m^2/g

t-Plot Micropore Area: 7.4690 m^2/g

t-Plot External Surface Area: 144.0522 m^2/g

BJH Adsorption cumulative surface area of pores between 1.7000 nm and 300.0000 nm diameter: 137.813 m^2/g

BJH Desorption cumulative surface area of pores between 1.7000 nm and 300.0000 nm diameter: 155.1126 m^2/g

Pore Volume

Single point adsorption total pore volume of pores less than 69.8048 nm diameter at p/p° = 0.971478049 : 0.224022 cm^3/g

t-Plot micropore volume: 0.001476 cm^3/g

BJH Adsorption cumulative volume of pores between 1.7000 nm and 300.0000 nm diameter: 0.279339 cm^3/g

BJH Desorption cumulative volume of pores between 1.7000 nm and 300.0000 nm diameter: 0.291424 cm^3/g

Pore Size

Adsorption average pore width (4V/A by BET): 5.91395 nm

BJH Adsorption average pore diameter (4V/A): 8.1078 nm

BJH Desorption average pore diameter (4V/A): 7.5152 nm

Sample: Majed active carrbon with cata.2015
Operator: MAJED oct.2, 2015
Submitter:
File: C:\DATA\MAJED\000-213.SMP

Started: 10/2/2015 8:14:25PM
Completed: 10/3/2015 3:40:00AM
Report Time: 10/3/2015 12:25:48PM
Sample Mass: 0.2532 g
Cold Free Space: 87.7548 cm³
Low Pressure Dose: None

Analysis Adsorptive: N2
Analysis Bath Temp.: 77.332 K
Thermal Correction: No
Warm Free Space: 27.9507 cm³ Measured
Equilibration Interval: 10 s
Automatic Degas: Yes

Isotherm Tabular Report

Relative Pressure (p/p°)	Absolute Pressure (mmHg)	Quantity Adsorbed (mmol/g)	Elapsed Time (h:min)	Saturation Pressure (mmHg)
			00:56	758.652283
0.010382216	7.875463	1.08181	01:25	
0.032893834	24.950260	1.28613	01:38	
0.063011019	47.792900	1.43257	01:45	
0.078819094	59.781738	1.49573	01:50	
0.100150859	75.959824	1.57006	01:54	
0.120399813	91.316078	1.63536	01:58	
0.140421447	106.499374	1.69537	02:02	
0.160496667	121.722763	1.75284	02:06	
0.180567602	136.942352	1.80785	02:10	
0.200429005	152.002487	1.86087	02:14	
0.248805871	188.687408	1.98238	02:18	
0.302402132	229.329178	2.11621	02:22	
0.352944079	267.653259	2.24424	02:26	
0.400619577	303.800873	2.36924	02:31	
0.450603358	341.698792	2.50491	02:35	
0.500351338	379.414825	2.64792	02:40	
0.550429819	417.381653	2.80260	02:44	
0.600453128	455.303223	2.97111	02:49	
0.650656097	493.357086	3.15840	02:55	
0.700422891	531.080566	3.36770	03:00	
			03:02	758.221619
0.750149216	568.770081	3.61392	03:07	
0.799867692	606.453247	3.90913	03:14	
0.821166088	622.591370	4.05878	03:19	
0.850433824	644.771057	4.29215	03:24	
0.875074646	663.439941	4.52301	03:30	
0.899858366	682.216431	4.80343	03:36	
0.924451643	700.845520	5.15902	03:43	
0.948511361	719.064575	5.65505	03:52	
0.971478049	736.449158	6.46154	04:03	
0.982321010	744.647034	7.05668	04:12	
0.991222915	751.370605	7.66950	04:22	
0.995201275	754.361694	8.08246	04:32	
0.983216772	745.260437	7.80971	04:39	
0.974600286	738.710022	7.50400	04:47	
0.949100563	719.339966	6.49375	05:05	
			05:07	757.912598
0.918061725	695.810547	5.67629	05:19	

0.906172026	686.799194	5.47083	05:26
0.879712248	666.744995	5.10673	05:33
0.850498001	644.603149	4.79631	05:41
0.826554563	626.456116	4.58688	05:46
0.800885917	607.001526	4.38956	05:51
0.750738949	568.994507	4.06545	05:58

Sample: Majed active carrbon with cata.2015
Operator: MAJED oct.2, 2015
Submitter:
File: C:\DATA\MAJED\000-213.SMP

Started: 10/2/2015 8:14:25PM
Completed: 10/3/2015 3:40:00AM
Report Time: 10/3/2015 12:25:48PM
Sample Mass: 0.2532 g
Cold Free Space: 87.7548 cm³
Low Pressure Dose: None

Analysis Adsorptive: N2
Analysis Bath Temp.: 77.332 K
Thermal Correction: No
Warm Free Space: 27.9507 cm³ Measured
Equilibration Interval: 10 s
Automatic Degas: Yes

Isotherm Tabular Report

Relative Pressure (p/p°)	Absolute Pressure (mmHg)	Quantity Adsorbed (mmol/g)	Elapsed Time (h:min)	Saturation Pressure (mmHg)
0.700553889	530.958618	3.79193	06:05	
0.650729849	493.196350	3.55783	06:10	
0.600612677	455.211914	3.34915	06:16	
0.550798783	417.457336	3.16189	06:21	
0.500647104	379.446747	2.98217	06:26	
0.455938729	345.561707	2.67826	06:35	
0.392350076	297.367065	2.42916	06:40	
0.337293922	255.639313	2.28509	06:45	
0.303055210	229.689362	2.19977	06:49	
0.250721433	190.024933	2.07105	06:53	
0.200388298	151.876816	1.94583	06:57	
0.143300176	108.609009	1.79527	07:01	

Sample: Majed active carrbon with cata.2015
Operator: MAJED oct.2, 2015
Submitter:
File: C:\DATA\MAJED\000-213.SMP

Started: 10/2/2015 8:14:25PM
Completed: 10/3/2015 3:40:00AM
Report Time: 10/3/2015 12:25:48PM
Sample Mass: 0.2532 g
Cold Free Space: 87.7548 cm³
Low Pressure Dose: None

Analysis Adsorptive: N2
Analysis Bath Temp.: 77.332 K
Thermal Correction: No
Warm Free Space: 27.9507 cm³ Measured
Equilibration Interval: 10 s
Automatic Degas: Yes

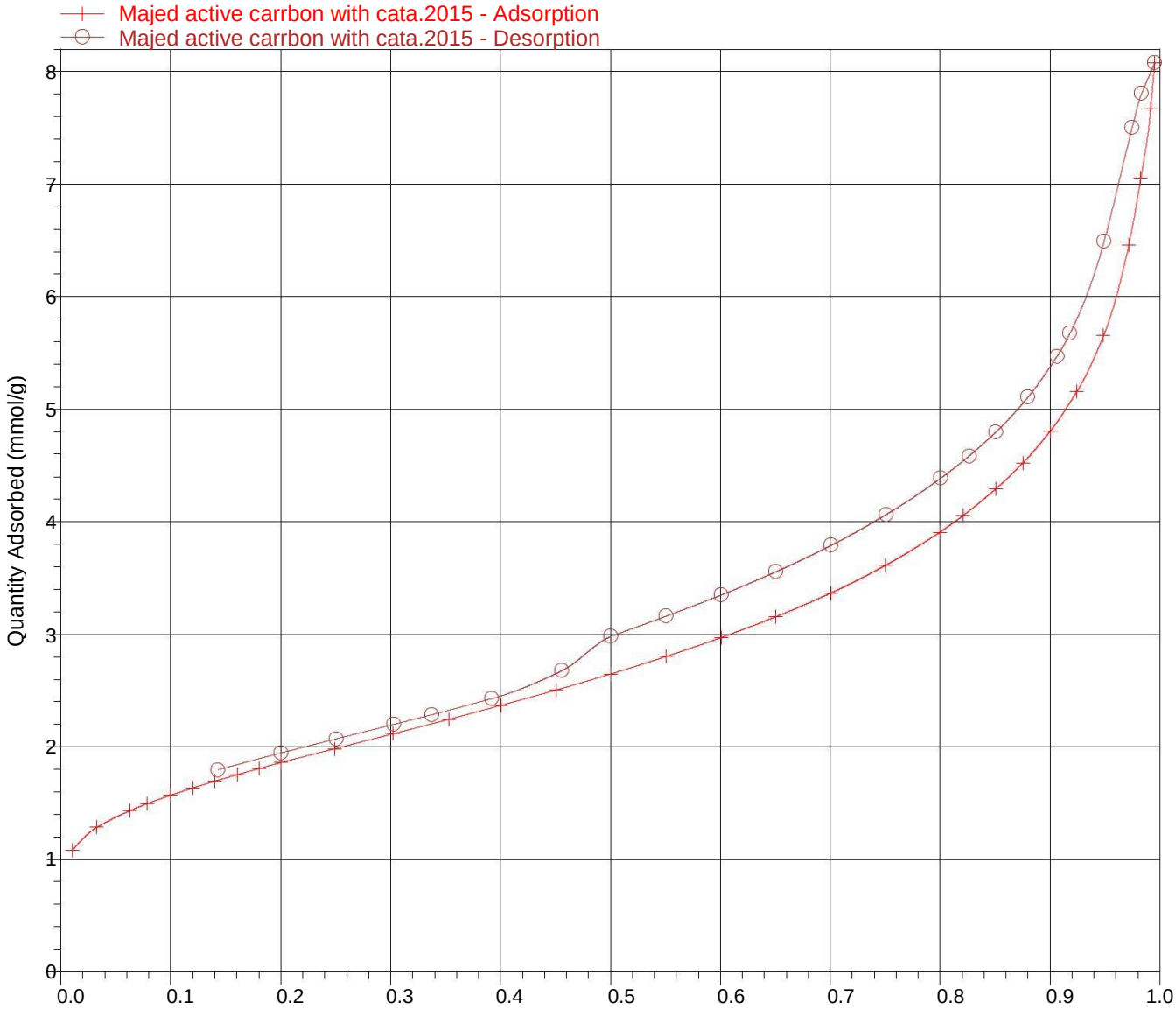

Figure 54: Isotherm Linear Plot

C.4 BET Analysis for Petcoke Before Impregnation

Quantachrome NovaWin2 - Data Acquisition and Reduction

for NOVA instruments

©1994-2006, Quantachrome Instruments

version 2.2

Analysis Report

Operator:1 Date:2013/07/08 Operator:1 Date:9/18/2015

Sample ID: Nova 2200E Filename: D:\QCDATA\Physisorb\Majed sample from Dr Sharif.qps

Sample Desc: Comment:

Sample weight: 0.0749 g Sample Volume: 0 cc

Outgas Time: 3.0 hrs OutgasTemp: 300.0 C

Analysis gas: Nitrogen Bath Temp: 77.3 K

Press. Tolerance:0.100/0.100 (ads/des)Equil time: 60/60 sec (ads/des) Equil timeout: 240/240 sec (ads/des)

Analysis Time: 467.4 min End of run: 2013/07/08 16:11:16 Instrument: Nova Station A

Cell ID: 33

Adsorbate Nitrogen Temperature 77.350K

Molec. Wt.: 28.013 g Cross Section: 16.200 Å² Liquid Density: 0.808 g/cc

Relative Pressure P/Po	Volume@STP cc/g	1 / [W((Po/P) - 1)]
6.27140e-02	373.1782	1.4346e-01
8.53920e-02	380.7947	1.9617e-01
1.05149e-01	385.5174	2.4387e-01
1.25188e-01	389.1453	2.9423e-01
1.42403e-01	391.6825	3.3920e-01

1.66811e-01	394.6003	4.0595e-01
1.85318e-01	396.4666	4.5906e-01
2.05435e-01	398.1982	5.1951e-01
2.26038e-01	399.7163	5.8460e-01
2.46790e-01	401.1205	6.5356e-01
2.67668e-01	402.5154	7.2653e-01
2.88879e-01	403.6585	8.0521e-01
3.08826e-01	404.9227	8.8289e-01
3.29542e-01	405.9670	9.6872e-01
3.49814e-01	407.1694	1.0572e+00

BET summary

Slope = 3.155

Intercept = -9.918e-02

Correlation coefficient, r = 0.995518

C constant= -30.810

Surface Area = 1139.612 m^2/g

Analysis Report

Operator:1 Date:2013/07/08 Operator:1 Date:9/18/2015

Sample ID: Nova 2200E Filename: D:\QCDATA\Physisorb\Majed sample from Dr Sharif.qps

Sample Desc: Comment:

Sample weight: 0.0749 g Sample Volume: 0 cc

Outgas Time: 3.0 hrs OutgasTemp: 300.0 C

Analysis gas: Nitrogen Bath Temp: 77.3 K

Press. Tolerance:0.100/0.100 (ads/des)Equil time: 60/60 sec (ads/des) Equil timeout: 240/240 sec (ads/des)

Analysis Time: 467.4 min End of run: 2013/07/08 16:11:16 Instrument: Nova Station A

Cell ID: 33

Adsorbate Nitrogen Temperature 77.350K

Molec. Wt.: 28.013 g Cross Section: 16.200 Å² Liquid Density: 0.808 g/cc

Total Pore Volume summary

Total Pore Volume

Total pore volume = 6.647e-01 cc/g for pores smaller than -33116.1 Å (Radius) at P/Po = 1.00029

V-t method summary

Thickness method: DeBoer

Slope = 3.409

Intercept = 381.600

Correlation coefficient, r = 0.747996

Micropore volume = 0.590 cc/g

Micropore area = 1086.874 m²/g

External surface area = 52.737 m²/g

C.5 BET Analysis for Petcoke After Impregnation

micromeritics®

Sample: Majed petcoke with cata.2015
Operator: MAJED oct.2, 2015
Submitter:
File: C:\DATA\MAJED\000-214.SMP

Started: 10/3/2015 12:43:10PM
Completed: 10/3/2015 5:41:51PM
Report Time: 10/4/2015 2:58:26PM
Sample Mass: 0.1786 g
Cold Free Space: 90.0115 cm³
Low Pressure Dose: None

Analysis Adsorptive: N2
Analysis Bath Temp.: 77.333 K
Thermal Correction: No
Warm Free Space: 28.0776 cm³ Measured
Equilibration Interval: 10 s
Automatic Degas: Yes

Summary Report

Surface Area

Single point surface area at p/p° = 0.201020610: 37. 1338 m²/g

BET Surface Area: 37.7058 m²/g

Langmuir Surface Area: 51.5974 m²/g

t-Plot Micropore Area: 16.5836 m²/g

t-Plot External Surface Area: 21.1222 m²/g

BJH Adsorption cumulative surface area of pores
between 1.7000 nm and 300.0000 nm diameter: 7.325 m²/g

BJH Desorption cumulative surface area of pores
between 1.7000 nm and 300.0000 nm diameter: 0.3850 m²/g

Pore Volume

Single point adsorption total pore volume of pores
less than 79.0758 nm diameter at p/p° = 0.974895587 : 0.019137 cm³/g

t-Plot micropore volume: 0.007163 cm³/g

BJH Adsorption cumulative volume of pores
between 1.7000 nm and 300.0000 nm diameter: 0.009936 cm³/g

BJH Desorption cumulative volume of pores
between 1.7000 nm and 300.0000 nm diameter: 0.004822 cm³/g

Pore Size

Adsorption average pore width (4V/A by BET): 2.03012 nm

BJH Adsorption average pore diameter (4V/A): 5.4258 nm

BJH Desorption average pore diameter (4V/A): 50.1030 nm

Sample: Majed petcoke with cata.2015
Operator: MAJED oct.2, 2015
Submitter:
File: C:\DATA\MAJED\000-214.SMP

Started: 10/3/2015 12:43:10PM
Completed: 10/3/2015 5:41:51PM
Report Time: 10/4/2015 2:58:26PM
Sample Mass: 0.1786 g
Cold Free Space: 90.0115 cm³
Low Pressure Dose: None

Analysis Adsorptive: N2
Analysis Bath Temp.: 77.333 K
Thermal Correction: No
Warm Free Space: 28.0776 cm³ Measured
Equilibration Interval: 10 s
Automatic Degas: Yes

Isotherm Tabular Report

Relative Pressure (p/p°)	Absolute Pressure (mmHg)	Quantity Adsorbed (mmol/g)	Elapsed Time (h:min)	Saturation Pressure (mmHg)
			00:57	758.769897
0.011118213	8.431630	0.28729	01:52	
0.033384891	25.313129	0.34831	02:11	
0.067763153	51.374428	0.39892	02:21	
0.080428217	60.974022	0.41285	02:25	
0.100738627	76.369453	0.42930	02:28	
0.120600228	91.423752	0.44244	02:31	
0.140728105	106.679016	0.45322	02:34	
0.160837576	121.919434	0.46238	02:37	
0.180754113	137.012711	0.46967	02:40	
0.201020610	152.371857	0.47633	02:42	
0.250876640	190.156708	0.48278	02:45	
0.301199392	228.293091	0.48648	02:48	
0.350938401	265.984802	0.48760	02:51	
0.420191391	318.463989	0.48600	02:54	
0.470328854	356.452820	0.48558	02:57	
			03:00	757.857727
0.520108618	394.168335	0.48451	03:02	
0.569574335	431.656311	0.48286	03:05	
0.619481835	469.479095	0.47978	03:08	
0.669333523	507.259583	0.47632	03:10	
0.719225922	545.070923	0.47339	03:12	
0.769237113	582.972290	0.47336	03:15	
0.819302746	620.914917	0.47456	03:19	
0.820136057	621.546448	0.47843	03:22	
0.850385298	644.471069	0.48072	03:24	
0.893875937	677.430786	0.48552	03:27	
0.900123309	682.165405	0.48963	03:29	
0.925090811	701.087219	0.49913	03:32	
0.949866877	719.863953	0.51564	03:35	
0.974895587	738.832153	0.55197	03:37	
0.980442533	743.035950	0.57231	03:41	
0.990431789	750.606384	0.61668	03:43	
0.994777937	753.900146	0.65891	03:46	
0.973572051	737.829102	0.58787	03:49	
0.932772376	706.908752	0.54413	03:52	
0.906777068	687.208008	0.53522	03:55	
0.881638427	668.156494	0.53232	03:58	
0.856448645	649.066223	0.53198	04:00	

0.831387560	630.073486	0.53269	04:03
0.806519118	611.226746	0.53544	04:06
0.781294947	592.110413	0.53777	04:09
0.731389501	554.289185	0.54387	04:12
0.681134204	516.202820	0.54942	04:14
0.630978692	478.192078	0.55567	04:17

Sample: Majed petcoke with cata.2015
Operator: MAJED oct.2, 2015
Submitter:
File: C:\DATA\MAJED\000-214.SMP

Started: 10/3/2015 12:43:10PM
Completed: 10/3/2015 5:41:51PM
Report Time: 10/4/2015 2:58:26PM
Sample Mass: 0.1786 g
Cold Free Space: 90.0115 cm³
Low Pressure Dose: None

Analysis Adsorptive: N2
Analysis Bath Temp.: 77.333 K
Thermal Correction: No
Warm Free Space: 28.0776 cm³ Measured
Equilibration Interval: 10 s
Automatic Degas: Yes

Isotherm Tabular Report

Relative Pressure (p/p°)	Absolute Pressure (mmHg)	Quantity Adsorbed (mmol/g)	Elapsed Time (h:min)	Saturation Pressure (mmHg)
0.580980670	440.300690	0.56247	04:20	
0.530948217	402.383209	0.56862	04:22	
0.481197643	364.679352	0.56879	04:25	
0.431341767	326.895691	0.57126	04:28	
0.380895599	288.664673	0.57583	04:31	
0.330801013	250.700104	0.57890	04:34	
0.281113438	213.043991	0.58074	04:36	
0.231036026	175.092438	0.57973	04:39	
0.200614578	152.037308	0.57734	04:42	
0.141047498	106.893936	0.56466	04:45	

Sample: Majed petcoke with cata.2015
Operator: MAJED oct.2, 2015
Submitter:
File: C:\DATA\MAJED\000-214.SMP

Started: 10/3/2015 12:43:10PM
Completed: 10/3/2015 5:41:51PM
Report Time: 10/4/2015 2:58:26PM
Sample Mass: 0.1786 g
Cold Free Space: 90.0115 cm³
Low Pressure Dose: None

Analysis Adsorptive: N2
Analysis Bath Temp.: 77.333 K
Thermal Correction: No
Warm Free Space: 28.0776 cm³ Measured
Equilibration Interval: 10 s
Automatic Degas: Yes

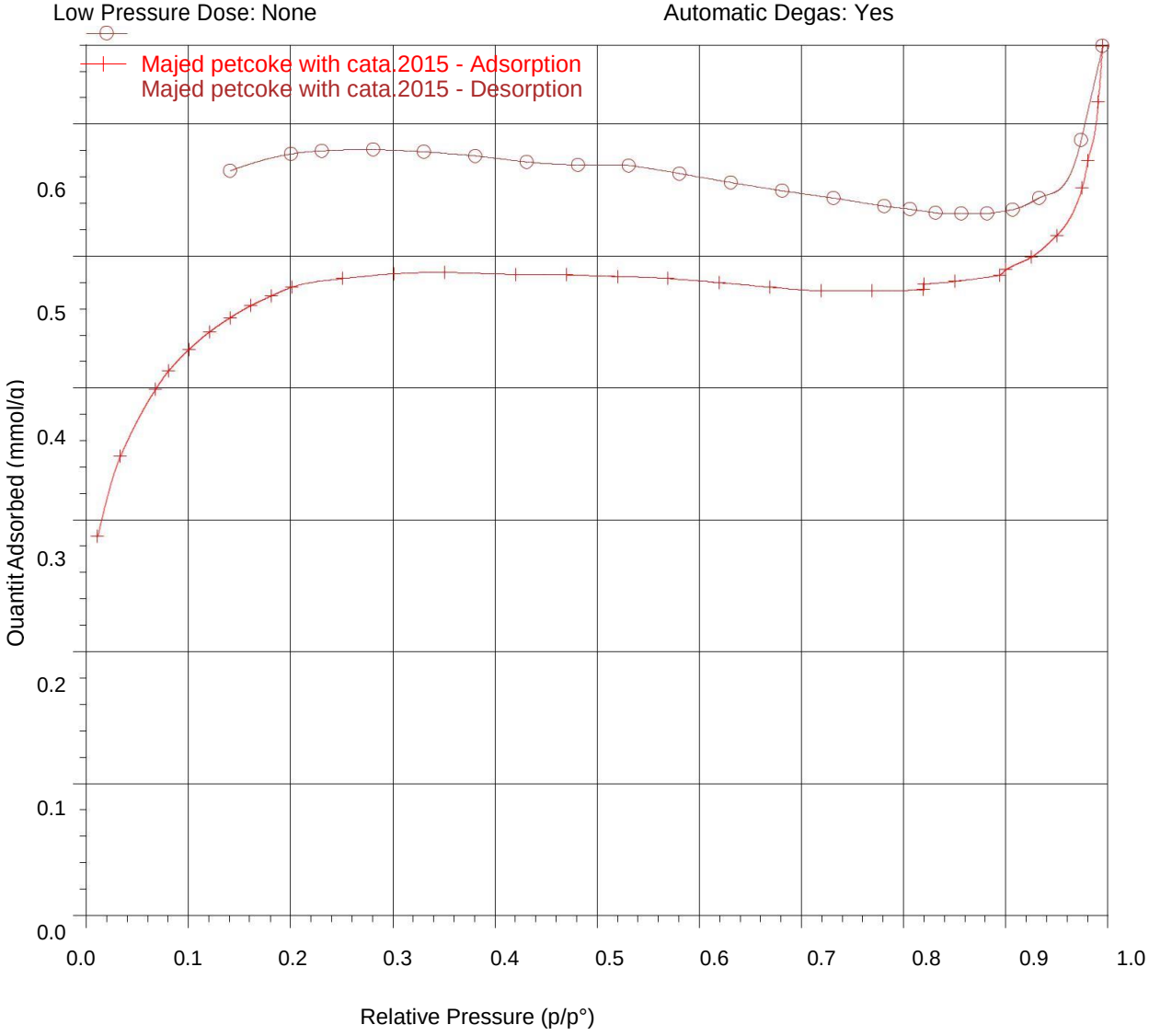

Figure 55: Isotherm Linear Plot

Appendix D C-MS Sample Scan

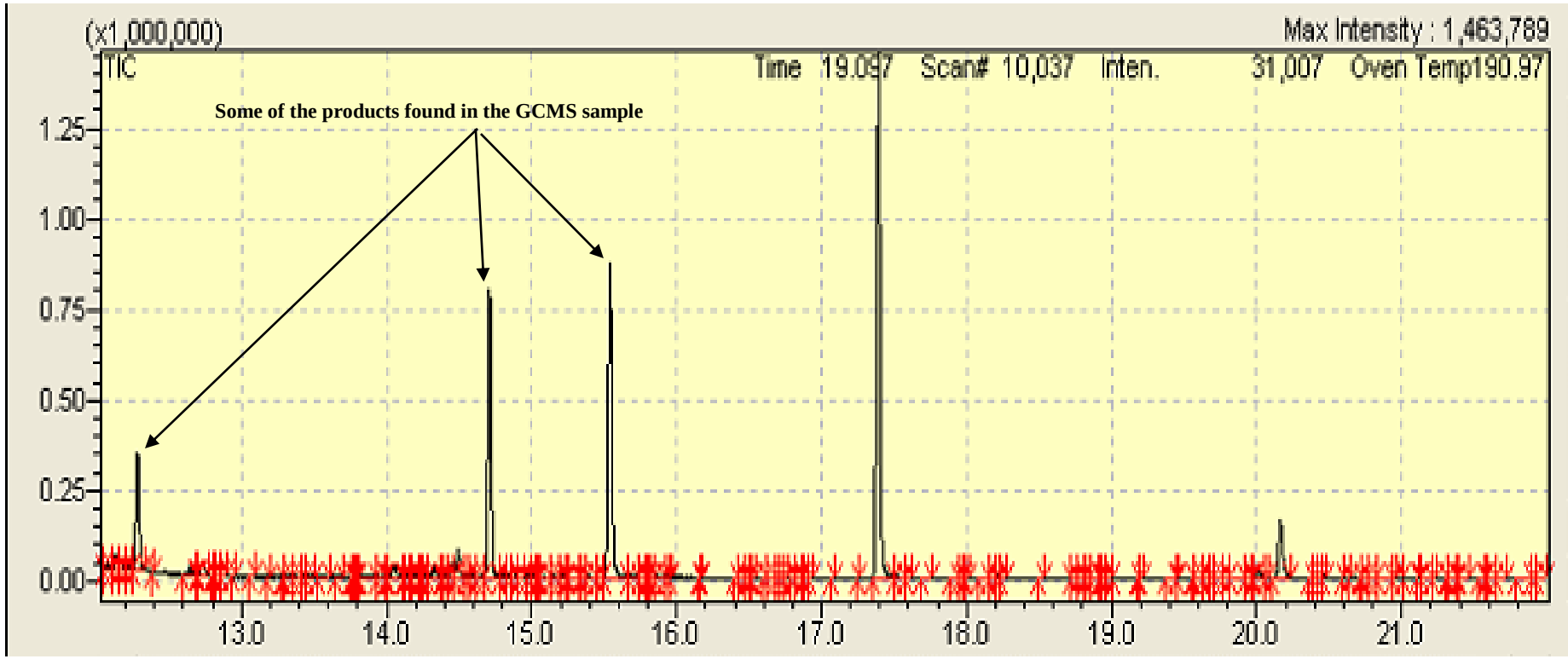

Figure 56: mass spect for a sample collected at 90 min for the HDS of DBT reaction at T=638 and P= 4.8 MPa

As shown in Figure 56 the GCMS was used to determine the concentration of the reaction species. In order to find the exact concentration, the GCMS should be calibrated. The calibration curve was constructed by analyzing the known concentrations of the feed and the products species. The GCMS showed the different areas of different known species' concentrations. The unknown sample's concentration was determined by fitting the sample's area in the calibration curve. More elaboration will follow.

As shown in Table 25 the calibration curve was constructed at a range of DBT concentration 0.1 – 2 wt%. The liquid inside the insert is 150 µL and we diluted it to 15 µL to maintain the GCMS column not to be damaged. Average density was calculated as follows

$$\rho_{ave} = \left(\frac{\%}{100}\right)_{\text{DBT}} \rho_{DBT} + \left(\frac{\%}{100}\right)_{\text{Decalin}} \rho_{Decalin}$$

Target initial sample (mg) = ρ_{ave}*diluted volume (15 µL)

$$\text{Target DBT conc (wt\%)} = \frac{\frac{(C_{DBT} * Target\ intial\ sample)}{100}}{\frac{(Target\ intial\ sample + Target\ DPE + Target\ Decalin)}{100}}$$

$$\text{Target DPE conc. (wt\%)} = \frac{(Target\ DPE)}{(Target\ intial\ sample + Trget\ DPE + Target\ Decalin)} * 100$$

Table 26 DBT calibration curve calculation

Sample name	Initial sample prep					Sample dilution									GCMS Analysis		
DBT	DBT (mg)	Decalin (mg)	DBT Concentration (wt%)	Avg.Density	Initial sample (uL)	Target Initial sample (mg)	Actual Initial sample (mg)	Target DPE (mg)	Actual DPE (mg)	Decalin (uL)	Target Decalin (mg)	Actual Decalin (mg)	Target DBT Concentration (wt%)	Actual DBT Concentration (wt%)	Target DPE Concentration (wt%)	Actual DPE Concentration (wt%)	DBTArea (-)
Zero point													0				0
DBT 1%1-1.qgd	0.905	895.936	0.10	0.90	15.00	13.45	13.355	0.25	0.237	80	71.68	72.4	0.02	0.02	0.2928	0.2756	115839
DBT 1%1-2.qgd	0.905	895.936	0.10	0.90	15.00	13.45	13.355	0.25	0.237	80	71.68	72.4	0.02	0.02	0.2928	0.2756	130490
DBT 1%1-3.qgd	0.905	895.936	0.10	0.90	15.00	13.45	13.355	0.25	0.237	80	71.68	72.4	0.02	0.02	0.2928	0.2756	140216
DBT 1-1.qgd	4.34	900.084	0.48	0.90	15.00	13.47	16.485	0.25	0.291	80	71.68	71.316	0.08	0.09	0.2928	0.3303	969295
DBT 1-2.qgd	4.34	900.084	0.48	0.90	15.00	13.47	16.485	0.25	0.291	80	71.68	71.316	0.08	0.09	0.2928	0.3303	1206488
DBT 1-3.qgd	4.34	900.084	0.48	0.90	15.00	13.47	16.485	0.25	0.291	80	71.68	71.316	0.08	0.09	0.2928	0.3303	1218281
DBT 2-1.qgd	9.033	897.561	1.00	0.90	15.00	13.49	13.908	0.25	0.285	80	71.68	73.914	0.16	0.16	0.2927	0.3235	2098927
DBT 2-2.qgd	9.033	897.561	1.00	0.90	15.00	13.49	13.908	0.25	0.285	80	71.68	73.914	0.16	0.16	0.2927	0.3235	2176825
DBT 2-3.qgd	9.033	897.561	1.00	0.90	15.00	13.49	13.908	0.25	0.285	80	71.68	73.914	0.16	0.16	0.2927	0.3235	2058170
DBT 3-1.qgd	13.575	880.34	1.52	0.90	15.00	13.52	13.434	0.25	0.276	80	71.68	72.305	0.24	0.24	0.2926	0.3209	3047023
DBT 3-2.qgd	13.575	880.34	1.52	0.90	15.00	13.52	13.434	0.25	0.276	80	71.68	72.305	0.24	0.24	0.2926	0.3209	2808127
DBT 3-3.qgd	13.575	880.34	1.52	0.90	15.00	13.52	13.434	0.25	0.276	80	71.68	72.305	0.24	0.24	0.2926	0.3209	2854409
DBT 4-1.qgd	18.326	900.98	1.99	0.90	15.00	13.55	13.463	0.25	0.309	80	71.68	74.863	0.32	0.30	0.2925	0.3486	3746641
DBT 4-2.qgd	18.326	900.98	1.99	0.90	15.00	13.55	13.463	0.25	0.309	80	71.68	74.863	0.32	0.30	0.2925	0.3486	3414162
DBT 4-3.qgd	18.326	900.98	1.99	0.90	15.00	13.55	13.463	0.25	0.309	80	71.68	74.863	0.32	0.30	0.2925	0.3486	3905784

By plotting actual DBT conc Vs DBT area we get

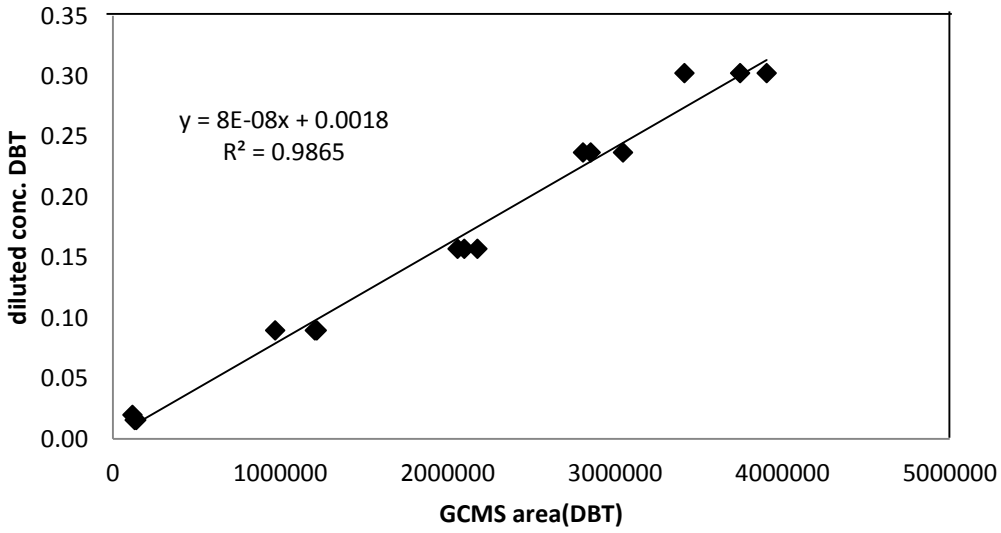

Figure 57: DBT calibration curve

Once we obtain the area of the unknown sample we lay it on Figure 57 to find the diluted conc. Of DBT.

D.1 Example of Sample Calculation

Table 27 : GCMS vail

GCMS vail contains	weight (mg)
DPE	0.25
Decalin	71.8
Diluted sample	13.45
	85.5

From the GCMS sample DBT weight = conc. Wt% of DBT (obtained from the curve after knowing its area) * Total weight $= \frac{0.2119}{100} * 85.5 = 0.181$ mg

DBT diluted conc. $= \frac{DBT\ weight}{Diluted\ volume} = \frac{0.181\ mg}{15\ \mu L} = 0.01208$ mg/µL

$$= \frac{1.207E{-}5\ g/\mu L}{184.26\ g/mol}$$

= 6.554E-8 mol/µL

= 6.55E-2 mol/L

To convert the diluted concentration to the actual concentration it has to be as follow

$$\frac{Diute\ DBT * Total\ GCMS\ vail\ volume}{Volume\ of\ the\ product\ in\ GCMS\ vail}$$

$$= \frac{6.55E{-}2 * (\frac{85.5}{0.9})}{(\frac{13.45}{0.9})} = 0.416$$

Appendix E Repeatability and Analysis Error

E.1 Conversion Calculation

After each reaction, we find the GCMS areas correspond to the DBT, BP, CHB, THDBT, and BCH by locate the areas in the calibration curves to obtain the concentration weight percent. To find the weight of each component, for instance, DBT, we multiply DBT conc.% into total weight of (DPE + Decalin +Product). Followed by that, we calculate the diluted moles of each component. Finally, to find the conversion, we divide the sum of the number of moles of the products by the total number of moles of the products + the remaining DBT in the reaction as shown in the following calculations:

BCH Conc%	0.011650668	
DBT	248695	
DBT conc%	0.021621908	
CHB Conc%	0.114441108	
TetraDBT	0.004039297	
BP Conc%	0.124547969	
DPE	0.248mg	
Decalin	71.004mg	
Product	14.058mg	
	0.29070	<-- DPE wt%
	0.01845	< -- mg DBT
	1.00107E-07	< --mole DBT
BP	0.10625	< -- mg BP
	6.8901E-07	< --mole BP in product
CHB	9.7630E-02	< -- mg BCH
	6.0920E-07	< --mole BCH in product
Tetra-DBT	3.4459E-03	< -- mg Tetra-DBT
	1.8301E-08	< -- mole Tetra DBT in product
BCH	9.939E-03	
	5.9767E-08	
%Conv	93.219	

sum of moles (prod.+remaining DBT)
1.4764E-06

E.2 Selectivity Calculations

To calculate the selectivity of any reaction, we collect the concentration weight percent of the products and normalize them to 100 and then we can get the selectivity. A calculation example will follow

component	conc.Wt%	normnalizing
BCH	0.002	0.025
CHB	0.032	0.342
BP	0.046	0.49
THDBT	0.013	0.143

E.3 Conversion Repeatability

The standard error was used to determine the variability of the measured data. The standard error equation is

$$\text{Se} = \sqrt{\frac{\sum_{i=1}^{m} SSQ*df}{\sum df}} \qquad \text{(E.1 1)}$$

Where X_i is the sample variable, X_{avg} is the average sample value, and df is the degree of freedom which is the number of samples minus one.

The repeatability runs for DBT conversions are given in the following table

Table 28: Conversions error calculation

Temperature	experiments	Average	SSQ	df
at 588 K	27.92			
	36.60			
	47.02	37.178	183.0553	2
at 603 K	60.23			
	49.09			
	81.97			
	55.11	61.602	615.5213	3
at 623 K	84.15			
	107.14			
	97.75			
	110.95	99.997	427.0217	3
at 638 K	119.07			
	105.26			
	120.94	115.09	146.6377	2
		$\sum_{i=1}^{m} SSQ$*df	1372.236	
		$\sum df$	10	
		Se^2	137.2236	
		Se	11.71425	

E.4 Product Selectivity Repeatability

The standard error was calculated for biphenyl as an example. The other products followed the same procedure.

Table 29: Error calculation of biphenyl

		Average	SSQ	df
BP at 603 K	1.93E-01			
	2.15E-01			
	1.94E-01	2.01E-01	0.000315	2
BP at 623 K	3.23E-01			
	2.80E-01			
	2.85E-01			
	2.69E-01	2.89E-01	0.001672	3
		$\sum_{i=1}^{m} SSQ$*df	0.001987	
		$\sum df$	5	
		Se^2	0.000397	
		Se	0.019936	

Appendix F Thermal Experiments Data

Many thermal runs were conducted at different temperature as shown in Table 30

Table 30: Thermal run data

Reaction time(min)	RPM	Temp	carbon Balance%	Conversion (Prod accum)
60	2000	588	104.26	2
90	2000	588	112.93	3
120	2000	588	100.94	3
30	2000	603	105.65	3
60	2000	603	100.85	3
90	2000	603	107.51	7
120	2000	603	101.60	7
30	2000	623	96.42	5
60	2000	623	103.95	10
90	2000	623	105.05	18
30	2000	638	96.64	6
60	2000	638	97.25	10
90	2000	638	101.23	18

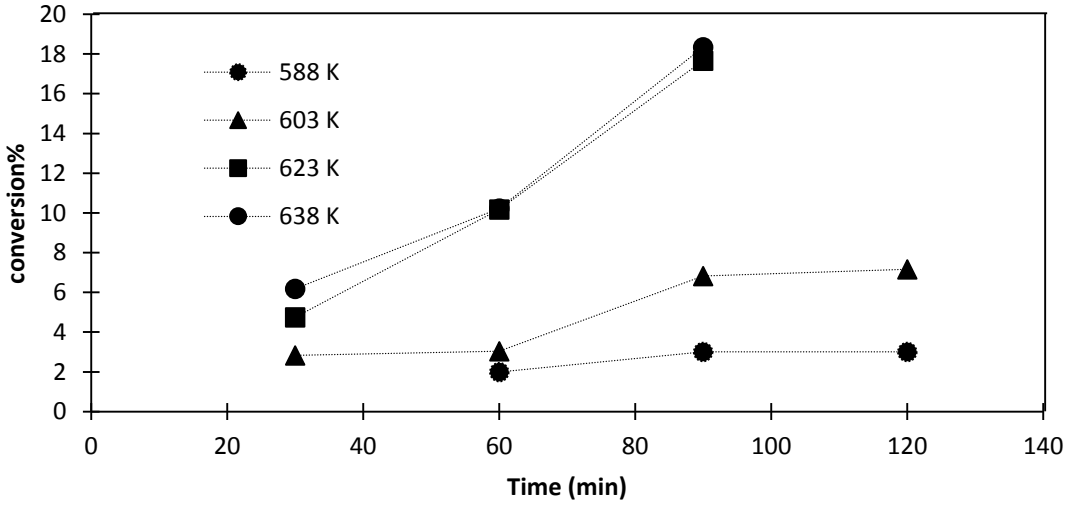

Figure 58: Comparison of different temperature amd reaction tmes for the thermal runs of HDS of DBT reaction

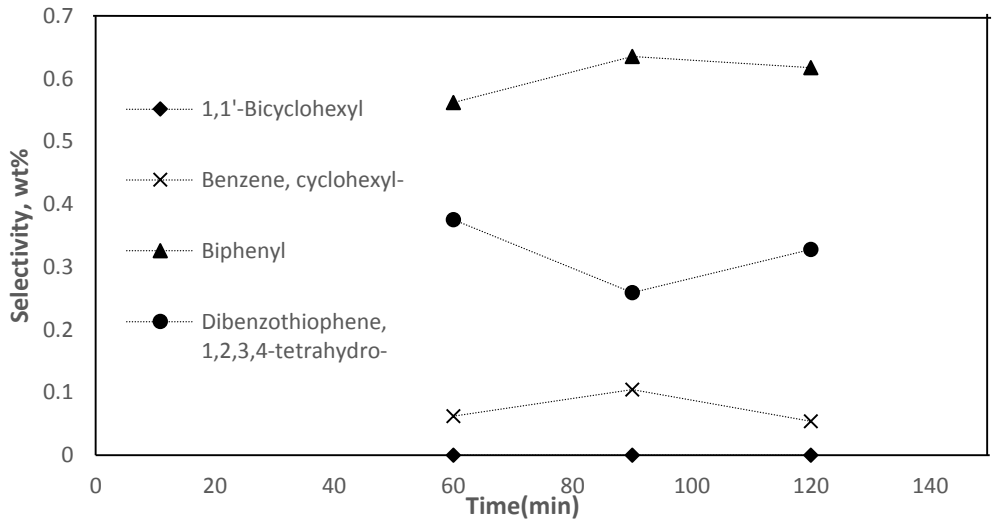

Figure 59: Selectivity of the thermal reaction at 588 K and 2000 RPM at different time

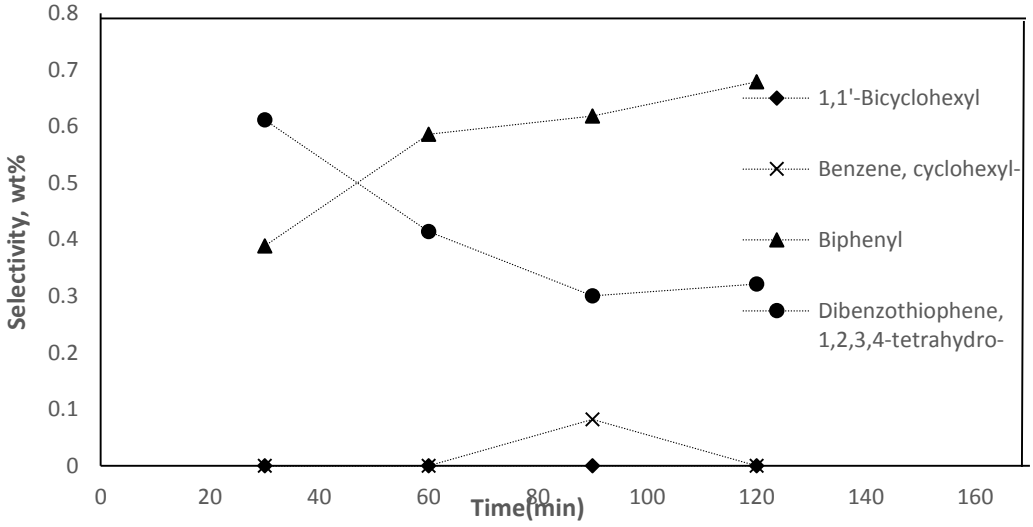

Figure 60: Selectivity of the thermal reaction at 603 K and 2000 RPM at different time

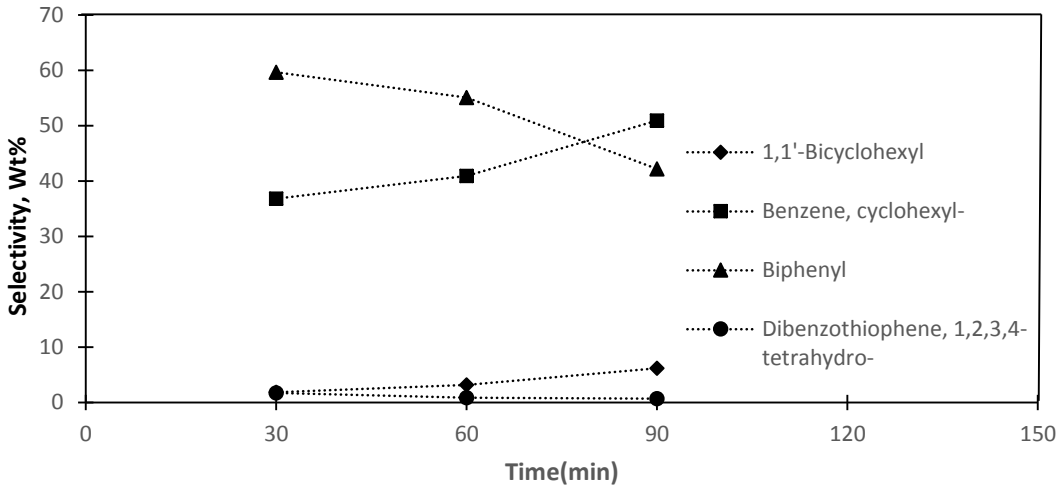

Figure 61: Selectivity of the thermal reaction at 623 K and 2000 RPM at different time

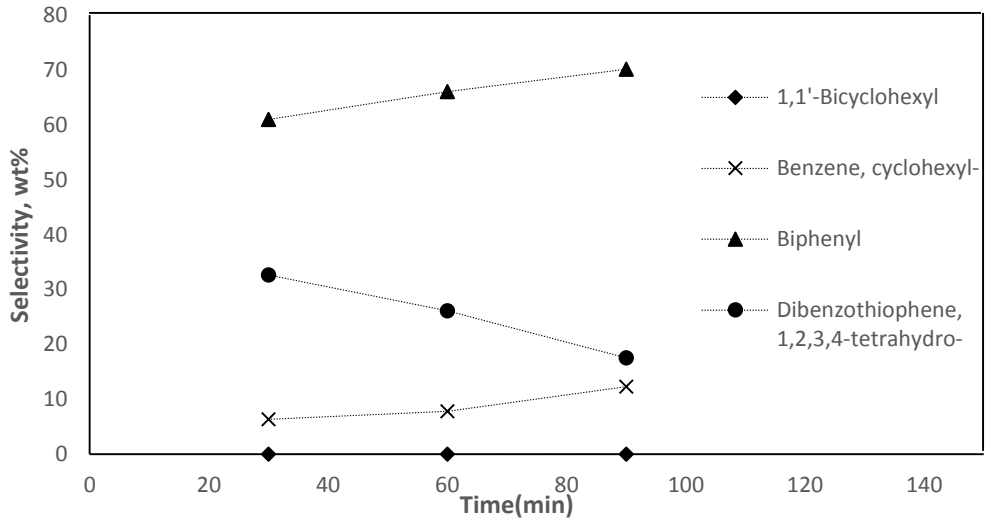

Figure 62: Selectivity of the thermal reaction at 638 K and 2000 RPM at different time

Appendix G Matlab Codes

These codes were used to model the HDS of DBT over NiMoS/AC and NiMoS/PC catalysts at different temperature 588 – 638 K. Least square function using Levenberg-Marquardt was used to estimate the kinetic parameters as well as their error.

G.1 Main Body Code

```
clear all
global nvar nx x0 y0
global verbose
global n1 n2 n3 n4 H2

verbose(1:2) = 1;
%
% x is the indep varaibale vector e.g. time measurements
% y is matrix of responses
% columns of y are responses y1, y2 (e.g. mol frac of component 1 and 2)
% rows of y are y values at the value of the indep variable (time) in x
% first row of y is initial value of response
% the program uses the Levenberg-Marquardt method to estimate parameters
% and calc statistics - done in leasqr and dfdp
% these two matlab m-files are designed for single repsonse
% the input data is re-aarnaged to yoied a single respone vector y
% the L-M requires the model to be calculated -this is done in modelmulti.m
% and assume sthe model is a series of ODEs, with the number of odes equalt
% to the number of responses.  The ODEs are calcualte din ODEfunm.  Note that
% this function must use teh correct model for each y
%
% INPUT
%
% input number of responses
%
% Order of reactions:
n1=1;       % order of CA
n2=1;       % order of CB
n3=1;       % order of CC
n4 = 1;
H2=1;   % Concentration of Hydrogen in liquid.
%
% Majed's data as of Novemver 25 2015
% time datq min)
T  =[0 60 90 120]';
44
nt=length (T)
x(1:nt-1)=T(2:nt)
x
nx=length(x)

CDBT=[5.98E-01 2.957E-01    2.545E-01   1.891E-01]';
```

```
CBCH= [0 1.111E-01  1.474E-01   1.454E-01]';

CBP=[0 7.456E-02    1.177E-01   1.471E-01]';

CCHB=[0 2.658E-02   2.552E-02   2.322E-02]';

CTHDBT=[0 5.222E-03 8.772E-03   1.481E-02]';


for j=1:nt-1
    y1(j)=CAX(j+1);
    y2(j)=CBX(j+1);
    y3(j)=CCX(j+1);
    y4(j)=CDX(j+1);
    y5(j)=CEX(j+1);
   end

nvar=5;
x0=0.;

oldx=x;
nx = length(x);
 y = [y1' y2' y3' y4' y5'];
 newy=y(:);
 oldy=reshape(newy,nx,nvar);
 x=x';
 newx=[x;x;x;x;x];

% y01(1:nx)=CAX(1);
 y02(1:nx)=CBX(1);
 y03(1:nx)=CCX(1);
 y04(1:nx)=CDX(1);
 y05(1:nx)=CEX(1);
 y01(1)=5.13E-01
 y01(2)=5.54E-01
 y01(3)=5.20E-01
 newy0=[y01';y02';y03'; y04'; y05'];
%
%INPUT DATA NOW IN CORRECT COLUMN FORMAT
%
 y0=newy0
 x=newx
 y=newy
%
%  provide initial parameter guesses
%
theta=[     5.0000e-003     8.0000e-003     2.0000e-003     4.0000e-003
8.0000e-003] ;
np=length(theta)
pin=theta

%
```

```
% Begin calculation by calling L-M leat squares routine
%
[f,p,kvg,iter,corp,covp,covr,stdresid,Z,r2]=leasqr(x,y,pin,'modelmulti');
disp('RESPONSE:')
if kvg ==1
    disp ('PROBELM CONVERGED')
    elseif kvg == 0
    disp('PROBLEM DID NOT CONVERGE')
end
format shortEng
oldf=reshape(f,nx,nvar);
oldr=reshape(y-f, nx, nvar);

% model value calculation
%ODEfunm(xatx,yatx,p,knt)
tspan=0:.1:120;
C0 = [y0(1);CBX(1);CCX(1);CDX(1);CEX(1)];
[t,Y]=ode45(@ODEfunm,tspan,C0,[],p);

CA  =Y(:,1);
CB  =Y(:,2);
CC  =Y(:,3);
CD  =Y(:,4);
CE  =Y(:,5);


%    figure;
%
%       subplot(2,4,1)
%
plot(T,CA_X_150_day2,'bo',T,CB_X_150_day2,'md',T,CC_X_150_day2,'r+',m,C_4MS_T
150_day2,'b--',m,C_HYD_T150_day2,'m--',m,C_C18_T150_day2,'r--')
%               title('T=150C')
%               ylabel({'Day 2';'Concentration (mol/L)'})
%               legend('4MS','HYD','C18',1)


    disp ('X-values:')
    disp (oldx')
    disp ('Y-values')
    disp(oldy)
    disp('f-values - i.e. model calculated responses')
    disp(oldf)
    disp('Residuals:')
    disp (oldr)
%     disp ('Standarddized residuals:')
%     disp (stdresid)
    disp ('Estimated parameter values are;')
    disp (p)
    disp ('Covariance of estimated parameters - sqrt of diagonal gives CL')
    disp (covp)
    disp('R2 values is:')
    disp (r2)
    plot (oldx,oldy,'d'), hold, plot (oldx,oldf)
```

```
   figure

plot(oldx(:),oldy(:,1),'bx',oldx(:),oldy(:,2),'ko',oldx(:),oldy(:,3),'r+',old
x(:),oldy(:,4),'gd',oldx(:),oldy(:,5),'mo',tspan,CA,'b--',tspan,CB,'k--
',tspan,CC,'r--',tspan,CD,'g--',tspan,CE,'m--')
          title('T=588, NiMoS/PC')
              xlabel('Time (min)')
              ylabel('Concentration (mol/L)')

legend('DBT','biphenyl','cyclohexylBenzene','1,2,3,4THDBT','1,1-Bicyclohexy')
```

G.2 Modelmulti Code

```
function f = modelmulti (x,pin)
% Solve a simple system of 2 ODE's  - 2 response variables
% find the solution at sepcified x values - corresponding to measured data
% first data point in x corresponds to initial condition
global nvar nx x0 y0
global verbose
global n1 n2 n3 n4 H2

 nxx=length(x);
yzero=reshape(y0,nx,nvar);

    for i = 1:nx
     xf = x(i);
     xoo=x0;
     yzed=yzero(i,:);
     [xmodel,ymodel] = ode45 (@ODEfunm,[xoo,xf], yzed,[],pin);
     yfinal(i,:)=ymodel(end,:);
    end
 f = yfinal(:);
```

G.3 ODE Codes

```
function yprime=ODEfunm(xatx,yatx,p,knt)
global nvar nx x0 y0
global verbose
global n1 n2 n3 n4 H2
%    disp('****************************YPRIME')
%    disp (knt)
%   nx
k1=p(1);
k2=p(2);
k3=p(3);
k4=p(4);
% k5=p(5);

%     yp(1)=-k1*yatx(1)-k2*yatx(1);
%     yp(2)=-k3*yatx(2)+k1*yatx(1);
%     yp(3)=-k5*yatx(3)+k4*yatx(4)+k3*yatx(2);
%     yp(4)=-k4*yatx(4)+k2*yatx(1);
%     yp(5)=-yp(1)-yp(2)-yp(3)-yp(4);
```

```
    yp(1)=-k1*yatx(1)-k2*yatx(1);
    yp(2)=k1*yatx(1);
    yp(3)=k3*yatx(4)-k4*yatx(3);
    yp(4)=-k3*yatx(4)+k2*yatx(1);
    yp(5)=-yp(1)-yp(2)-yp(3)-yp(4);
  yprime =[yp(1);yp(2)';yp(3)';yp(4)';yp(5)'];
```

G.4 Jacobian Matrix Calculation

```
function prt=dfdp(x,f,p,dp,func)
% numerical partial derivatives (Jacobian) df/dp for use with leasqr
% --------INPUT VARIABLES---------
% x=vec or matrix of indep var(used as arg to func) x=[x0 x1 ....]
% f=func(x,p) vector initialsed by user before each call to dfdp
% p= vec of current parameter values
% dp= fractional increment of p for numerical derivatives
%      dp(j)>0 central differences calculated
%      dp(j)<0 one sided differences calculated
%      dp(j)=0 sets corresponding partials to zero; i.e. holds p(j) fixed
% func=string naming the function (.m) file
%      e.g. to calc Jacobian for function expsum prt=dfdp(x,f,p,dp,'expsum')
%----------OUTPUT VARIABLES-------
% prt= Jacobian Matrix prt(i,j)=df(i)/dp(j)
%================================
m=length(x);n=length(p);      %dimensions
ps=p; prt=zeros(m,n);del=zeros(n,1);       % initialise Jacobian to Zero
for j=1:n
      del(j)=dp(j) .*p(j);    %cal delx=fract(dp)*param value(p)
           if p(j)==0
           del(j)=dp(j);     %if param=0 delx=fraction
           end
      p(j)=ps(j) + del(j);
      if del(j)~=0, f1=feval(func,x,p);
           if dp(j) < 0, prt(:,j)=(f1-f)./del(j);
           else
           p(j)=ps(j)- del(j);
           prt(:,j)=(f1-feval(func,x,p))./(2 .*del(j));
           end
      end
      p(j)=ps(j);     %restore p(j)
end
return
```

G.5 Least Square Codes

```
function [f,p,kvg,iter,corp,covp,covr,stdresid,Z,r2]= ...
      leasqr(x,y,pin,F,stol,niter,wt,dp,dFdp,options)
%function[f,p,kvg,iter,corp,covp,covr,stdresid,Z,r2]=
%                   leasqr(x,y,pin,F,{stol,niter,wt,dp,dFdp,options})
%
% Version 3.beta
%  {}= optional parameters
% Levenberg-Marquardt nonlinear regression of f(x,p) to y(x), where:
```

```
% x=vec or mat of indep variables, 1 row/observation: x=[x0 x1....xm]
% y=vec of obs values, same no. of rows as x.
% wt=vec(dim=length(x)) of statistical weights.  These should be set
%   to be proportional to (sqrt of var(y))^-1; (That is, the covariance
%   matrix of the data is assumed to be proportional to diagonal with
diagonal
%   equal to (wt.^2)^-1.  The constant of proportionality will be
estimated.),
%   default=ones(length(y),1).
% pin=vector of initial parameters to be adjusted by leasqr.
% dp=fractional incr of p for numerical partials,default=
.001*ones(size(pin))
%   dp(j)>0 means central differences.
%   dp(j)<0 means one-sided differences.
% Note: dp(j)=0 holds p(j) fixed i.e. leasqr wont change initial guess:
pin(j)
% F=name of function in quotes,of the form y=f(x,p)
% dFdp=name of partials M-file in quotes default is prt=dfdp(x,f,p,dp,F)
% stol=scalar tolerances on fractional improvement in ss,default stol=.0001
% niter=scalar max no. of iterations, default = 20
% options=matrix of n rows (same number of rows as pin) containing
%   column 1: desired fractional precision in parameter estimates.
%     Iterations are terminated if change in parameter vector (chg) on two
%     consecutive iterations is less than their corresponding elements
%     in options(:,1).  [ie. all(abs(chg*current parm est) < options(:,1))
%      on two consecutive iterations.], default = zeros().
%   column 2: maximum fractional step change in parameter vector.
%     Fractional change in elements of parameter vector is constrained to be
%     at most options(:,2) between sucessive iterations.
%     [ie. abs(chg(i))=abs(min([chg(i) options(i,2)*current param
estimate])).],
%     default = Inf*ones().
%
%          OUTPUT VARIABLES
% f=vec function values computed in function func.
% p=vec trial or final parameters. i.e, the solution.
% kvg=scalar: =1 if convergence, =0 otherwise.
% iter=scalar no. of interations used.
% corp= correlation matrix for parameters
% covp= covariance matrix of the parameters
% covr = diag(covariance matrix of the residuals)
% stdresid= standardized residuals
% Z= matrix that defines confidence region
% r2= coefficient of multiple determination

% All Zero guesses not acceptable
% Richard I. Shrager (301)-496-1122
% Modified by A.Jutan (519)-679-2111
% Modified by Ray Muzic 14-Jul-1992
%       1) add maxstep feature for limiting changes in parameter estimates
%          at each step.
%       2) remove forced columnization of x (x=x(:)) at beginning. x could be
%          a matrix with the ith row of containing values of the
%          independent variables at the ith observation.
%       3) add verbose option
```

```
%       4) add optional return arguments covp, stdresid, chi2
%       5) revise estimates of corp, stdev
% Modified by Ray Muzic 11-Oct-1992
%   1) revise estimate of Vy.  remove chi2, add Z as return values
% Modified by Ray Muzic 7-Jan-1994
%       1) Replace ones(x) with a construct that is compatible with versions
%          newer and older than v 4.1.
%       2) Added global declaration of verbose (needed for newer than v4.x)
%       3) Replace return value var, the variance of the residuals with covr,
%          the covariance matrix of the residuals.
%       4) Introduce options as 10th input argument.  Include
%          convergence criteria and maxstep in it.
%       5) Correct calculation of xtx which affects coveraince estimate.
%       6) Eliminate stdev (estimate of standard deviation of parameter
%          estimates) from the return values.  The covp is a much more
%          meaningful expression of precision because it specifies a
confidence
%          region in contrast to a confidence interval..  If needed, however,
%          stdev may be calculated as stdev=sqrt(diag(covp)).
%       7) Change the order of the return values to a more logical order.
%       8) Change to more efficent algorithm of Bard for selecting epsL.
%       9) Tighten up memory usage by making use of sparse matrices (if
%          MATLAB version >= 4.0) in computation of covp, corp, stdresid.
% Modified by Sean Brennan 17-May-1994
%          verbose is now a vector:
%          verbose(1) controls output of results
%          verbose(2) controls plotting intermediate results
%
% References:
% Bard, Nonlinear Parameter Estimation, Academic Press, 1974.
% Draper and Smith, Applied Regression Analysis, John Wiley and Sons, 1981.
%
%set default args

% argument processing
%

plotcmd='plot(x(:,1),y,''+'',x(:,1),f); shg';
%if (sscanf(version,'%f') >= 4),
vernum= sscanf(version,'%f');
if vernum(1) >= 4,
  global verbose
  plotcmd='plot(x(:,1),y,''+'',x(:,1),f); figure(gcf)';
end;
if (exist('OCTAVE_VERSION'))
  global verbose
end;

if(exist('verbose')~=1), %If verbose undefined, print nothing
    verbose(1)=0    %This will not tell them the results
    verbose(2)=0    %This will not replot each loop
end;
if (nargin <= 8), dFdp='dfdp'; end;
if (nargin <= 7), dp=.001*(pin*0+1); end; %DT
```

```
if (nargin <= 6), wt=ones(length(y),1); end;    % SMB modification
if (nargin <= 5), niter=20; end;
if (nargin == 4), stol=.0001; end;
%

y=y(:); wt=wt(:); pin=pin(:); dp=dp(:); %change all vectors to columns
% check data vectors- same length?
m=length(y); n=length(pin); p=pin;[m1,m2]=size(x);
if m1~=m ,error('input(x)/output(y) data must have same number of rows ')
,end;

if (nargin <= 9),
  options=[zeros(n,1) Inf*ones(n,1)];
  nor = n; noc = 2;
else
  [nor noc]=size(options);
  if (nor ~= n),
    error('options and parameter matrices must have same number of rows'),
  end;
  if (noc ~= 2),
    options=[options(noc,1) Inf*ones(noc,1)];
  end;
end;
pprec=options(:,1);
maxstep=options(:,2);
%

% set up for iterations
%
f=feval(F,x,p); fbest=f; pbest=p;
r=wt.*(y-f);
sbest=r'*r;
nrm=zeros(n,1);
chgprev=Inf*ones(n,1);
kvg=0;
epsLlast=1;
epstab=[.1 1 1e2 1e4 1e6];

% do iterations
%
for iter=1:niter,
  pprev=pbest;
  prt=feval(dFdp,x,fbest,pprev,dp,F);
  r=wt.*(y-fbest);
  sprev=sbest;
  sgoal=(1-stol)*sprev;
  for j=1:n,
    if dp(j)==0,
      nrm(j)=0;
    else
      prt(:,j)=wt.*prt(:,j);
      nrm(j)=prt(:,j)'*prt(:,j);
      if nrm(j)>0,
        nrm(j)=1/sqrt(nrm(j));
```

```
      end;
    end
    prt(:,j)=nrm(j)*prt(:,j);
  end;
% above loop could ? be replaced by:
% prt=prt.*wt(:,ones(1,n));
% nrm=dp./sqrt(diag(prt'*prt));
% prt=prt.*nrm(:,ones(1,m))';
  [prt,s,v]=svd(prt,0);
  s=diag(s);
  g=prt'*r;
  for jjj=1:length(epstab),
    epsL = max(epsLlast*epstab(jjj),1e-7);
    se=sqrt((s.*s)+epsL);
    gse=g./se;
    chg=((v*gse).*nrm);
%   check the change constraints and apply as necessary
    ochg=chg;
    for iii=1:n,
      if (maxstep(iii)==Inf), break; end;
      chg(iii)=max(chg(iii),-abs(maxstep(iii)*pprev(iii)));
      chg(iii)=min(chg(iii),abs(maxstep(iii)*pprev(iii)));
    end;
     if (verbose(1) & any(ochg ~= chg)),
       disp(['Change in parameter(s): ' ...
          sprintf('%d ',find(ochg ~= chg)) 'were constrained']);
     end;
    aprec=abs(pprec.*pbest);       %---
% ss=scalar sum of squares=sum((wt.*(y-f))^2).
    if (any(abs(chg) > 0.1*aprec)),%---  % only worth evaluating function if
      p=chg+pprev;                       % there is some non-miniscule change
      f=feval(F,x,p);
      r=wt.*(y-f);
      ss=r'*r;
      if ss<sbest,
        pbest=p;
        fbest=f;
        sbest=ss;
      end;
      if ss<=sgoal,
        break;
      end;
    end;                           %---
  end;
  epsLlast = epsL;
%   if (verbose(2)),
%     eval(plotcmd);
%   end;
  if ss<eps,
    break;
  end
  aprec=abs(pprec.*pbest);
%  [aprec chg chgprev]
  if (all(abs(chg) < aprec) & all(abs(chgprev) < aprec)),
    kvg=1;
```

```
    if (verbose(1)),
      fprintf('Parameter changes converged to specified precision\n');
    end;
    break;
  else
    chgprev=chg;
  end;
  if ss>sgoal,
    break;
  end;
end;

% set return values
%
p=pbest;
f=fbest;
ss=sbest;
kvg=((sbest>sgoal)|(sbest<=eps)|kvg);
if kvg ~= 1 , disp(' CONVERGENCE NOT ACHIEVED! '), end;

% CALC VARIANCE COV MATRIX AND CORRELATION MATRIX OF PARAMETERS
% re-evaluate the Jacobian at optimal values
jac=feval(dFdp,x,f,p,dp,F);
msk = dp ~= 0;
n = sum(msk);           % reduce n to equal number of estimated parameters
jac = jac(:, msk);  % use only fitted parameters

%% following section is Ray Muzic's estimate for covariance and correlation
%% assuming covariance of data is a diagonal matrix proportional to
%% diag(1/wt.^2).
%% cov matrix of data est. from Bard Eq. 7-5-13, and Row 1 Table 5.1

if vernum(1) >= 4,
  Q=sparse(1:m,1:m,(0*wt+1)./(wt.^2));  % save memory
  Qinv=inv(Q);
else
  Qinv=diag(wt.*wt);
  Q=diag((0*wt+1)./(wt.^2));
end;
resid=y-f;                                    %un-weighted residuals
covr=resid'*Qinv*resid*Q/(m-n);                 %covariance of residuals
Vy=1/(1-n/m)*covr;  % Eq. 7-13-22, Bard         %covariance of the data

jtgjinv=inv(jac'*Qinv*jac);         %argument of inv may be singular
covp=jtgjinv*jac'*Qinv*Vy*Qinv*jac*jtgjinv; % Eq. 7-5-13, Bard %cov of parm
est
d=sqrt(abs(diag(covp)));
corp=covp./(d*d');

covr=diag(covr);                % convert returned values to compact storage
stdresid=resid./sqrt(diag(Vy));  % compute then convert for compact storage
Z=((m-n)*jac'*Qinv*jac)/(n*resid'*Qinv*resid);
```

```
%%% alt. est. of cov. mat. of parm.:(Delforge, Circulation, 82:1494-1504,
1990
%%disp('Alternate estimate of cov. of param. est.')
%%acovp=resid'*Qinv*resid/(m-n)*jtgjinv

%Calculate R^2 (Ref Draper & Smith p.46)
%
r=corrcoef(y,f);
if (exist('OCTAVE_VERSION'))
  r2=r^2;
else
  r2=r(1,2).^2;
end

% if someone has asked for it, let them have it
%
 if (verbose(2)), eval(plotcmd); end,
 if (verbose(1)),
   disp(' Least Squares Estimates of Parameters')
   disp(p')
   disp(' Correlation matrix of parameters estimated')
   disp(corp)
   disp(' Covariance matrix of Residuals' )
   disp(covr)
   disp(' Correlation Coefficient R^2')
   disp(r2)
   sprintf(' 95%% conf region: F(0.05)(%.0f,%.0f)>=
delta_pvec''*Z*delta_pvec',n,m-n)
   Z
%   runs test according to Bard. p 201.
  n1 = sum((f-y) < 0);
  n2 = sum((f-y) > 0);
  nrun=sum(abs(diff((f-y)<0)))+1;
  if ((n1>10)&(n2>10)), % sufficent data for test?
    zed=(nrun-(2*n1*n2/(n1+n2)+1)+0.5)/(2*n1*n2*(2*n1*n2-n1-n2)...
      /((n1+n2)^2*(n1+n2-1)));
    if (zed < 0),
      prob = erfc(-zed/sqrt(2))/2*100;
      disp([num2str(prob) '% chance of fewer than ' num2str(nrun) ' runs.']);
    else,
      prob = erfc(zed/sqrt(2))/2*100;
      disp([num2str(prob) '% chance of greater than ' num2str(nrun) '
runs.']);
    end;
  end;
end

% A modified version of Levenberg-Marquardt
% Non-Linear Regression program previously submitted by R.Schrager.
% This version corrects an error in that version and also provides
% an easier to use version with automatic numerical calculation of
% the Jacobian Matrix. In addition, this version calculates statistics
% such as correlation, etc....
%
```

```
% Version 3 Notes
% Errors in the original version submitted by Shrager (now called version 1)
% and the improved version of Jutan (now called version 2) have been
corrected.
% Additional features, statistical tests, and documentation have also been
% included along with an example of usage.  BEWARE: Some the the input and
% output arguments were changed from the previous version.
%
%     Ray Muzic     <rfm2@ds2.uh.cwru.edu>
%     Arthur Jutan  <jutan@charon.engga.uwo.ca>
```

Appendix H Calculations of Arrhenius Equations

Arrhenius expression can be shown as follows

$$k_j = A_j * \exp\left(\frac{-E_{aj}}{R*T}\right) \qquad \text{(G1)}$$

National logarithm of G1 gives

$$\ln(k_j) = \ln(A_j) + \frac{-E_{aj}}{R} * \frac{1}{T} \qquad \text{(G2)}$$

By plotting $\ln(k_j)$ Vs $\frac{1}{T}$ as illustrated in Figure 77 the slope and the interception can be used to obtain the pre-exponetioal factor A_j and the activation energy E_a as follow:

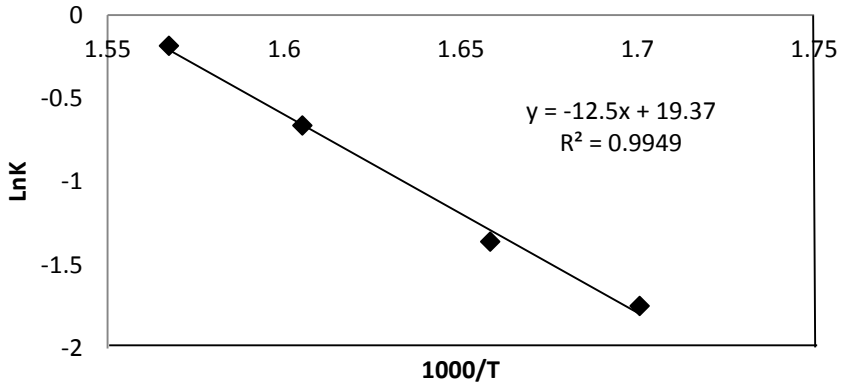

Figure 63: Arrhenius plot for NiMoS/AC for k1 at different temperature

$$\text{The slope} = \frac{-E_{aj}}{R} = -11.88$$

$$E_{a1} = -11.88 * 8.314 = 104 \text{ kJ/mol}$$

$$\text{Intercept} = \ln(A) = 19.37$$

$$A = 2.5 * 10^8 \text{ cm}^3/(g_{cat} * s$$

Appendix I Thermodynamic Calculations to Determine the Reaction Phase.

I.1 Reaction Phase Determination

Aspen software was use to simulate the current study reaction and determine the phase of the reaction inside the reactor. As shown in Figure 64 and Table 31, after setting the conversion to zero to determine the DBT phase inside the reactor, it was found to be liquid (refer to Table 30 LIQPRO column):

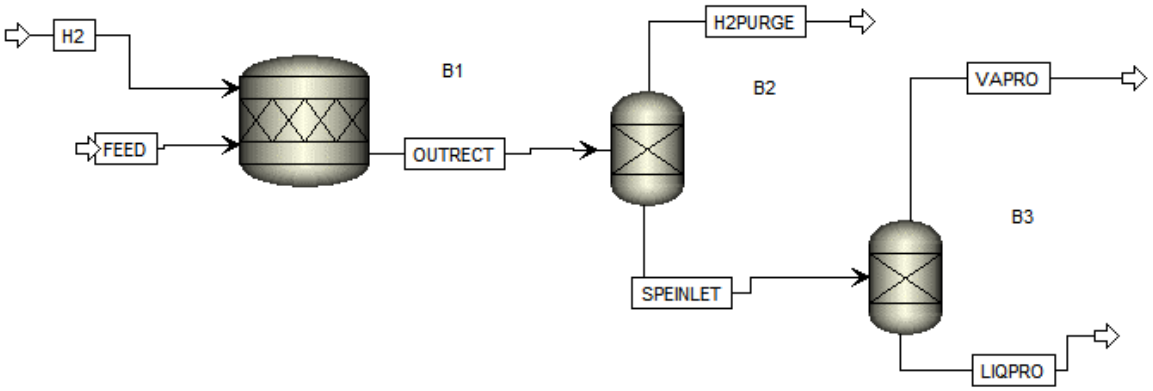

Figure 64: HDS of DBT reaction flowchart

Table 31 Aspen result for HDS of DBT at conversion set to zero

	FEED	H2	H2PURGE	LIQPRO	OUTRECT	SPEINLET	VAPRO
	B1	B1			B2	B3	
			B2	B3	B1	B2	B3
	LIQUID	VAPOR	VAPOR	LIQUID	MIXED	LIQUID	MIXED
Substream: MIXED							
Mole Flow kmol/hr							
DIBENZOT	0.0108541	0	0	0.0108432	0.0108432	0.010843	0
DECALIN	0.7088458	0	0	0.7088458	0.7088458	0.708846	0
CYCLO-01	0	0	0	0	1.81E-06	1.81E-06	1.81E-06
DIPHE-01	0	0	0	7.24E-06	7.24E-06	7.24E-06	0
HYDRO-01	0	0	0	0	1.09E-05	1.09E-05	1.09E-05
BICYC-01	0	0	0	0	1.81E-06	1.81E-06	1.81E-06
$C_{12}H_{12}S$	0	0	0	0	0	0	0
SULFUR	0	0	0	0	0	0	0
H_2	0	0.1488184	0.1487804	0	0.1487804	0	0
Total Flow kmol/hr	0.7196999	0.1488184	0.1487804	0.7196963	0.8684912	0.719711	1.45E-05
Total Flow kg/hr	100	0.3	0.2999234	99.99912	100.3	100.0001	9.61E-04
Total Flow l/min	1.855203	1.445154	2.740963	2.925255	6.639883	2.925296	2.47E-04
Temperature C	25	24	365	365	365	365	365
Pressure bar	42.40276	42.40276	48	48	48	48	48
Vapor Frac	0	1	1	0	0.2495916	0	0.9045203
Liquid Frac	1	0	0	1	0.7504084	1	0.0954796
Solid Frac	0	0	0	0	0	0	0
Enthalpy cal/mol	-50932.84	-6.872138	2372.776	-21945.11	-17344.26	-21944.8	-2503.228
Enthalpy cal/gm	-366.5636	-3.409002	1177.042	-157.9396	-150.1828	-157.939	-37.70937
Enthalpy cal/sec	-10182.32	-0.2840835	98.06183	-4387.171	-4184.259	-4387.19	-0.0100631
Entropy cal/mol-K	-228.5736	-7.438328	-2.356278	-168.05	-138.8462	-168.047	-32.62025
Entropy cal/gm-K	-1.645044	-3.689867	-1.168858	-1.20946	-1.20226	-1.20945	-0.4914011
Density mol/cc	6.47E-03	1.72E-03	9.05E-04	4.10E-03	2.18E-03	4.10E-03	9.75E-04
Density gm/cc	0.8983741	3.46E-03	1.82E-03	0.5697458	0.2517615	0.569743	0.0647494
Average MW	138.9468	2.01588	2.01588	138.9463	115.4876	138.9448	66.38213
Liq Vol 60F l/min	1.844838	0.1328398	0.1328058	1.844828	1.977654	1.844848	2.05E-05

I.2 H_2S Partial Pressure Calculation

First of all let's show the feed calculations:

We want 1000 uL, or roughly 1 g of total mixed feed with 3600 ppm Mo (or 0.36wt%)

Table 32 Mo, Ni, CS_2 molecular weight

Model compound	DBT	Unit
Desired conc.	2	wt%
Mr Mo	95.96	g/mol
Mr CS2	76.131	g/mol
Mr Ni	58.693	g/mol

Table 33 Desired metal wt%

Catalyst	18wt% NiMo/C	unit
Mo conc in cat	15	wt%
Ni conc in cat	3	wt%
Desired Metal conc.	0.36	wt%

Table 34 Feed preparation calculation

Catalyst conc	0.36	wt%				
Total mass	1	g				
DBT mass	0.019400616	g	19.40	mg	15.5	uL
Decalin mass	0.950630202	g	950.63	mg	1061.0	uL
Metal mass	0.0036	g				
Catalyst mass	0.02	g	20.00	mg		
Mo moles	3.75156E-05	mol				
Ni mass	0.00072	g				
Ni moles	1.22672E-05	mol				
Stoich S required	8.72985E-05	mol				
CS2 for 3 x stoich S	0.000130948	mol				
	0.009969181	g	9.97	mg	7.9	uL
Total additives	0.049369798	g				
			1000.00			

From Table 34 we conclude:

Mass of DBT + Decalin	970.03mg
Mass of Mo	3.6
DBT conc	2.000mg wt%
Mo loading	3.6000E-01 wt%
catalyst mass	
Metal	3.6 mg
Support	16.4
TOTAL CATALYST MASS	20 mg

Now let's calculate number of moles of S needed to sulphide the catalysts

From Table 34 number of moles of Mo = 37.52 micromoles

Number of S needed to sulphide the catalysts = 37.52*2=75.05 micromoles

We are using ~ 10 mg of CS_2 which equals 131.34 micromoles

If $CS_2 \rightarrow 2H_2S$ which means 2 moles of H_2S will be generated for 1 mole of CS_2

Now H_2S number of moles = 2*131.34 =262.67 micrometers

H_2S remaining after MoS_2 formation = 262.67-75.05 =187.63

Reactor volume = $\frac{\pi}{4}$*d^2*h = $\frac{\pi}{4}$*0.006^2*0.25 =7.07E-0.6 m^3

$P_{H_2S} = \frac{187.63*0.000001*8.314*613}{7.07E-6/1000}$ = 135.28 kPa